Development of the TiO$_2$-coated Silk Fibroin Filters

for Treatment of Gaseous Formaldehyde in Indoor Air

Miss Janjira Triped

A Dissertation Submitted in Partial Fulfillment of the Requirements

for the Degree of Doctor of Philosophy Program in Environmental Management

(Interdisciplinary Program)

Graduate School

Chulalongkorn University

Academic Year 2015

Copyright of Chulalongkorn University

การพัฒนาแผ่นกรองไหมไฟโบรอินที่เคลือบด้วยไททาเนียมไดออกไซด์
เพื่อการบำบัดก๊าซฟอร์มัลดีไฮด์ในอาคาร

นางสาวจันทร์จิรา ตรีเพชร

Thesis Title	Development of the TiO_2-coated Silk Fibroin Filters for Treatment of Gaseous Formaldehyde in Indoor Air
By	Miss Janjira Triped
Field of Study	Environmental Management
Thesis Advisor	Assistant Professor Wipada Sanongraj, Ph.D.
Thesis Co-Advisor	Assistant Professor Wipawee Khamwichit, Ph.D.

Accepted by the Graduate School, Chulalongkorn University in Partial Fulfillment of the Requirements for the Doctoral Degree

---Dean of the Graduate School

(Associate Professor Sunait Chutintaranond, Ph.D.)

THESIS COMMITTEE

---Chairman

(Assistant Professor Chantra Tongcumpou, Ph.D.)

---Thesis Advisor

(Assistant Professor Wipada Sanongraj, Ph.D.)

---Thesis Co-Advisor

(Assistant Professor Wipawee Khamwichit, Ph.D.)

---Examiner

(Assistant Professor Achariya Suriyawong, Ph.D.)

---Examiner

(Associate Professor Nurak Grisdanurak, Ph.D.)

---External Examiner

(Assistant Professor Bovornlak Oonkanond, Ph.D.)

จันทร์จิรา ตรีเพชร : การพัฒนาแผ่นกรองไหมไฟโบรอินที่เคลือบด้วยไททาเนียมไดออกไซด์ เพื่อการ
บำบัดก๊าซฟอร์มัลดีไฮด์ในอาคาร (Development of the TiO$_2$-coated Silk Fibroin Filters for
Treatment of Gaseous Formaldehyde in Indoor Air) อ.ที่ปรึกษาวิทยานิพนธ์หลัก: ผศ. ดร.
วิภาดา สนองราษฎร์, อ.ที่ปรึกษาวิทยานิพนธ์ร่วม: ผศ. ดร. วิภาวี ขำวิจิตร, 180 หน้า.

งานวิจัยนี้มุ่งเน้นการสังเคราะห์แผ่นกรองไหมไฟโบรอินที่เคลือบด้วยไททาเนียมไดออกไซด์และการนำไป
ประยุกต์ใช้เพื่อการบำบัดมลภาวะอากาศภายในอาคารโดยกระบวนการโฟโตคะตะไลติกออกซิเดชัน ก๊าซฟอร์มัลดี
ไฮด์ซึ่งเป็นหนึ่งในมลภาวะอากาศภายในอาคารที่สำคัญได้ถูกเลือกในการศึกษานี้ งานวิจัยนี้สามารถแบ่งออกได้เป็น
4 เฟส ประกอบด้วย เฟสที่ 1 การตรวจติดตามความเข้มข้นของก๊าซฟอร์มัลดีไฮด์ในอาคารห้องปฏิบัติการกายวิภาค
ศาสตร์และการสำรวจข้อมูลสุขภาพทั่วไป เฟสที่ 2 การสังเคราะห์แผ่นกรองไหมไฟโบรอินและการศึกษาลักษณะ
ทางสัณฐานวิทยาและคุณสมบัติทางกายภาพ เฟสที่ 3 การบำบัดก๊าซฟอร์มัลดีไฮด์ในห้องจำลองขนาดเล็กโดยการใช้
แผ่นกรองไหมไฟโบรอินที่สังเคราะห์ได้และแผ่นกรองอากาศทางการค้า และเฟสที่ 4 การประยุกต์ใช้แผ่นกรองไหม
ไฟโบรอินสังเคราะห์ที่เคลือบด้วยไททาเนียมไดออกไซด์เพื่อกระบวนการโฟโตคะตะไล ติกออกซิเดชั่นของการบำบัด
ก๊าซฟอร์มัลดีไฮด์ในห้องจำลองขนาดใหญ่ ผลการศึกษาเฟสที่ 1 ความเข้มข้นสูงสุดของก๊าซฟอร์มัลดีไฮด์ที่ตรวจพบ
มีค่าเท่ากับ 15.66 ± 0.00 พีพีเอ็ม ผลจากการสำรวจข้อมูลทั่วไปด้านสุขภาพ พบว่าอาการป่วยที่เกิดขึ้นมากที่สุด
ได้แก่ อาการหัวใจเต้นผิดปกติ สำหรับเฟสที่ 2 ได้ทำการสังเคราะห์และวิเคราะห์ลักษณะสัณฐานของแผ่นกรองไหม
ไฟโบรอินสังเคราะห์ที่เคลือบด้วยไททาเนียมไดออกไซด์ด้วยกล้องจุลทรรศน์อิเล็กตรอนแบบส่องกราด ยูวีวิสสเปรก
โตโฟโตมิเตอร์ ฟูเรียร์อินฟราเรด การวิเคราะห์คุณสมบัติทางความร้อน ไอโซเทอมการดูดซับและการคายซับของ
ก๊าซไนโตรเจนบนแผ่นกรองไหมไฟโบรอิน และคุณสมบัติทางกายภาพด้วยวิธีการความเค้นดึง ผลจากการศึกษาด้วย
กล้องจุลทรรศน์อิเล็กตรอนแบบส่องกราด แสดงให้การกระจายตัวค่อนข้างดีของไททาเนียมไดออกไซด์บนพื้นผิวแผ่น
กรองไหม ค่าระดับพลังงาน (band gap energy) เท่ากับ 3.18 อิเล็กตรอนโวลต์ การศึกษาประสิทธิภาพการบำบัด
ก๊าซฟอร์มัลดีไฮด์ในห้องจำลองขนาดเล็กที่มีขนาด 40x45x50 ลูกบาศก์เซนติเมตร โดยศึกษาผลของความเข้มข้น
เริ่มต้นของก๊าซฟอร์มัลดีไฮด์ ปริมาณตัวเร่งปฏิกิริยา (ไททาเนียมไดออกไซด์) และอัตราการไหลของอากาศ ผลจาก
การศึกษาพบว่าประสิทธิภาพการบำบัดก๊าซฟอร์มัลดีไฮด์สูงที่สุดเท่ากับร้อยละ 68.23 ± 0.44 ที่ความเข้มข้นเริ่มต้น
เท่ากับ 5.0 พีพีเอ็ม ปริมาณตัวเร่งปฏิกิริยาที่ร้อยละ 5 (น้ำหนักของไททาเนียมไดออกไซด์ต่อปริมาตรของตัวทำ
ละลาย) และที่อัตราการไหลของอากาศ 5 ลิตรต่อนาที ยิ่งไปกว่านั้นผลที่ได้จากจลนพลศาสตร์เผยให้เห็นว่าอัตรา
การเกิดปฏิกิริยาโฟโตคะตะไลสิซเป็นไปตามปฏิกิริยาอับดับหนึ่ง (first order reaction) ค่าคงที่ของอัตราการ
เกิดปฏิกิริยา (simplified L-H reaction) เท่ากับ 0.0061 ต่อนาที สำหรับการประยุกต์ใช้แผ่นกรองไหมไฟโบรอินที่
เคลือบไททาเนียมไดออกไซด์เพื่อการบำบัดก๊าซฟอร์มัลดีไฮด์ในห้องจำลองขนาดใหญ่ที่มีขนาด   1.2x1.2x1.85
ลูกบาศก์เมตร ที่อัตราการไหลของอากาศ 84.40 ลูกบาศก์ฟุตต่อนาที พบว่ามีประสิทธิภาพการบำบัดก๊าซฟอร์มัลดี
ไฮด์ประมาณร้อยละ 54.72 ± 1.75

สาขาวิชา	การจัดการสิ่งแวดล้อม	ลายมือชื่อนิสิต ....
ปีการศึกษา	2558	ลายมือชื่อ อ.ที่ปรึกษาหลัก
		ลายมือชื่อ อ.ที่ปรึกษาร่วม ....

5487758220 : MAJOR ENVIRONMENTAL MANAGEMENT

KEYWORDS: INDOOR AIR / FORMALDEHYDE (HCHO) / PHOTOCATALYTIC OXIDATION PROCESS (PCO) / TiO2-COATED SILK FIBROIN (SF) FILTERS

JANJIRA TRIPED: Development of the TiO_2-coated Silk Fibroin Filters for Treatment of Gaseous Formaldehyde in Indoor Air. ADVISOR: ASST. PROF. DR. WIPADA SANONGRAJ, Ph.D., CO-ADVISOR: ASST. PROF. DR. WIPAWEE KHAMWICHIT, Ph.D., 180 pp.

This research focuses on synthesis of TiO_2-coated silk fibroin (SF) filters and their application for treatment of indoor air contaminant via photocatalytic oxidation process (PCO). Formaldehyde (HCHO), one of major indoor air contaminants, was selected in this study. This work can be divided into 4 phases including: phase 1 monitoring of HCHO concentrations in a gross anatomy laboratory (GAL) and general health survey, phase 2 synthesis of SF filters and study of morphological structure and physical properties, phase 3 treatment of HCHO in a small reactor using the synthesized SF filters and commercial filter, and phase 4 application of the TiO_2-coated SF filters for PCO of HCHO in a large modeling room. For the first phase, the highest HCHO concentration observed was 15.66 ± 0.00 ppm. The result of general health survey showed that the most medical symptom occurred was irregular heartbeat. For the second phase, TiO_2-coated SF filters were synthesized and analyzed for morphological structure by Scanning electron microscopy (SEM), UV–VIS spectrophotometer, Fourier transform infra-red spectroscopy (FT-IR), Thermogravimetric analysis (TGA), isotherm of adsorption and desorption of nitrogen gas on the SF filter, and physical properties by tensile strength method. The SEM images revealed that the TiO_2 was relatively well scattered on SF surface. The band gap energy was 3.18 eV. The removal efficiency of HCHO in a small reactor with 40x45x50 cm^3 was conducted for impact of initial HCHO concentration, catalyst (TiO_2) dosage, and air flow rate. From the studies, the highest removal efficiency of approximately 68.23 ± 0.44 % was obtained at initial concentration of 5.0 ppm, catalysis dosage of 5.0 % (TiO_2 wt /vol.sol.), and air flow rate of 5 L/min. Moreover, the results derived from the kinetic model revealed that the photocatalytic rate follows the first order reaction. The simplified L-H reaction rate constant was calculated to be 0.0061 min^{-1}. For application of the TiO_2-coated SF filters for treatment of HCHO in a large modeling room of 1.2x1.2x1.85 m^3 at air flow rate of 84.40 ft^3/min, it was found that the removal efficiency of HCHO was approximately 54.72 ± 1.75 %.

Field of Study: Environmental M nagement   Student's Signature ------------------------------

Academic Year: 2015   Advisor's Si   nature------------------------------

                                            Co-Advisor's Signature ------------------------------

ACKNOWLEDGEMENTS

CONTENTS

LIST OF TABLES

LIST OF FIGURES

CHAPTER I

INTRODUCTION

1.1   Statement of problem

The Environmental Protection Agency found that indoor air pollution is one of the top risks to human health [1] as populations in developed countries spend more than 80% of their time in closed areas. There are several sources of indoor air pollutants, including outdoor pollution human activities, and releases of pollutants from household and decoration materials[2].

Studies of indoor air quality (IAQ) have shifted gradually to indoor volatile organic compounds (VOC). Formaldehyde (HCHO), an indoor VOC and a major indoor air contaminant, is a colorless gas with a strong odor that is commonly used as a preservative in medical laboratories and mortuaries, as an industrial fungicide, germicide, and disinfectant, and is found in building materials and household products such as chemicals, particle board, household products, glues, permanent press fabrics, paper product coatings, fiberboard, and plywood [3]

The use of formaldehyde occurs extensively in hospitals for disinfection and the preservation of tissue samples in histopathology laboratories [4] Concentrations of formaldehyde are from time to time high, such as during tissue disposal, preparation of formalin, and changing of tissue processor solutions [5].

During an anatomy class, the evaporation of formaldehyde from cadavers and embalming fluid could negatively affect medical students' and instructors' health. In 1977, the Ministry of Interior of Thailand declared that formaldehyde concentrations in situations where people work for eight hours could not be over 3 ppm [6]. The threshold limit value set by the American Conference of Governmental Industrial Hygienists is 0.3 ppm[7]. In Japan, the maximum level for working environments is 0.25 ppm [8] Ohmichi, Komiyama [9] found that indoor formaldehyde concentrations in anatomy laboratories were 0.45, 0.38, and 0.68 ppm for the 4th, 10th, and 18th sessions respectively, whereas personal exposure concentrations in the 4th, 10th, and 18th sessions were 1.02, 1.08, and 0.89 ppm for medical students and 0.80, 0.45, and 0.51 ppm for instructors respectively.

Formaldehyde removal is vital for the improvement of IAQ and human health due to carcinogenic risk [10]. Acute and chronic exposure to formaldehyde by inhalation by humans has been associated with problematic respiratory symptoms and eye, nose, and throat irritation. Formaldehyde solution splashes in the eye can cause injuries ranging from transient discomfort to severe, permanent corneal clouding and loss of vision [11, 12]. Chronic symptoms from formaldehyde exposure are nasal cancer and nasopharyngeal cancer. Exposure to formaldehyde concentrations ranging from 0.1 to 5 ppm can cause skin irritation, burning eyes, tearing, rhinorrhea, and upper respiratory irritation, while exposure 5 to 20 ppm can cause coughing, chest tightening or pain, difficulty in breathing, headache, and

palpitation. Exposure to 50 to 100 ppm and more can cause pneumonia, pulmonary edema, and death [13, 14].

Formaldehyde from furnishings and decorating materials frequently causes cancer and the development of titanium oxide (TiO_2) coated silk fibroin filter for photocatalytic degradation of formaldehyde and the investigation of photocatalytic reaction kinetics has theoretical and practical significance. In recent years, the application of heterogeneous photocatalysis in the removal of contaminants in air and wastewater has aroused great interest[15].

Photocatalytic oxidation (PCO) is a remediation technology which offers a number of advantages over conventional technologies. It can play a significant role in the reduction of the energy consumption of a building, lowering indoor air contaminant levels, and the improvement of the well-being of occupants. Most PCO technology is implemented in buildings as in-duct systems, located either on the return air duct, the supply air duct, or portable air cleaners. For such systems, ultra-violet (UV) lamps provide high energy radiation and thus promote electron transition within the catalyst. PCO is a promising air purification technology for trace contaminant degradation because it can degrade a broad range of VOC to water (H_2O) and carbon dioxide (CO_2) at room temperature and atmospheric pressure without significant energy input [16, 17]

Photocatalytic degradation of environmental contaminants has been studied in the past two or three decades. In early 1970s, Fujishima and Honda [18]

discovered the phenomenon of photo-induced water cleavage on TiO_2 electrodes. [19, 20] developed a differential dynamic fixed-bed reactor to study the heterogeneous photo-catalysis for partial oxidation of paraffin. However, earlier work mainly dealt with the treatment of wastewater. Using PCO to remove trace-level organic contaminants in air has recently received considerable attention since this technology can be potentially applied for air purification in office buildings, factories, homes, cars, and spacecraft.

The whole PCO process may be divided into six elemental mass transfer processes occurring in series: 1) advection (VOC and precursor species are carried by airflows); 2) external diffusion of reagent species through the boundary layer (BL) surrounding the catalyst or catalyst pellet; 3) adsorption onto the catalyst surface; 4) chemical reaction at the catalyst surface; 5) desorption of reaction product(s); 6) boundary layer diffusion of product(s) to the main flow. In the PCO reaction, pure or doped metal oxide semiconductors, such as TiO_2, ZnO, CdS, Fe (III)-doped TiO_2, are commonly used as the photo-catalysts. TiO_2 is widely used as a photocatalyst due to its superior characteristics [20] because (a) it is inexpensive, safe, and very stable showing high photocatalytic efficiency, (b) it promotes ambient temperature oxidation of the major classes of indoor air pollutants, (c) complete degradation of a broad range of pollutants can be achieved under certain operating conditions, and (d) no chemical additives are required. Pierre-Alexandre B. et al, (2010)[21] studied the characterization of new photocatalytic textile for HCHO removal from indoor air

by coating with TiO_2. The result has demonstrated efficiency to remove the formaldehyde, priority pollutant of indoor air.

Silk fibroin (SF) fiber obtained from silk cocoons is one of the filters used in air conditioners to ensure the production of clean air. Recently, re-generated silk solutions have been used to form a variety of bio-materials, such as gels, sponges and films, for medical applications [22]

SF in aqueous solutions from de-gummed *Bombyx mori* silk or *Bombyx mori* glands have been used to prepare silk fiber and fiber with sub-micron diameters was successfully obtained[23]. Recently, SF fiber from silk cocoons such as *Bombyx mori* has been explored to exploit the excellent characteristics of this protein as a textile fiber in the production of bio-material cosmetic creams, lotions, make-up, powder, bath preparations, and pharmaceuticals [24-26]. Natural silk fiber is one of the strongest materials due to the dominance of well-orientated β-sheet structures of protein chains [27, 28] The inner filaments of fiber fibroin are embedded in an outer rubbery coating made up of sericin. High purity SF can be obtained easily from degummed silk cocoon. Briefly, silk cocoons of *Bombyx mori* were degummed with 0.5 wt% Na_2CO_3 solution and washed with de-ionized water to remove the sericin [23].

Silk fiber has been used for decades. Recently SF from silkworm sources including Thai silkworm *Bombyx mori* (Nangnoi Srisaket 1) has been considered as a potential bio-material for a range of tissue engineering applications due to its non-

toxicity to cells, good mechanical properties, and slow degradation rate [29, 30]. Triped, J. et al., [31] found that SF fiber can be applied for the removal of indoor air particulate.

In this study, cost-effective and straightforward fabrication of photocatalytic filters is achieved by coating the SF filters with TiO_2. The photocatalytic destruction of gaseous formaldehyde using the TiO_2-coated SF filters was conducted in the modeling room to examine the removal efficiency of formaldehyde.

1.2 Objectives

1. To measure gaseous formaldehyde concentrations in the gross anatomy laboratory in the Division of Anatomy, College of Medicine and Public Health, Ubon Ratchathani University, Thailand.

2. To do the survey on health information of medical students who have been exposed to formaldehyde emission in gross anatomy laboratory.

3. To synthesize TiO_2-coated SF filters from silk cocoons by degumming process and TiO_2-coating method.

4. To examine the characteristics and mechanical properties of the TiO_2-coated SF filters.

5. To investigate the efficiency of TiO_2-coated SF filters for the removal of gaseous formaldehyde using the photocatalytic oxidation process in a closed modelling room.

1.3 Hypothesis

1. TiO_2-coated SF filters can be readily prepared by the de-gumming and paint brushing processes.

2. Gaseous formaldehyde can be efficiently removed (≥80%) via the photo-catalytic oxidation process using the TiO_2 –coated SF filer.

1.4 Scopes of study

The research is divided into four phases as follows:

Phase 1: Monitoring of Formaldehyde Concentrations in A Gross Anatomy Laboratory and General Health Survey

The Hand-held Formaldehyde Meter (HAL-HFX205) was used for the measurement of gaseous formaldehyde in the gross anatomy laboratory. Study of formaldehyde exposure was a cross-sectional health survey on the second and the third year medical students in the Division of Anatomy, College of Medicine and Public Health, Ubon Ratchathani University, Thailand.

Phase 2: Synthesis of SF filters and study of morphological structure and physical properties

The SF fiber from silk cocoons was degummed by boiling them in 0.5% (w/w) sunlight solution for sericin extraction. The SF fiber was uniformly reformed into rectangular- shaped filters and coated with TiO_2.

The morphological structure of the TiO_2-coated SF filters was observed using a scanning electro microscope (SEM). The optical property and structure of TiO_2-

coated SF filters were inspected following the UV/VIS, FT-IR spectrophotometer, and Thermogravimetric analysis (TGA) method . The specific surface area, specific pore volume, and pore size were analyzed by Barret Joyner Halendar (BJH) method. The mechanical properties of the synthesized SF fibers were measured. Static uniaxial tension tests were carried out at room temperature by the use of a universal material test machine LR5K (Lloyd instruments, USA).

Phase 3: Treatment of formaldehyde in a small reactor using the synthesized SF filters and commercial air filter

The removal efficiency of the TiO_2-coated SF filters was examined through the photo-catalytic destruction of gaseous formaldehyde in a closed reactor with the dimensions of 40 cm × 45 cm × 50 cm. The initial concentrations, catalyst dosages, and air flow rates were varied to investigate the suitable conditions for the removal of formaldehyde.

Phase 4: Application of the TiO_2 coated SF filters for photocatalytic oxidation (PCO) of formaldehyde in a large modeling room

The removal efficiency of the TiO_2-coated SF filters was examined through the photo-catalytic destruction of gaseous formaldehyde in a large modeling room with the dimensions of 1.20 m ×1.20 m × 1.85 m. The initial concentration was varied. The catalyst dosage and air flow rate were fixed as 2.50 % (wt./vol. sol.) and 84.40 ft^3/min, respectively to investigate the potential use of the synthesized SF filter as an air purifier.

CHAPTER II

BACKGROUND AND LITERATURE REVIEWS

2.1 Indoor air environment

Indoor air quality (IAQ) has received immense attention in the early 1990s. This is because studies [32] showed that the level of pollutants in indoor environments is actually higher than in outdoor environments. In addition, people generally spend more than 80 % of their time in indoors, which contributes a higher risk from inhalation of pollutants than outdoors [33]. In 1995, USEPA identified indoor air pollution is one of the top environmental risk [34].

Indoor air environments must meet the requirement of thermal comfort and IAQ. Thermal comfort is affected by many factors, which mainly include air temperature, air humidity, air velocity, mean radiant temperature, human clothing, and activity levels. The wide use of air conditioning helps to improve thermal comfort, but health problems associated with poor IAQ appear more frequently (e.g., SBS) [35]. Many experts believe that IAQ may be the most important and relatively overlooked environmental issue of our times. It is indoor pollutants that lead to poor IAQ. Indoor air pollutants consist of both particle pollutants and gaseous pollutants [36].

Sulfur dioxide, nitrogen oxide, volatile organic compounds (VOCs), and particulates are the four major components of air pollution and are the main causes

of environmental damage and many diseases, including cancer. Studies of IAQ have shifted gradually to indoor volatile organic compounds (VOCs). Formaldehyde (HCHO), as a major indoor air contaminant, is a colorless gas with a strong odor that is commonly used as a preservative in medical anatomy laboratories and mortuaries, as an industrial fungicide, germicide, and disinfectant, and is found in building materials and household products such as chemicals, particle board, household products, glues, permanent press fabrics, paper product coatings, fiberboard, and plywood. Its removal is vital for improving IAQ and human being's health due to carcinogenic risk [3].

2.2 Formaldehyde

General information on exposure

❖ Technical products and impurities

"Formaldehyde" is the chemical substance, HCHO, Chemical Abstracts Service Registry No. 50-00-0. Trade names: BFV; FA; Fannoform; Floguard 1015; FM 282; Formalin; Formalin 40; Formalith; Formol; FYDE; Hoch; Ivalon; Karsan; Lysoform; Morbicid; Paraform; Superlysoform.

Formaldehyde is an important chemical used widely by industry to manufacture building materials and numerous household products. It is also a by-product of combustion and certain other natural processes. Thus, it may be present in substantial concentrations both indoors and outdoors. Formaldehyde (sometimes called "formalin" a mixture of formaldehyde and alcohol usually methanol) is a

clear colorless liquid with a pungent odor detectable at 1 parts per million (ppm). It is most commonly available commercially as a 30–50% (by weight) aqueous solution. In dilute aqueous solution, the predominant form of formaldehyde is its monomeric hydrate, methylene glycol. In more concentrated aqueous solutions, oligomers and polymers that are mainly polyoxy methylene glycols are formed and may predominate. Methanol and other substances (e.g. various amine derivatives) are usually added to the solutions as stabilizers, in order to reduce intrinsic polymerization [37]..

Formaldehyde is marketed in solid form as its cyclic trimer, trioxane $((CH_2O)_3)$, and its polymer, paraformaldehyde, with 8–100 units of formaldehyde [4, 38].
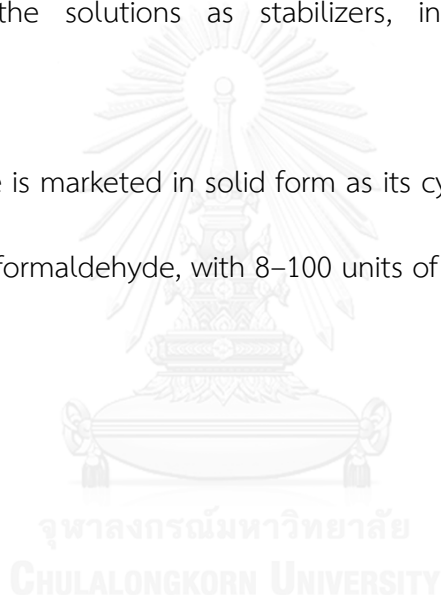
Table 2. 1 Chemical and physical properties of formaldehyde

Properties	Information
Description	Colorless gas
Molecular formula	CH_2O
Molecular weight	30.03 g/mol
Speciic gravity	0.815 at −20°C/4°C
Melting point	−92°C
Boiling point	−19.5°C
Log K_{ow}	0.35
Water solubility	400 g/L at 25°C
Vapor pressure	3,890 mm Hg at 25°C
Vapor density relative to air	1.067
Dissodation constant (pKa)	13.27 at 25°C
Flashpoint	300° C
Explosive limits	7% - 73%
Solubility	soluble in water, alcohol, either and other polar solvents
Odor threshold	0.05-0.5 ppm
Metabolites	formic acid
Conversion factor	1 ppm in air = 1.24 mg/m^3 at 25° C

❖ **Production**

Formaldehyde has been produced commercially since 1889 by the catalytic oxidation of methanol. Various specific methods were used in the past, but only two are widely used currently: the silver catalyst process and the metal oxide catalyst process.

The silver catalyst process is conducted in one of two ways: (i) partial oxidation and de-hydrogenation with air in the presence of silver crystals, steam and excess methanol at 680–720°C and at atmospheric pressure (also called the BASF process; methanol conversion, 97–98%); and (ii) partial oxidation and dehydrogenation with air in the presence of crystalline silver or silver gauze, steam and excess methanol at 600–650°C (primary conversion of methanol, 77–87%); the conversion is completed by distilling the product and recycling the unreacted methanol. Carbon monoxide, carbon dioxide, methyl formate and formic acid are by products.

In the metal oxide (Formox) process, methanol is oxidized with excess air in the presence of a modified iron molybdenum vanadium oxide catalyst at 250–400°C and atmospheric pressure (methanol conversion, 98–99%). By-products are carbon monoxide, dimethyl ether and small amounts of carbon dioxide and formic acid [38, 39].

❖ Use

The most extensive use of formaldehyde is in the production of resins with urea, phenol and melamine, and of polyacetal resins. Formaldehyde-based resins are used as adhesives and impregnating resins in the manufacture of particle-board, plywood, furniture and other wood products; for the production of curable moulding materials (appliances, electric controls, telephones, wiring services); and as raw materials for surface coatings and controlled release nitrogen fertilizers. They are also

used in the textile, leather, rubber and cement industries. Further uses are as binders for foundry sand, stone wool and glass wool mats in insulating materials, abrasive paper and brake linings [38, 39].

Formaldehyde itself is used to preserve and disinfect, for example, human and veterinary drugs and biological materials (viral vaccines contain 0.05% formalin as an inactivating agent), to disinfect hospital wards and to preserve and embalm biological specimens.

Formaldehyde and medications that contain formaldehyde are also used in dentistry [40]. Formaldehyde is used as an antimicrobial agent in many cosmetics products, including soaps, shampoos, hair preparations, deodorants, lotions, make up, mouthwashes and nail products. Formaldehyde is also used directly to inhibit corrosion, in mirror finishing and electro plating, in the electro deposition of printed circuits and in the development of photographic films[38].

❖ **Histopathology and disinfection in hospitals**

Formalin is commonly used to preserve tissue samples in histopathology laboratories. Concentrations of formaldehyde are sometimes high, e.g. during tissue disposal, preparation of formalin and changing of tissue processor solutions (Belanger and Kilburn, 1981). The usual mean concentration during exposure is approximately 0.6 mg/m^3.

Levels of formaldehyde were measured in 10 histology laboratories using area samplers for 1–4 h for a study of neurobehavioral and respiratory symptoms.

Concentrations of formaldehyde in areas where tissue specimens were prepared and sampled were 0.25–2.3 mg/m^3 [41]. In two studies in Israel, pathology staff were divided into two groups: those who had low exposure (mean, 0.5 mg/m^3), which included laboratory assistants and technicians, and those who had high exposure (mean, 2.8 mg/m^3), which included physicians and hospital orderlies, based on 15 min samples[42].

❖ **Embalming and anatomy laboratories**

Formaldehyde is used as a tissue preservative and disinfectant in embalming fluids. Some parts of bodies that are to be embalmed are also cauterized and sealed with a hardening compound that contains paraformaldehyde powder. The concentration of formaldehyde in the air during embalming depends on its content in the embalming fluid, the type of body, ventilation and work practices; mean levels are approximately 1 ppm. Embalming of a normal intact body usually takes approximately 1 h. Disinfectant sprays are occasionally used, and these may release small amounts of solvent, such as isopropanol [43] . Methanol is used as a stabilizer in embalming fluids, and concentrations of 0.5–22 ppm have been measured during embalming. Low levels of phenol have also been detected in embalming rooms [44].

Levels of formaldehyde measured in anatomy laboratories in China for a cytogenetic study averaged 0.51 mg/m^3 over a 3-h period; the peak occurred while cadavers were being dissected [45]. A cross-sectional study on the cytogenetic effects of formaldehyde on anatomy students in China found personal exposures of 2.92

mg/m^3 [46]. The concentration of formaldehyde in the air in pathology and anatomy laboratories in Turkey did not exceed 2 and 4 mg/m^3, respectively [no other information available], when measured in a study of cytogenetic responses [47].

Health effects of formaldehyde

The International Agency for Research on Cancer (IARC) is internationally recognised for evaluation of compounds, complex mixtures and industrial processes with a carcinogenic potential (hazard identification). Frequently, the IARC classification is mentioned in the documentation used for setting an OEL. Also, the first ACGIH classification from 1992 of carcinogenicity was linked as closely as possible with the IARC classification. Additional modifications introduced in 1998 were partly influenced by the MAK classification [48].

Formaldehyde is regulated by OSHA as a carcinogen (Standard 1910.1048) and is listed in IARC Group 2A ("probable human carcinogen") in the IARC Monographs on the Evaluation of Carcinogenic Risks to Humans. This substance is classified as a "select carcinogen" under the criteria of the OSHA Laboratory Standard [49].

❖ **Acute toxicity**

Formaldehyde is known to induce acute poisoning, cause irritation, as well as other immunotoxic effects. In 1998, 17 employees of a pharmaceutical company who continuously inhaled formaldehyde vapors showed symptoms of irritated eyes, tearing, sneezing, coughing, chest congestion, fever, heartburn, lethargy, and loss of appetite. As a result of the poisoning, some even experienced vomiting, abdominal

pain, and nodal tachycardia [50]. In 2000, a 32 year old male experienced abdominal pain, bloody stool, hematemesis, and a high serum alanine-amino transferase (ALT) level of 105 µg/L after imbibing 300 mL of formaldehyde contaminated water [51]. Another 26 year old male died of extreme abdominal pain, cyanosis, and gastric mucosal degeneration just two hours after drinking a cup of water containing concentrated formaldehyde [52]. Sixty students at a middle school discovered they were poisoned 30 min after consuming formaldehyde preserved Pacific saury fish. They all reported symptoms of nausea, while 83% experienced vomiting, and 50% experienced dizziness [53].

❖ **Chronic toxicity**

Long-term exposure to elevated levels of formaldehyde in the occupational setting has resulted in upper and lower airway irritation; eye irritation; and degenerative, inflammatory and hyperplastic changes of the nasal mucosa in humans [54]. Chronic exposure to formaldehyde can result in symptoms of neurasthenia, which include headaches, dizziness, sleep disorders, and memory loss. Many reports indicate that chronic exposure to formaldehyde increases the chances of headache and dizziness by 30–60% [55]. Recently, the association between exposure to chemicals including formaldehyde and amyotrophic lateral sclerosis (ALS) mortality was assessed in a prospective cohort study investigating 1 million participants in the American Cancer Society's Cancer Prevention Study II [56]. The study from Armon (2003) [57] shown that apart from age and gender, cigarette smoking is perhaps the

most consistent non-genetic risk factor for ALS Formaldehyde is a by-product of cigarette smoke, which may account for up to 10–25% of indoor air formaldehyde exposure [58].

Guideline for reducing exposure to formaldehyde in indoor air

USEPA suggests step to reduce formaldehyde in indoor air as follows: increase ventilation for reducing exposure to formaldehyde and other indoor pollutants by bringing more outdoor air into indoor air. Open windows and doors whenever possible. Extra ventilation during warm weather can be remove greater amounts of formaldehyde than ventilation when temperatures are cool. Consider installing a whole house fan or a fresh-air ventilation system. Increasing ventilation by opening doors and windows and installing an exhaust fans. This can be helpful for newer homes that are tightly insulated [59].

Maintain moderate temperature and humidity levels and provide adequate ventilation can reduce exposure to formaldehyde. The rate at which formaldehyde is released is accelerated by heat and may also depend somewhat on the humidity level. Therefore, the use of dehumidifiers and air conditioning to control humidity and to maintain a moderate temperature can help reduce formaldehyde emissions. Drain and clean dehumidifier collection trays frequently so that they do not become a breeding ground for microorganisms. Increasing the rate of ventilation in home will also help in reducing formaldehyde levels [59].

2.3 VOCs treatment methods

Several methods have been designed to reduce VOCs in indoor air.

Some of them are as follows:

- Activated carbon adsorption

- Thermal oxidation

- Biological method

- Photocatalytic oxidation process

The common methods are as follows:

Activated carbon

Activated carbon is commonly used as an adsorbent of gases and vapors because of its large surface area and large pore volumes. Molecules, when adsorbed on the carbon surface, are strongly held by adsorption forces that are enhanced in small pores [60]. Absorption and adsorption methods do not really degrade the pollutants but instead transfer them into a secondary solid waste stream [61] The disposal or treatment of adsorbent after using induces consequently problem of solid waste treatment.

Thermal oxidation

Thermal oxidation systems, also known as fume incinerators, are not simple flares or after burners. The modern thermal oxidizer is designed to accomplish from 95% to 99% destruction of virtually all VOCs. These systems can be designed to

handle a capacity of 1,000 to 500,000 cfm (cubic feet per minute) and VOC concentration ranges from 100 to 2,000 ppm. Nominal residence time ranges from 0.5 to 1.0 s. Available with thermal energy recovery options to reduce operating costs, thermal oxidizers are very popular [62, 63]. Thermal oxidation systems are combust VOCs at temperatures of 1,300–1,800°F. Actual operating temperature is a function of the type and concentration of material in the vent stream and the desired Destruction and Removal Efficiency (DRE). Compounds that are difficult to combust or that are present at low inlet concentrations will require greater heat input and retention time in the combustion zone to ensure that the desired DRE is accomplished. Operation with insufficient VOC content to supply thermal input requirements necessitates the use of external fuel sources.

Biological method

The bio-filtration process, which was originally developed for the odour abatement of waste gases, has proven recently to be an effective and inexpensive method for the removal of VOCs produced during various industrial activities [64]. This technique is based on the ability of micro-organisms (generally bacteria) to convert, under aerobic conditions, organic pollutants to water, carbon dioxide and bio-mass. Bio-filter success is dependent upon the degradability of the contaminants [65, 66]. Anthropogenic compounds may contain complex bonding structures that resist microbial enzymatic reactions. Oxidation may not be complete, and may even form degradation by-products more toxic than the original compounds [67].

Moreover, a relatively long acclimation period is needed to use microorganisms in biological system [68, 69].

Photocatalytic oxidation process

The last one is the photocatalytic oxidation process that requires a light source and a photocatalyst. As a treatment method, this process has more advantages among others in terms of treatment efficiency and economy [70]. Photocatalytic oxidation has attracted considerable attention for degrading organics, given its generation of powerful and non-selective oxidant active species [71, 72] Furthermore, numbers of VOCs with small and large molecular weights can be successfully photocatalytically degraded under various conditions, indicating photocatalytic technology's excellent and non-selective ability to remove VOCs [73-75]. Therefore, this research focuses on heterogeneous photocatalysis as an advanced oxidation technology for degradation of VOCs in gas phase.

2.3.1 Photocatalytic oxidation process

The process of photocatalysis is emerging as a promising technology in environmental control through the oxidation and degradation of organic contaminants. It has been widely established as an alternative physical chemical process for the elimination of toxic, hazardous organic substances and metals in waste water, drinking water, and air [76]. The process involves a semi-conductor activated by ultraviolet (UV) radiations being used as a catalyst to destroy organic contaminants. There are two types of reaction in the photocatalytic process [77].

Homogenous photocatalysis

These reactions occur in a single phase, for example the reaction between a β-ketone and HOCl as written in equation (2.1) [78].

$$R - (C=O) - CH_4 + HOCl \longrightarrow CHCl_3 + \text{Products (2.1)}$$
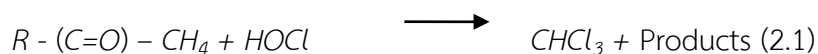
Heterogeneous Photocatalysis

In recent years, interest has been focused on the use of semiconductor materials as photocatalysts for the removal of organic and inorganic species from aqueous or gas phases. This method has been used in environmental protection due to its ability to oxidize the organic and inorganic substrates [79].

In heterogeneous photocatalysis two or more phases are used in the photo-catalytic reaction. A light source with semiconductor material is used to initiate the photoreaction. The catalysts can carry out substrate oxidations and reductions simultaneously. UV light of long wavelengths and possibly even sunlight [78].

2.3.2 Principles of photocatalytic oxidation

The process of photocatalysis is emerging as a promising technology in environmental control through the oxidation and degradation of organic contaminants. It has been widely established as an alternative physical chemical process for the elimination of toxic, hazardous organic substances and metals in waste water, drinking water, and air. The process involves a semiconductor activated by ultraviolet (UV) radiations being used as a catalyst to destroy organic contaminants.

The air purification technique of PCO commonly uses nano-semiconductor catalysts and ultraviolet (UV) light to convert organic compounds in indoor air into benign and odorless constituents water vapor (H_2O) and carbon dioxide (CO_2)[80]. Photocatalytic degradation of environmental contaminants has been studied in the past two or three decades. In early 1970s, Fujishima and Honda, 1972 discovered the phenomenon of photo induced water cleavage on TiO_2 electrodes. Formenti et al., (1971)[18] developed a differential dynamic fixed-bed reactor to study the heterogeneous photo-catalysis for partial oxidation of paraffin. However, earlier work mainly dealt with the treatment of wastewater. Using PCO to remove trace level organic contaminants in air has recently received considerable attention since this technology can be potentially applied for air purification in office buildings, factories, homes, cars, and spacecraft.

Most PCO reactors use nano titania (TiO_2) as the catalyst that is activated by UV light. Fig. 2.1 shows the schematic of the UV-PCO process of VOCs using TiO_2 as the catalyst. An electron in an electron-filled valence band (VB) is excited by photo-irradiation to a vacant conduction band (CB), leaving a positive hole in the VB. These electrons and positive holes drive reduction and oxidation reactions, respectively, of compounds adsorbed on the surface of a photocatalyst [81].
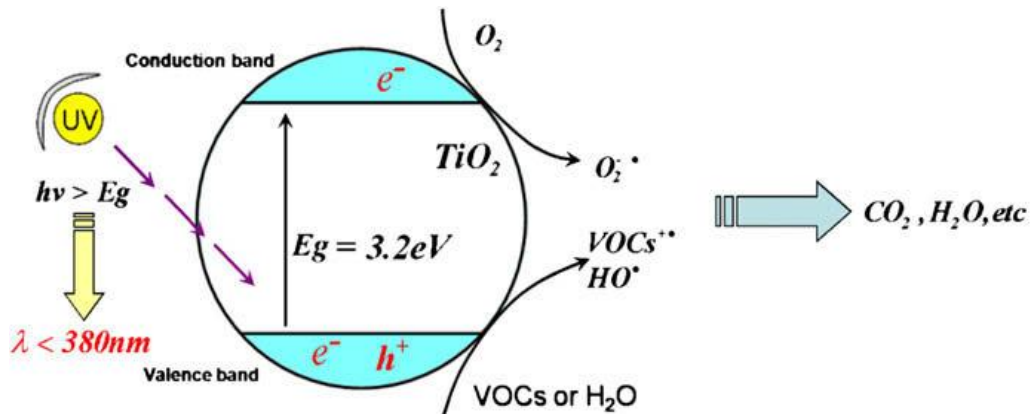
Fig. 2. 1 Schematic of TiO2 UV photocatalytic oxidation process of VOCs[82]

$$TiO_2 \xrightarrow{h\nu} e_{cb}^-(TiO_2) + h_{vb}^+(TiO_2) \qquad (1)$$
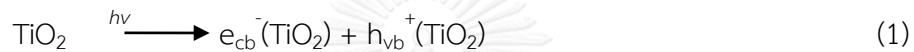
where *cb* is the conduction band and *vb* is the valence band.

In the above reaction, h_{vb}^+ and e_{cb}^- are powerful oxidizing and reducing

agents, respectively. The oxidation and reduction reactions can be expressed as:

Oxidation reaction: $\quad h_{vb}^+ + OH^- \longrightarrow OH^* \qquad (2)$

Reduction reaction: $\quad e_{cb}^- + O_{2ads} \longrightarrow O_{2ads}^- \qquad (3)$

When organic compounds are chemically transformed by a PCO device, it is

the hydroxyl radical (OH*), derived from the oxidation of adsorbed water or adsorbed

OH^-, that is the dominant oxidant. Its net reaction with a VOC can be expressed as

equation (3-4) [82].

$$OH^* + VOC + O_2 \longrightarrow nCO_2 + mH_2O \qquad (4)$$

The process of PCO has several advantages [83]: (1) Generally Recognized As

Safe (GRAS): the common photocatalyst is anatase TiO_2, an n-type semiconductor

oxide which is also a component of some toothpastes and pharmaceutical

suspensions; (2) mild oxidant: kinetic studies demonstrated that the ultimate source of oxygen during oxidation is molecular oxygen, a far milder oxidant than hydrogen peroxide or ozone; (3) ambient temperature: photocatalysis appears to be active at room temperature; (4) general: while several mechanistic pathways for oxidation have been proposed, the dominant view is that the hydroxyl radical (or some other equally strong oxidant) is photo-generated on the titanium surface; the potency of this oxidant is responsible for the titanium's broad activity toward various contaminants (such as aromatics, alkanets, olefins, halogenated hydrocarbons, and odor compounds).

❖ **Adsorption process**

Adsorption is a process that occurs when a gas or liquid solute accumulates on the surface of a solid or a liquid (adsorbent) forming a molecular or atomic film known as the adsorbate. It is different from *absorption* in which a substance diffuses into a liquid or solid to form a solution. The term *sorption* encompasses both processes, while *desorption* is the reverse process. Adsorption is operative in most natural physical, biological, and chemical systems and is widely used in industrial applications such as activated charcoal, synthetic resins, and water purification [84].

❖ **Irradiation process**

As the essential component to the PCO reaction process, the UV light (wavelength and intensity) has a great effect on the PCO reaction rate. Theoretically, the UV light with wavelength less than <380 nm could activate titanium

photocatalysts. Although some researchers developed a visible light responsive photo-catalyst, the germicidal lamp (UV-C, 254 nm) and fluorescent black-light lamp (300–370 nm) were more commonly used [85]. It was reported that more intermediates were produced using a germicidal source than using a black light. In addition, an ultraviolet light-emitting diode (UV-LED), long lasting, robust, small in size and high in efficiency, was also applied as the UV source during PCO oxidation (Chen et al., 2005). The commercial UV-LED used in PCO has a typical output of   12–20 mW [84, 86]. However, its peak wavelength is normally greater than 360 nm and requires a specific responsive photo-catalyst for its application.

The reaction rate increased with increasing light intensity, as the heterogeneous photo-catalytic reaction depends on the irradiation of TiO_2 surface by UV light to produce electron/hole pairs, even though part of them recombined [87]. Egerton and King (1979) [88] found that the influence of UV intensity on the reaction rate can be separated into two regimes: a first-order regime where the electron-hole pairs are consumed more rapidly by chemical reactions than by recombination, and a half-order regime where the recombination rate dominates.

❖ **Mechanism of generation of oxidation species**

The whole PCO process may be divided into six elemental mass transfer processes occurring in series, namely 1) advection (VOCs and precursor species are carried by airflows), 2) external diffusion of reagent species through the boundary layer (BL) surrounding the catalyst or catalyst pellet, 3) adsorption onto the catalyst

surface, 4) chemical reaction at the catalyst surface, 5) desorption of reaction product(s), and 6) boundary layer diffusion of product(s) to the main flow (Fig. 2.2) **[89]**.

1 : Advection   4 : Surface reactions
2 : BL diffusion of reagent species   5 : Desorption of reaction product(s)
3 : Adsorption of reagent species   6 : BL Diffusion of reaction product(s)
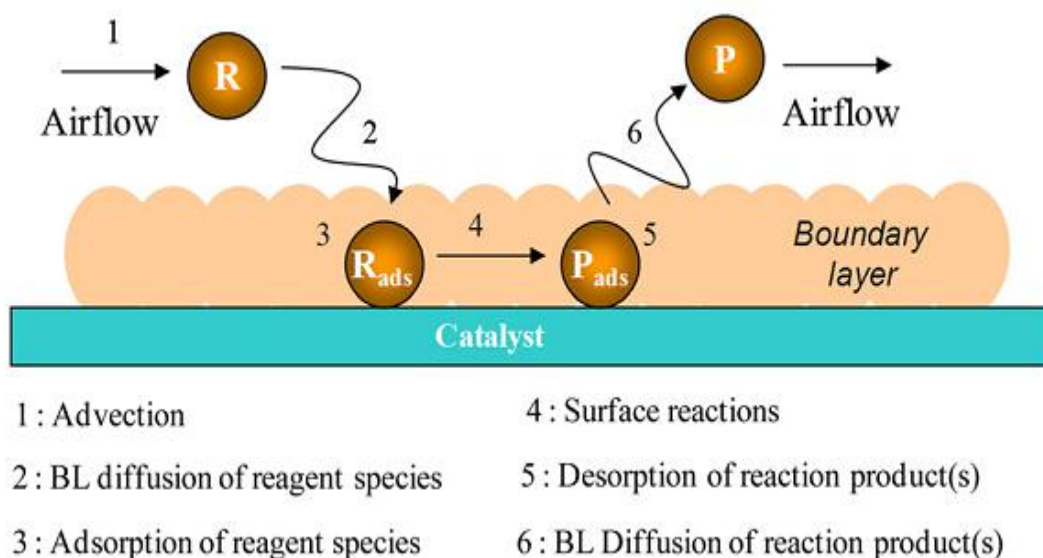
Fig. 2. 2 Elemental mass transfer processes involved in the photocatalytic oxidation of VOCs with a non-porous catalyst [89]

In the PCO reaction, pure or doped metal oxide semiconductors (e.g., TiO_2, ZnO, CdS, Fe (III)-doped TiO_2) are commonly used as the photocatalyst [20]:

There are two routes through which OH radicals can be formed. The reaction of the valence-band holes (h_{vb}^+) with either adsorbed H_2O or with the surface OH^- groups on the TiO_2 particle [90] can be written as in equations (5) and (6).

$$TiO_2 (h_{vb}^+) + H_2O_{ads} \longrightarrow TiO_2 + HO^*_{ads} + H^+ \qquad (5)$$

$$TiO_2 (h_{vb}^+) + HO^-_{ads} \longrightarrow TiO_2 + HO^*_{ads} \qquad (6)$$

In general, donor (D) molecules such as H_2O will adsorb and react with a hole in the valence band and an acceptor (A) such as dioxygen will also be adsorb and reacted with the electron in the conduction band (e_{cb}^-), according to equations (7) and (8)

$$TiO_2\ (h_{vb}^+) + D_{ads} \longrightarrow TiO_2 + D_{ads}^+ \qquad (7)$$

$$TiO_2\ (e_{cb}^-) + A_{ads} \longrightarrow TiO_2 + A_{ads}^- \qquad (8)$$
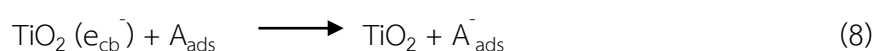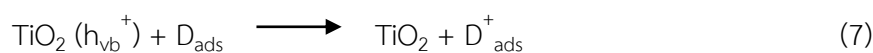
It is generally accepted that oxygen plays an important role in PCO process. Oxygen can trap conduction-band electrons to form superoxide ion (O_2^{*-}) as in equation (9). These superoxide ions can react with hydrogen ions (formed by splitting water) forming HO_2^* [78].

$$TiO_2\ (e_{cb}^-) + O_{2ads} + H^+ \longrightarrow O_2^{*-} + H^+ \longrightarrow TiO_2 + HO_2^* \quad (9)$$

H_2O_2 could be formed from HO_2^* via reactions (3-10) [78].

$$TiO_2\ (e_{cb}^-) + HO_2^* + H^+ \longrightarrow H_2O_2 \qquad (10)$$
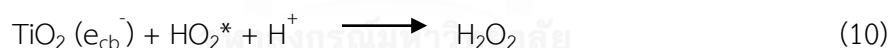
Cleavage of H_2O_2 by one of the reactions (11, 12, and 13) may yield an OH radical [78].

$$H_2O_2 + h\nu \longrightarrow 2HO^* \qquad (11)$$

$$H_2O_2 + O_2^* \longrightarrow HO^* + O_2 + HO^- \qquad (12)$$

$$H_2O_2 + TiO_2\ (e_{cb}^-) \longrightarrow HO^* + HO^- + TiO_2 \qquad (13)$$
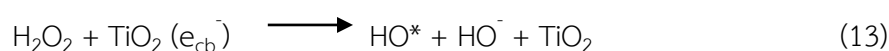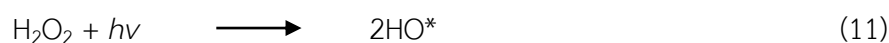
Photoreduction, photooxidation, and adsorption occur on or near the particle surface. The illumination of semiconductor particles such as TiO_2 generates e_{cb}^- and h_{vb}^+ as described previously. A competitive reaction occurs between water,

oxygen, organic molecules, and trace metals which may be present in the system [91].

A possible mechanism of TiO_2 photocatalytic oxidation of HCHO was purposed by Yang et al., (2000) [92] as follows:

$$TiO_2 \xrightarrow{hv} e_{cb}^- + h_{vb}^+ \tag{14}$$

$$h_{vb}^+ + OH^- \longrightarrow OH^* \quad or \quad h_{vb}^+ + H_2O$$

$$\longrightarrow OH^* + H^+ \tag{15}$$

$$e_{cb}^- + O_{2\,(ads)} \longrightarrow O_2^- \tag{16}$$

$$HCOH + OH^* \longrightarrow COH^* + H_2O \tag{17}$$

$$COH^* + OH^* \longrightarrow HCOOH \tag{18}$$

$$COH^* + O_2^{*-} \longrightarrow HCO_3^- \xrightarrow{-H^+} HCOOOH \xrightarrow{+H^+} \xrightarrow{HCHO} HCOOH \tag{19}$$

$$HCOOH \xrightarrow{h_{vb}^+} COO \xrightarrow{OH^*} H_2O + {}^*CO_2^- \quad or$$

$$HCOO^- \xrightarrow{[O],\; OH^*,\, h_{vb}^+} H^+ + CO_2^{*-} \tag{20}$$

$$CO_2^{*-} \longrightarrow CO_2 \tag{21}$$
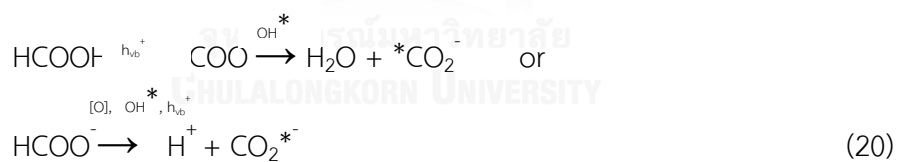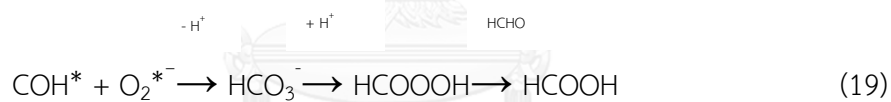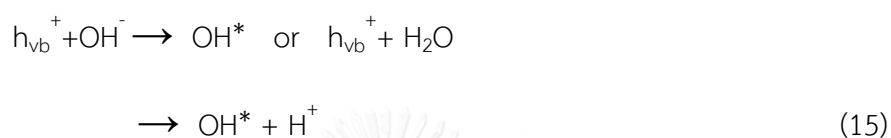
2.3.3 Appilcation of PCO

❖ Anti-Bacterial Application

Photocatalytic oxidation can destroy bacteria during this process and has been found to be more effective than any other antibacterial agents. This is due to the fact that the photocatalytic oxidation process continuously destroys the bacterial cells that are spreading in the air and covering on the surfaces of materials [93].

❖ Deodorizing Application

Some odor in the indoor air is occurred from VOCs. Therefore, the hydroxyl radicals from PCO accelerate the breakdown of VOCs by destroying the molecular bonds. This reaction will promote the breakdown of organic gases to form a single molecule that is not harmful to humans. Some of the examples of odor molecules are tobacco, formaldehyde, nitrogen dioxide, urine, fecal, gasoline, and many other hydro carbon molecules found in the atmosphere [94]. Moreover, photocatalytic oxidation with the high oxidizing effect can remove smoke, pollen, bacteria, viruses and harmful gases as well as seize the free bacteria in the air by 99.9% [95].

❖ Air Purifying Application

The PCO can be applied for the reduction or elimination of polluted compounds in the air such as the volatile organic compounds which arise from various construction materials. Also, high photocatalytic oxidation activity can be

used to protect lamp-houses and walls in tunneling, as well as to prevent tent fabrics 14 and cloth materials from becoming dark from impurities in the air [96].

❖ Self-Cleaning Application

Most of the exterior walls of buildings become soiled because of automotive exhaust fumes which contain oily components. When building materials are coated with a photocatalyst, such as a protective film of titanium, it provides the self-cleaning building by becoming antistatic, super oxidative, and hydrophilic. The hydrocarbons from automotive exhaust are oxidized causing the dust collected on the walls to wash away by rainfall or manual washing. The advantage is the building exterior is easily cleaned at any time [97].

❖ Water Purification Application

Photocatalytic oxidation process can oxidize organic pollutants into non-toxic substances, such as CO_2 and water. Moreover, the photocatalytic oxidation can disinfect certain bacteria. PCO is very effective not only for removing further hazardous organic compounds but also for destroying a variety of microorganisms in the secondary wastewater treatment[98]..

2.3.4 Photocatalytic materials

A wide range of semiconductors may be used for photocatalysis, such as TiO_2, ZnO, MgO, WO_3, Fe_2O_3, and CdS. The ideal photocatalyst should process have the following properties (1) photoactivity, (2) biological and chemical inertness, (3)

stability toward photo-corrosion, (4) suitability towards visible or near UV light, (5) low cost, and (6) lack of toxicity.

TiO_2 is known to have excellent pigmentary properties, high ultraviolet absorption, and high stability. These allow it to be used in different applications, such as electro ceramics, glass, and in the photocatalytic degradation of chemicals in water and air. It has been used in the form of a suspension or a thin film in water treatment [99].

Titanium dioxide has different crystalline forms, the most common being anatase and rutile. The third crystalline form is bookie, which is uncommon and unstable. Anatase is the most stable form by 8-12 KJ mol,$^{-1}$ and can be converted to rutile by heating to temperatures of ~ 700 °C [100]. The density of rutile is greater at 4.26 g/ml while anatase has a density of 3.9 g/ml. In the photocatalysis applications, it is known that anatase is more efficient than rutile, having a more open structure.

TiO_2 has a large band gap of 3.2 eV. According to the activation energy, it was limited by the radiation wavelength that was equal to or below the UV light spectrum. There are three characteristics of TiO_2 crystalline forms, i.e. anatase, rutile, and brookite as shown in Figure 2.3. The anatase form has been found to have the most favorable characteristics for PCO, as it appears to be the most active and consistent, the irradiation with light of 385 nm or less will generate complete electron hole pairs in anatase structure of TiO_2 [101].
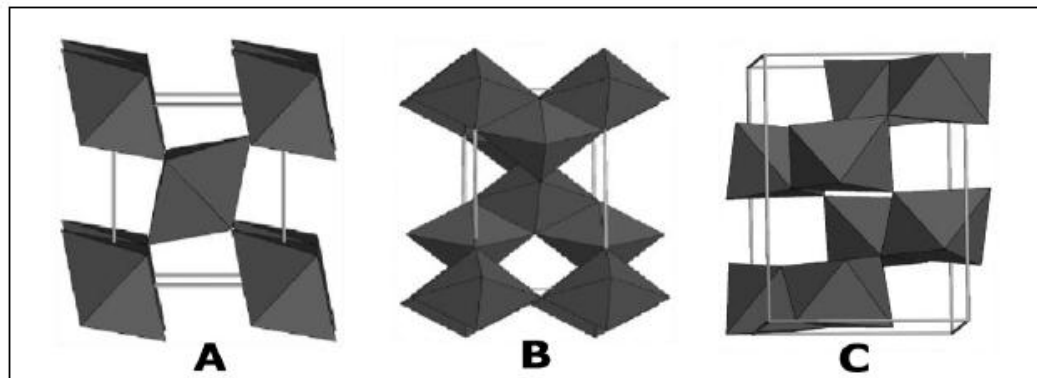
Fig. 2. 3 Crystalline Structures of TiO_2

2.4 Silkworm silk

Silk is a natural biopolymer produced by silkworms during the formation of their cocoon. There are two main types of the silkworms, mulberry silk or *Bombyx mori* which is also called cultivated silk, and wild silk such as *Samia Cynthia ricini* or *A.pernyi*. Cultivated silk are fine, almost white and soft filaments with luster. The world silk production consists of nearly 80-85% of cultivated silks. While wild silks are coarser, more irregular and brownish in appearance, they are never as white as the cultivated silk filament. Thai silk is one of the mulberry silkworm (*Bombyx mori)* silks but it differs somewhat in the appearance. It is yellower in colour, the filaments are coarser, and it has more silk gum. The process of remove sericin is known as degumminig. The silk fiber can be divided from silkworm into 2 types that are [102].

1. **Mulberry silk** (*Bombyx mori*) is produced by cultivated silkworm. The cultivated silkworm is fed with mulberry leaves.

2. **Wild silk** is produced by wild silkworm .This type often referred as Tussah silk .The wild silkworm is fed with oak leaves.

The wild silkworm is hard to culture and the silk fibers obtained from wild silkworm are coarser, more irregular, and brownish in appearances. While the silk fibers obtained from cultivated silkworm are fine, almost white (when degummed), and soft fiber with lusture. Moreover, wild silkworm' fiber has more silk gum (e.g. up to 38%) than *Bombyx mori (B. mori)* silkworm' fiber (20-25%). From these characteristic, silk fiber produced by *B. mori* silkworm is well known and has been studied extensively in biomaterial application.

Silk consists of two natural macromolecular proteins, fibroin and sericin. Both of their molecular weights range from about 10,000 to over 300,000 Da. Fibroin is continuous protein with crystalline structure and is water-insoluble. It can be regenerated in several forms such as gel, powder, fiber, or membrane.

The domesticated silkworm (*B. mori*) silk fibroin fibers are about 10–25 mm in diameter and consist of two proteins: a light chain (_26 kDa) and heavy chain (_390 kDa) which are present in a 1:1 ratio and linked by a single disulfide bond. These proteins are coated with a family of hydrophilic proteins called sericins (20–310 kDa) [103]. The disulfide linkage between the Cys-c20 (20th residue from the carboxyl terminus) of the heavy chain and Cys-172 of the light chain holds the fibroin together

and a 25 kDa glycoprotein, named P25, is noncovalently linked to these proteins [104].

Silk fibroin is purified from sericins by boiling silk cocoons in an alkaline solution (Fig. 2.4 and Fig. 2.5). Twenty-five to thirty percent of the silk cocoon mass is sericin, which is removed during the de-gumming process
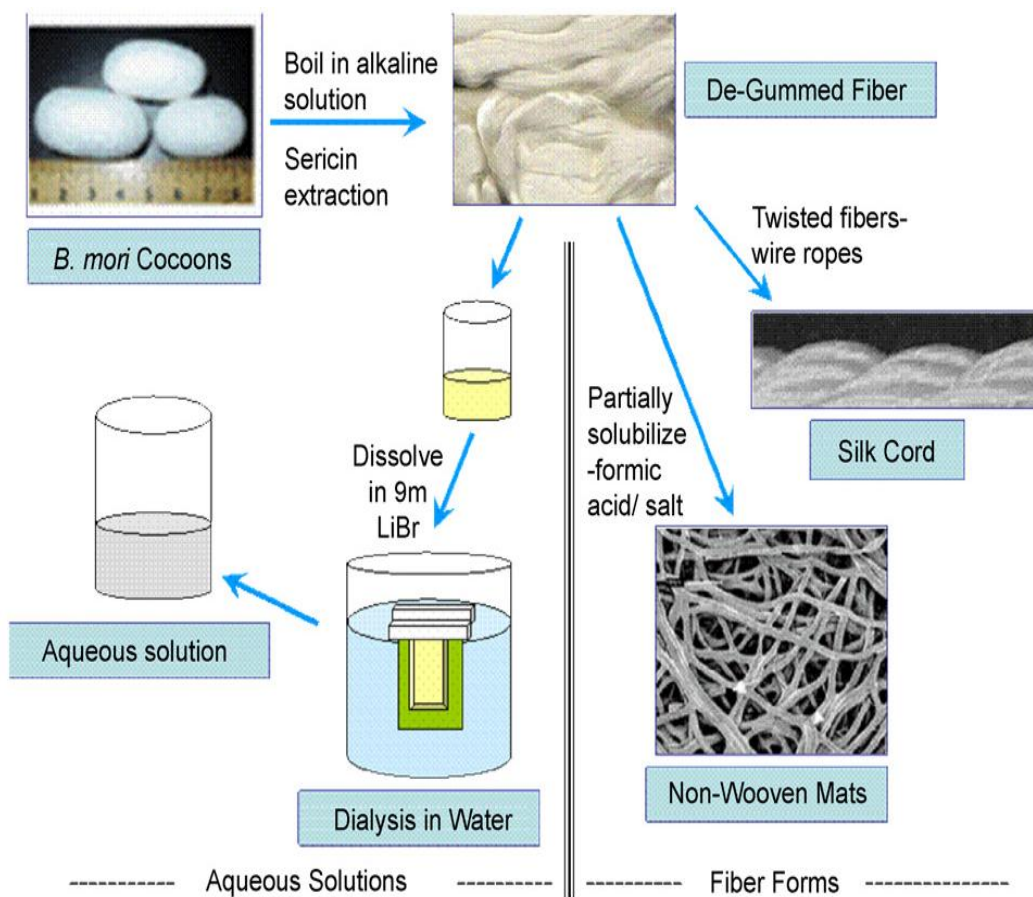
Fig. 2. 4 Silk fibroin is purified from sericins via boiling in an alkaline solution
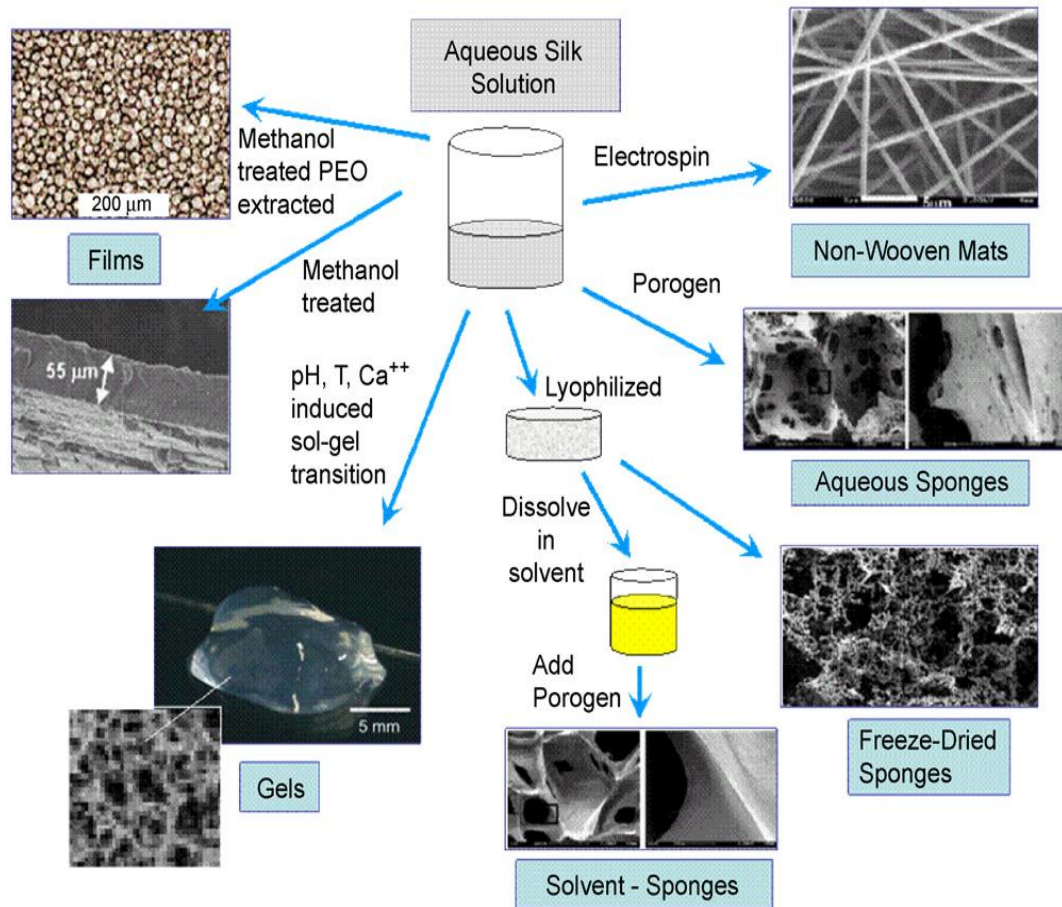
Fig. 2. 5 Processing of silk morphologies from aqueous silk fibroin solution into non-woven silk fibers; aqueous- and solvent-based porous sponges; hydrogels and films

.

Fibroin is one of the candidate materials for biomedical application because of its various characteristic such as good biocompatibility, good oxygen and water vapor permeability, and minimal inflammatory reaction. Additionally, fibroin has been used in cosmetic, medical material for human health, and food additive.

Serisin, or silk gum is a globular protein, an amorphous structure, water soluble glue and it also has some impurities such as waxes, fats, and pigments. Serisin constitutes 25-30% of silk protein and it envelops the fibroin fiber with continuing sticky layer and that provide the cohesion of the cocoon by gluing silk threads together. Removal of sericin from the silk fibroin is achieved by the process call degumming. When subjected to the degumming process, physically, chemically, or enzymologically, the sericin protein is degraded into polypeptide. The sericin peptide has excellent moisture absorption and releases a lot of biological activities such as antioxidant, anti-cancer activities and can be applied to degradable biomaterials. Furethermore, sericin is also used as a coating material for natural and artificial fibers which can prevent abrasive skin injuries[102].

2.4.1 *Bombyx mori* silk fibroin structure

The amino acid composition of silk fibroin from *B. mori* consists primarily of glycine (Gly) (43%), alanine (Ala) (30%) and serine (Ser) (12%) [105]. The heavy chain consists of 12 domains that form the crystalline regions in silk fibers, which are interspersed with primary sequence that is non-repetitive and thus forms fewer organized domains in the fibers. The crystalline domains in the fibers consist of Gly-X

repeats, with X being Ala, Ser, Threonine (Thr) and Valine (Val). The crystalline forming domains consist of an average of 381 residues (596 in size in the seventh domain to 36 in the 12th domain). Each domain consists of sub-domain hexa peptides including: GAGAGS, GAGAGY, GAGAGA or GAGYGA where G is glycine, A is alanine, S is serine and Y is tyrosine. These subdomains end with tetra peptides such as GAAS or GAGS. The less crystalline forming regions of the fibroin heavy chain, also known as linkers, are between 42 and 44 amino acid residues in length. All the linkers have an identical 25 amino acid residue (non-repetitive sequence), which is composed of charged amino acids not found in the crystalline regions [106]. The primary sequence results in a hydrophobic protein with a natural coblock polymer design. Efficient secretion of fibroin is believed to be due in part to the formation of a disulfide bond between the heavy and light fibroin chains. A naked pupa mutation in *B. mori* has been mapped to the same locus as of the light chain on the 14th chromosome. The resulting fibroin light chain does not have a disulfide bond with the fibroin heavy chain and the cocoon has less than 0.3% fibroin protein content.

Silk fibroin (SF) is a core structural protein and is coated by sericin (silk gum), a family of glue- like proteins that hold the fibroin core fibers together. The sericin is a minor component of fiber (i.e. 25% of the weight of raw silk) and it also has some purities such as waxes, fat, and pigments. Silk fibroin is a fibrous protein unlike sericin which is a globular protein. The elemental compositions in SF are listed in the Table 2.2

Table 2. 2 The composition of elements in silk fibroin [107]

Element	Percentages of element
Carbon	48-49
Hydrogen	6.40-6.51
Nitrogen	17.35-18.89
Oxygen	26.00-27.90
Sulphur	Slightly

The Silk fibroin is a semi-crystalline protein polymer that consists of beta-sheet crystals and non-crystalline amorphous regions Gosline, *et al.*, 1987[108]. Silk fibroin is a linear polypeptide whose chemical composition comprised of few types of amino acid of alternating of Glycine (Gly) residue with two thirds Alanine (Ala) and one third Serine (Ser). Fibroin has a highly repetitive primary structure that contains of the motif -Gly-Ala-Gly-Ala-Gly-Ser- along its sequence. It is composed of the alpha form consisting of crank shaft, pleated beta-sheet formation (Fibroin I) and the beta formation consisting of anti-parallel pleated beta-sheet formation (Fibroin II) [109]. The polypeptide chains (Fig. 2.6) always form anti- parallel β-sheet because this

structure has hydrogen bonds (H-bond) between peptide groups on adjacent beta

strands and these H-bonds can stabilize structure.

Sericin, on the other hand, is a mixture of proteins, which contains Ser, Thr

and Tyr. It is amorphous and soluble in water. [108]
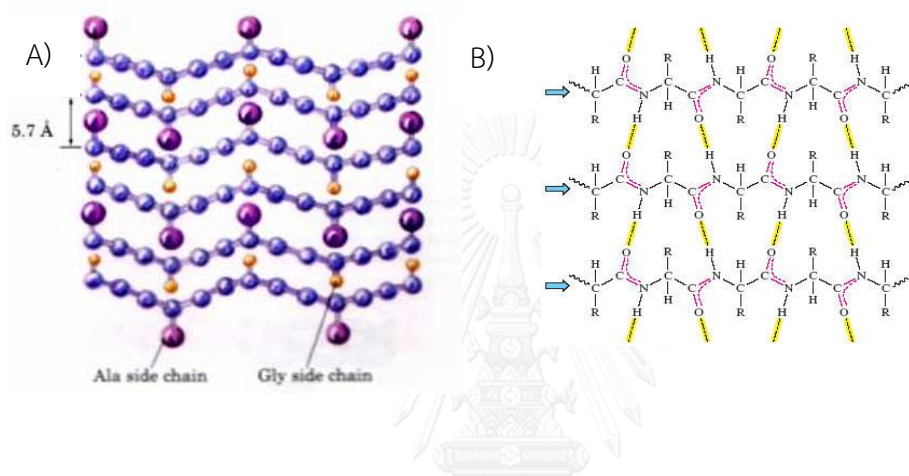
Fig. 2. 6 A) and B) The polypeptide chain of silk fibroin consists of layers antiparallel
β-sheets rich in Ala and Gly residues

Silk fibers after degumming are approximately 900-1,700 meters long and the

diameter ranges from 9 to 11 microns. Silk fibers are extremely strong. A filament of

silk is stronger than steel with an equal diameter, but the strength of the fiber is

reduced greatly when it is wet (about 80-85% of the dry strength). If silk fiber is

heated at 140° C , it will remain unaffected for a long period of time but it is

decomposed very quickly at the temperature of 175 ° C or higher. As show in Fig. 2.4,

because the silk fibers have extensive hydrogen bonding, the abundant hydrophobic

nature of their proteins, and the significant crystalline structure of the polypeptide

chains in silk fibroin, so silk fibers are insoluble in most solvents, including water, dilute acid and alkali.

Table 2. 3 The composition of amino acid in silk fiber (%) [106]

Type	Side group(R-group)	Amino acid	Proportion
Inert	-H		
	-CH$_3$	Glycine	46.39
	-CH(CH$_3$)$_2$	Alanine	44.55
	-CH$_2$CH(CH$_3$)$_2$	Valine	0.50
	-CH(CH$_3$)CH$_2$CH$_3$	Leucine	0.05
	-CH$_2$C$_6$H$_5$	Isoleucine	0.08
		Phenylalanine	0.02
Acidic	-CH$_2$COOH	Aspartate	0.17
	-CH$_2$CH$_2$COOH	Glutamate	1.03
Basic	-CH$_2$CH$_2$CH$_2$CH$_2$NH$_2$	Lysine	0.07
	-(CH$_2$)$_3$NHC(NH)NH$_2$	Arginine	0.17
Hydroxyl	-CH$_2$OH	Serine	7.17
	-CH(OH)CH$_3$	Threonine	0.15
	-CH$_2$C$_6$H$_4$OH	Tyrosine	0.14

Ring	$-CH_2$ CH_2 $-CH_2$	Proline	0.02
Sulfur	$-CH_2-S-S-CH_2-$ $-CH2CH_2-S-CH_3$	Cysteine Methionine	0.02 0.04

Table 2.3 lists the composition of amino acid in silk fibers. There are different proportions of amino acid residues in fibroin and sericin. Fibroin has higher proportions of alanine, glycine, and serine than leading to antiparallel β - pleated sheet formation. The crystalline regions of silk fibers are composed mainly of repeating unit of amino acid in silk fibroin chains. *Bombyx mori* and *A.pernyi* silk fibroin are composed mainly of -(alanine-alanine)n -sequences, while -(glycine-alanine) n -repetitions are characteristic to *Bombyx mori* silk fibroin. A small amount of cysteine and methioinine residues give a very small amount of sulfur in the fiber [102].

A number of silk polymorphs have been reported, including the glandular state prior to crystallization (silk I), the spun silk state which consists of the β-sheet secondary structure (silk II), and an air/water assembled interfacial silk (silk III, with a helical structure). The silk I structure is the water-soluble state and upon exposure to heat or physical spinning easily converts to a silk II structure. The silk I structure is

observed in vitro in aqueous conditions and converts to a β-sheet structure when exposed to methanol or potassium chloride. The β-sheet structures are asymmetrical with one side occupied with hydrogen side chains from glycine and the other occupied with the methyl side chains from the alanines that populate the hydrophobic domains. The β-sheets are arranged so that the methyl groups and hydrogen groups of opposing sheets interact to form the intersheet stacking in the crystals. Strong hydrogen bonds and van der Waals forces generate a structure that is thermodynamically stable. The inter- and intra-chain hydrogen bonds form between amino acids perpendicular to the axis of the chains and the fiber. The silk II structure excludes water and is insoluble in several solvents including mild acid and alkaline conditions [105].

The silk II structure is identified by the ^{13}C chemical shifts that are indicative of anti- parallel β-sheet, while the silk I structure gives the chemical shifts that are related with a loose helix. The two structures can undergo a conformational transition from silk depending on any factors such as solvent, temperature, or shear and tensile stresses [104]. The region of anti- parallel β-sheet is a crystal region which results in the stability and mechanical features of silk fibroin.

2.4.2 Constituent and crystal structure

❖ Constituent

Silk fibroin consists of a light (L) chain polypeptide and a heavy (H) chain polypeptide linked together via a sin-gle disulfide bond at the C-terminus of H-chain, forming a H–L complex [103]. Vepari C. et al., (2007) [110] and Inoue S. et al., (2000) [111] noted that the H–L complex also binds glycoprotein P25 in a ratio of 6:1 via hydrophobic interactions to form an elementary micellar unit. Necessarily, the formation of such a micellar unit enables the transportation of a large amount of fibroin through silk gland lumen toward the spinnerets before spinning into fibers.

Vepari C. et al., (2007)[110] and Takahashi Y. et al., (1999) [112] presented in silk fibroin material, H-chains form discrete β-sheet crystallites serving as the main structural component responsible for the superior mechanical properties, while L-chain plays little mechanical role as its size is much smaller than H-chain and besides, its sequence is also not associated with the formation of the crystalline region in silk fibroin. The β-sheet crystallites are in turn embedded in a less-ordered (i.e., semi-amorphous) matrix. In terms of amino acid composition, the H-chain comprises primarily the three simplest amino acids, i.e., glycine (G) (∼43–46%), alanine (A) (∼25–30%) and serine (S) (∼12%), whereas tyrosine (Y) (the larger amino acid with a polar side chain)

occurs at ～5%. The next most abundant amino acid in H-chain is valine (V) (～2%), and this is followed by aspartic acid (D), phenylalanine (F), glutamic acid (E), threonine (T), isoleucine (I), leucine (L), proline (P), arginine (R), lysine (K) and histidine (H), present in much smaller percentages (i.e., less than 2% each) [110].

Organizationally, the silk fibroin H-chain is a highly regular biopolymer that consists of 12 hydrophobic domains interspersed with 11 hydrophilic domains (Fig. 2.8). The hydrophobic domains contain amino acids in repetitive sequence (i.e., therefore also referred to as repetitive domains), while the hydrophilic domains contain amino acids in non-repetitive sequence (i.e., also referred to as non-repetitive domains) [113-115]

Zhou C.Z. et al., (2001) [103, 106]and Zhou C.Z. et al., (2000) [103] also found that the repetitive domains (comprising mainly glycine, alanine, serine, and also tyrosine, valine and threonine in lesser proportion) are capable of organizing themselves together into β-sheet crystallites via intramolecular or intermolecular forces including hydrogen bonds, van der Waals forces, and hydrophobic interactions, leading to the formation of highly ordered crystalline regions in silk fibroin. On the other hand, the non-repetitive domains (comprising mainly charged/acidic amino acids, e.g., glutamic acid, aspartic acid, arginine and lysine, which are not found in the repetitive domains) form non-

crystalline(semi-amorphous) region in silk fibroin [116]. Structurally, 11 out of 14 prolines in a H-chain are p resent at one each for all the 11 hydrophilic domains (also known as linkers), that serve as β -turns to allow the chain reversal and facilitate folding into a micellar structure during silk processing in vivo [103, 106]

❖ Crystal structure

The crystal structure of fibroin in silk fibers has been investigated by X-ray diffraction (XRD). The XRD patterns revealed that its molecular chains are orderly aligned along the axis of the silk fibers (Fig. 2.7). Together with chemical analysis, it was proposed that the chains are made up of glycine and alanine with occasional substitution by other amino acids. The chains are held together by strong inter-actions, discovered to be hydrogen bonds between amide linkages of the adjacent chains [117, 118]. To clarify the packing of the chains, Marsh et al. , (1955) [117] proposed a pseudo unit based on the two established principles for proteins, i.e., the planarity of the six atoms in each amide linkage, and the tendency toward maximizing the number of hydro-gen bonds during molecular arrangement. The repeats of the pseudo unit form β-sheet crystallites, that constitute β -strands with antiparallel arrangement (i.e., adjacent β -strands run in the opposite direction) rather than parallel arrangement (i.e., adjacent β -strands run in the same direction).

This is mainly because, there are shorter linear hydrogen bonds (2.76 ° A) between antiparallel β-strands as compared to longer non-linear hydrogen bonds (2.97 ° A) between parallel β-strands (i.e., a bond angle deviating by 20°from linearity) (Fig. 2.7), that can offer greater stability to the β-sheet crystallites[117, 118]
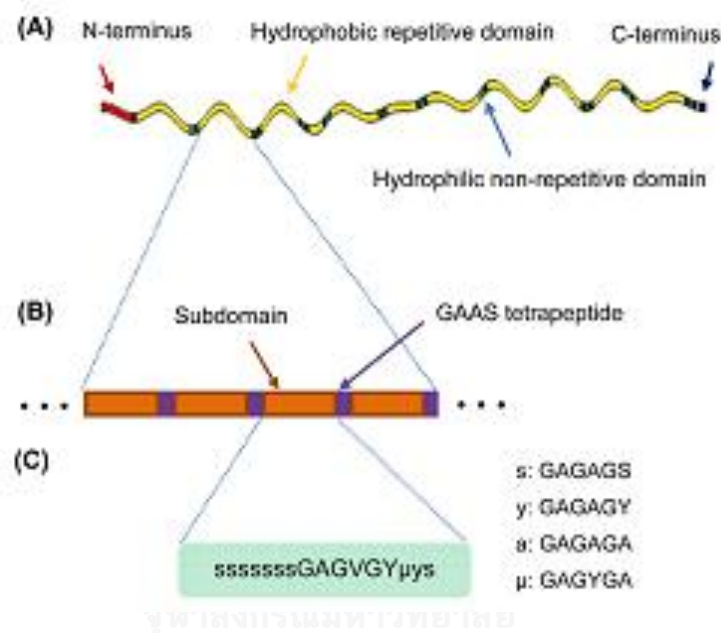
Fig. 2. 7 A) Each fibroin heavy chain (H-chain), B) Each repetitive domain consists of subdomains separated by GAAS tetrapeptides, C) Each subdomain in turn consists of different repeating units of hexapeptides [106, 115]

Garrett R.H. et al., (2007) [119] and Marsh R. et al., (1995)[117] also presented on the pseudo unit, the side chains of adjacent β-strands are similar within each face in a β-sheet. In such a polar arrangement, the front face of the β-sheet projects only the glycine side chains (β H) (i.e., glycine face), while the back face of the same sheet projects only the alanine side

chains (–CH$_3$) (i.e., alanine face), as illustrated in Fig. 2.9. The β -sheets are stacked into a β -sheet crystal-lite in such a way that similar faces of adjacent β -sheets are facing each other (i.e., front-to-front and back-to-back). Important clues that led to the revelation of such front-to-front and back-to-back stacking of β -sheets were the intersheet distances, generated after feeding X-ray equatorial reflections data into Patterson function – a convolution function, commonly used to solve crystal structures. The calculated intersheet distances between two glycine faces (front-to-front) or two alanine faces (back-to-back) are 3.7 and 5.5˚A, respectively. According to the pseudo unit, the β -sheet crystallite adopts an orthorhombic crystal lattice with unit cell dimensions a = 9.20, b = 9.40, and c = 6.97˚A where a is the direction along the stacking of β -sheets, b is the direction in a β -sheet perpendicular to the strand axis, and c is the direction along the strand axis [117].

Takahashi Y. et al., (1999) [112]; Kaplan D.L. et al., (1998)[105] investigated the subsequent yield that similar results. Up till today, the polar-antiparallel arrangement in the β –sheet crystallites is still widely accepted. XRD is a straightforward method for analyzing single crystalline materials, but has limitations in revealing the crystal structure of polycrystalline silk fibroin. The earlier efforts only extracted very general illustration of its molecular

organization, lacking atomic resolution details. Even if fibroin can be recrystallized into single crystal state in solution, the data obtained might not be fully representative of that in its fibrous state [120]. in the β-sheet crystallite was still unascertained only until recent confirmation from NMR that the crystalline region could also accommodate serine and tyrosine residues [120, 121]. Experimentally, a glycylalanyl peptide containing serine (S) and tyrosine (Y) residues (i.e., AGYGAGAGAGY-GAGAGSGAASGAGAGAGAG) was successfully crystallized into the Silk II form (i.e., the stable β-sheet structure in silk fibers), as characterized by ^{13}C CP/MAS nuclear magnetic resonance (NMR) spectroscopy. However, some degree of local disorder is present in the structure, often recognized as being amorphous by XRD techniques.
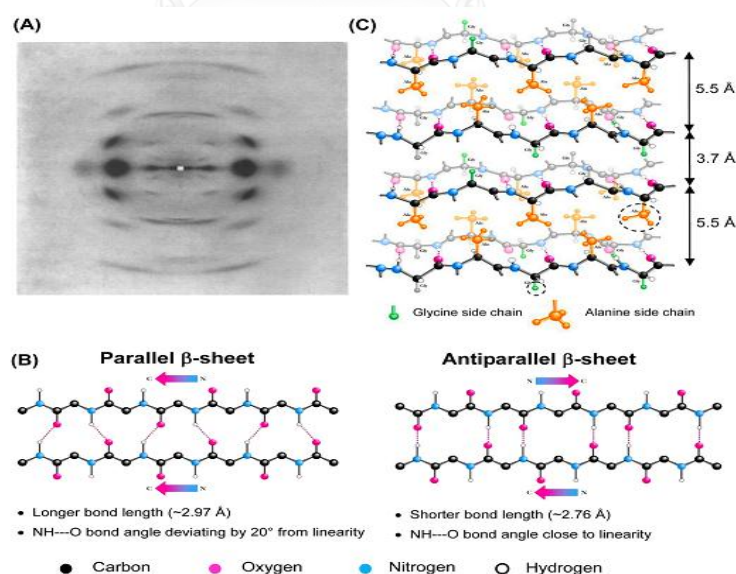
Fig. 2. 8 A) X-ray diffraction (XRD) pattern for silk fibroin fibers , B) Bond length and bond angle in parallel and antiparallel fibroin β-sheets , C) Widely accepted polar-stacking of antiparallel β-sheets [122]

2.4.3 *Bombyx mori* silk sericin

The sericin coating constitutes 25–30% of the weight of *B. mori*'s silk fibre, and helps in the formation of silk cocoon by gluing the fibres together. It is made of sericins, gum-like proteins that vary in their molecular weight between 10 and 300 kDa, and are rich in the amino acid serine. It is also thought to contain carotenoids, which are responsible for cocoon pigmentation. Sericins are known to have several extraordinary properties: they resist oxidation, are antibacterial, UV resistant, and can absorb and release moisture easily [123]. These properties are valuable in the protection of silk from microbial degradation, animal digestion, and other damaging processes. Recent studies show some surprising properties of sericin; dietary sericin has been suggested to suppress the development of colon tumours by reducing cell proliferation, and creating oxidative stress and nitric acid production. It has also been found, under certain conditions, to induce bone-like apatite deposition [124]. However, sericin is still considered an obstacle for *B. mori* silk biocompatibility, despite the coating being soluble in hot alkaline water and therefore removable. As discussed later in this review, insufficient sericin removal is still an issue in many biomedical applications.

2.4.4 Structure of silk threads

It is now clear that there is a strong connection between the structure of silk fibres and their physical (and mechanical) properties. Structural organisation from protein sequence, through protein folding to the assembly of the fibrils appears to

play a role in the toughness and elasticity of silk fibers[106]. Relating structural features and patterns to physical properties is valuable as it could contribute to the ability to control the properties of future man-made silk analogous (for example, an ability to control mechanical properties by introducing a certain structural features to the thread during spinning could be beneficial). However, an understanding the structure of silk threads is still a challenge. Below is a review of the main structural features of silkworm and spider silks, starting at the overall thread organization and going down to the protein makeup.

Most natural silk threads known to date are thought to consist of an inner silk core of polymer protein, a protein skin, and some type of coating. The core exhibits nanofibrils, with some assembled into bundles called microfibrils. Generally, the coating functions as glue, but there is some evidence that it may also act as a fungicidal or bactericidal agent. It may also have a role during the extrusion process. Micro-morphological studies show that the substructure of spider silks is very similar to that of mulberry silkworm silks. *B. mori* silk fiber has been shown to be composed of two protein-monofilaments (named brins) embedded in a gluelike sericin coating. A similar structure has been observed in other silkworms silk. The brins are fibroin filaments made up of bundles of nanofibrils, approx 5 nm in diameter, with a bundle diameter of around 100 nm. The nanofibrils are oriented parallel to the axis of the fibre, and are thought to interact strongly with each other [125]. A schematic representation of the structure of *B. mori* thread is shown in Fig. 2.9
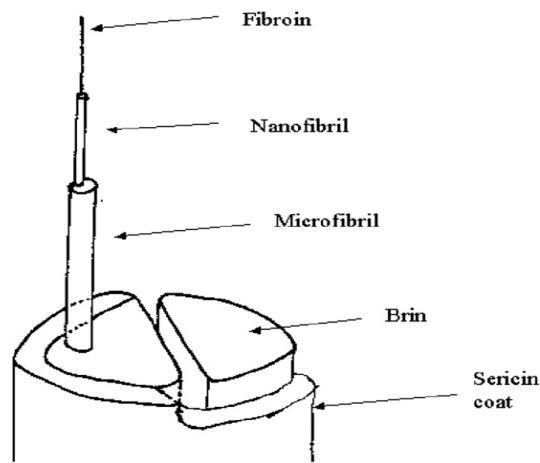
Fig. 2. 9 The structure of a raw silk filament [125]

Fig. 2.9 present the structure of raw silk filament, which contains microfibrils that are packed together to form the fibril bundle. The several fibril bundles produce a single strand of fibroin. Sericin envelops two strand of fibroin together to form a raw silk filament. Both contain elongated tubular cavities or vacuoles called canaliculi. The role of these canaliculi may be to facilitate controlled crack formation in the fibres when it is stretched or loaded. Although thread diameter varies across silk types and species, the mean width of nanofibrils appears to be independent of the fibre size, ranging 90–170 nm [126].

A comparison of mechanical properties (Table 2.4) suggests that *Bombyx mori* silk provide a remarkable combination of strength and toughness. The distinguishing features of the silk fibroin filaments following extraction of sericin are the very high strength in combination with excellent elasticity in comparison with these other

biomaterials. In additionally, these fibers display resistance to failure in compression that distinguishes them from other high performance fiber such as Kevlar.

Table 2. 4 Comparison of mechanical properties of common silks (silkworm and spider dragline) to several types of biomaterial fibers and tissues commonly used today

Material	Tensile Strength (MPa)	Modulus(GPa)	% Strain at break
B. mori silk (w/ sericin)[a]	500	5–12	19
B. mori silk (w/o sericin)[b]	610–690	15–17	4–16
B. mori silk[c]	740	10	20
Spider silk[d]	875–972	11–13	17–18
Collagene	0.9–7.4	0.0018–0.046	24–68
Collagen X-linked[f]	47–72	0.4–0.8	12–16
PLA[g]	28–50	1.2–3.0	2–6
Tendon (comprised of mainly collagen)	150	1.5	12
Bone	160	20	3
Kevlar (49 fiber)	3600	130	2.7
Synthetic Rubber	50	0.001	850

[a]*Bombyx mori* silkworm silk—determined from bave (multithread fibers naturally

produced from the silk worm coated in sericin).

[b]*Bombyx mori* silkworm silk—determined from single brins (individual fibroin filaments

following extraction of sericin).

[c]*Bombyx mori* silkworm silk—average calculated from data in Ref. Cunniff , P. M., *et al*., 1994

[d] Nephila clavipes silk produced naturally and through controlled silking.

[e] Rat-tail collagen Type I extruded fibers tested after stretching from 0% to 50%.

[f] Rat-tail collagen dehydrothermally cross-linked and tested after stretching from 0% to 50%.

[g] Polylactic acid with molecular weights ranging from 50,000 to 300,000.

Because of the impressive mechanical properties including biological properties, biocompatibility and biodegradability, the SF has been interested in various not only textile fields but also in reinforcing composites, food additive, cosmetic, and biomedical fields. Particularly, SF has been researched extensively in the biomedical fields. The applications of SF in the biomedical fields are controlled drug-delivery carrying, cell culture substrate, sutures, tissue engineering matrix, and wound dressing. The SF can be prepared as regenerated SF in various forms such as gel, powders, membranes, or fibers depending on desired application.

In 2006, Gopal, *et al*.,[127] investigated a permeability of the electrospun nanofibrous membrane with varying parameters of the membrane structure such as fiber diameter, porosity and thickness. It was reported that an electrospun Polyvinylidene fluoride nanofibers (PVDF) membrane could be used for separation of microscale particles and an application to an affinity membrane was also reported

for electrospun cellulose nanofiber having large surface area to volume ratio. The viability of developing a fibrous membrane via electrospun nanofibrous web for liquid separation and demonstrates its applicability in particulate removal. Polyvinylidene fluoride nanofibers were electrospun into membranes and characterized to relate its structural properties to membrane separation properties and performance. Characterization of these electrospun membranes revealed that they have similar properties to that of conventional microfiltration membranes. The electrospun membranes were used to separate 1, 5 and 10 μm polystyrene particles. The electrospun membranes were successful in rejecting more than 90% of the micro-particles from solution. This work opens up the avenue of exploring the use of nanofibers for more mainstream application in the separation technology as a potential membrane for pre-treatment of water prior to reverse osmosis or as pre-filters to minimize fouling and contamination prior to ultra- or nano-filtration [127].

Chen W. X. et al (2005)[128], applied silk fibroin fibers (SF) by studying Copper(II)-silk fibroin complex fibers as air-purifying materials for removing ammonia. Ammonia is one of the most common pernicious in-door gases, especially in new buildings and newly renovated houses. In addition, the concentration of ammoniais much higher in some livestock farms, lavatories, and special workshops . The most convenient and common method for removing harmful indoor gases was to install gas filters in air-conditioners, and such filters are traditionally made of activated

carbon. A new alternative method of removing ammonia with metal-silk fibroin complex fibers through a coordination displacement reaction was proposed and studied. In this research, the spring cocoon shells were degummed in a 2% (wt%) marseilles soap and 0.1% (wt%) Na_2CO_3 solution. The results show that the $Cu(O)_4$ complex is more effective than the $Cu(N)_4$ complex in term of ammonia adsorption. It is highly desirable to prepare a deodorizing material that has both high copper(II) content and a $Cu(O)_4$ complex structure. Based on study, a novel deodorizing fiber was prepared as follows: silk fibroin fibers was first treated with tannic acid (TA), then was dipped into the cuprammonia solution to obtain the $Cu(O)_4$ complex containing 8.5% (wt%) copper(II). A new deodorizing functional silk fibroin fiber was prepared by designing the coordination structure. They found that these functional fibers remove ammonia quickly, and their adsorbing capacity is very high at room temperature. Moreover, such fibers can be regenerated by heating [128].

2.5 Kinetic study

Chemical kinetics study examines the rate and mechanism by which one chemical species is converted to another. The rate is the mass or moles of a product produced or reactant consumed per unit time. Reaction kinetics gives information about the reaction rates and the mechanism by which the reactants are converted to the products. To kinetically analyze the obtained experimental data of the formaldehyde decomposition, the widely used equation for describing the mechanism of the destruction of organic compounds, the Langmuir–Hinshelwood (L-

H) was applied. The LH kinetics is the most commonly used kinetic model to explain the kinetics of the heterogeneous catalytic processes.

Formaldehyde photodegradation

The photocatalytic rate of organic contaminants over illuminated TiO_2 fitted L–H kinetics [129-131]. There is only one contaminant in this experiment, and a single-site L–H model is introduced to evaluate photocatalytic degradation rates:

$$r = -\frac{dCt}{dt} = \frac{kKCt}{1+KCo} \qquad (2.5\text{-}1)$$

where;

r is the reaction rate (ppm h^{-1})

t is the illumination time (h)

k is the apparent kinetic constant (ppm h^{-1})

K is the adsorption equilibrium constant (ppm^{-1})

Ct is the contaminant concentration at times (ppm)

If KCt is well less than 1, the reaction is a first-order reaction with a constant reaction rate coefficient. Eq.(2.5-1) can be rewritten as Eq.(2.5-2). When C_0 is small, first-order oxidation kinetics can be observed:

$$r = -\frac{dCt}{dt} = K'Ct \qquad (2.5\text{-}2)$$

$$-\frac{dCt}{Ct} = K'dt \qquad (2.5\text{-}3)$$

Where K' is the apparent first-order reaction coefficient (h^{-1})

The integrated form of Eq. (2.5-3) is

$$Ct = Co \; e^{-K't} \qquad\qquad (2.5\text{-}4)$$

By using logarithmic function, Eq.(2.5-4) can be linearly expressed as Eq.(2.5-5)

$$ln\frac{Ct}{Co} = -K't \qquad\qquad (2.5\text{-}5)$$

First order reaction depends on the concentration of only one reactant (a unimolecular reaction). k is the first order rate constant, which has units of 1/time.

[132]

CHAPTER III

METHODOLOGY

3.1 Research overview

The main objective of this study is to synthesize TiO_2-coated SF filters for indoor air formaldehyde (HCHO) removal by using the PCO process. They were degummed with sunlight soap, and were studied the characterization, physical properties, and mechanical properties. The TiO_2-coated SF fiber was studied the efficiency of formaldehyde removal by the effect of TiO_2 dosage, initial indoor air concentration, and air flow rate of air condition. This research was divided into 4 phases. Research flow chart can be illustrated in Fig. 3.1.

Phase 1: Monitoring of formaldehyde concentrations in a gross anatomy laboratory and general health survey

⬇

Phase 2: Synthesis of SF filters and study of morphological structure and physical properties of SF filters

⬇

Phase 3: Treatment of formaldehyde in a small reactor using the synthesized SF filters and commercial air filter
- ➤ Impact of initial formaldehyde concentration
- ➤ Impact of catalyst (TiO_2) dosage
- ➤ Impact of air flow rate

  Kinetics study of HCHO treatment

⬇

Phase 4: Application of the TiO_2 coated SF filters for photocatalytic oxidation (PCO) of formaldehyde in a large modeling room

⬇

Cost comparison between the SF filters and the commercial air filter

Fig. 3. 1 Flow chart of the research

3.2 Chemicals and Materials

    3.2.1 Chemicals

1) Formaldehyde (HCHO) solution analytical grade from Ajax Finechem Pty Ltd.

2) Alkalinity (Sunlight soap)

3) Poly (Ethylene-CO-Vinyl acetate) 25% by wt. Analytical grade from ALDRICH Chemistry, USA.

4) Ecoterric T80 analytical grade from Ajax Finechem Pty Ltd, Austria

5) Titanium dioxide (TiO_2) Brand Tipaque code A-220 (Anatase)

    3.2.2 Materials

    1) Commercial Filter (Polyester class Eu 2 thickness 0.5 mm, Fig. 3.2
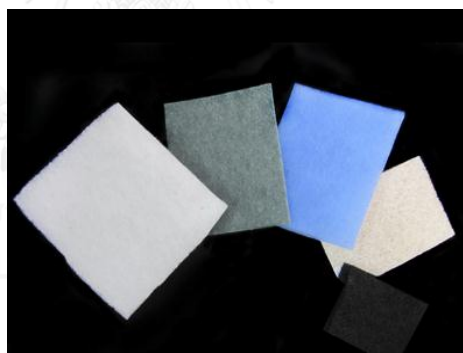
Fig. 3. 2 Commercial filters polyester class Eu 2

2) Cocoons of the *Bombyx mori* silkworm was collected from a local farm in Ubonratchatani province, Thailand.

Fig. 3. 3 Silk cocoons

3.3 Experimental and equipment

3.3.1 Monitoring of formaldehyde concentrations in a gross anatomy laboratory

Formaldehyde measurement

Gaseous formaldehyde concentrations in the gross anatomy laboratory in the Division of Anatomy, College of Medicine and Public health, Ubon Ratchathani University, Thailand, was measured using the Handheld Formaldehyde Meter (HAL-HFX205). The device was placed at the location towards the center of the room where it is approximately 1 meter away from the cadaver bed. The duration time was every 20 min from 9 am to 4 pm, three days a week during October to December 2012. This period covered the on and off school time. Three case studies of measurement were conducted as follows: 1) no practical study, 2) 2nd year medical student class, and 3) 3rd year medical student class. A sample integration

time is equal to 20 s. The calibration of the apparatus will be done with formaldehyde permeation cartridge.

Monitoring of formaldehyde concentrations in a gross anatomy laboratory was studied by using Hand-held formaldehyde meter (HAL-HFX205, USA) for the measurement of gaseous formaldehyde concentration as shown in Fig. 3.4. The HAL-HFX205 is a compact personal monitor that can provide a rapid indication of hazardous airborne formaldehyde levels. The HCHO concentration was continuously measured every 5 minutes with auto save capability in ppm unit.

Fig. 3. 4 Hand-held formaldehyde meter (HAL-HFX205, USA)

Health Questionnaire

Population and Questionnaire: The study of formaldehyde exposure was a cross-sectional health survey on the second and the third year medical students of College of Medicine and Public health, Ubon Ratchathani University, Thailand.

In questionnaire, there was a statement explained to medical students about the objective of a personal health survey. The questionnaire was designed to collect general information, information of practice anatomy laboratory, and the general health information. This process was performed during the first semester of the academic year 2012.

Data on general information, such as age, gender, birth place, present address, levels of education, were also designed to collect demographic information and to gather information on the amount of time spent in anatomy laboratory. The questions related to health information especially symptoms associated with poor respiratory health were also included. For this study the questionnaire was designed in part of information of practice anatomy laboratory and questions related to health information on potential known disease that occur of medical symptom during the year 2012.

Data Analysis

Formaldehyde concentrations data were analyzed with descriptive statistics. The difference of mean of formaldehyde concentrations in indoor air of gross anatomy laboratory were tested by using Wilcoxon Mann-Whitney method.

Furthermore the data from questionnaires were analyzed as percentage of each symptom by using SPSS for Windows.

3.3.2 Synthesis of SF filters: Pure Silk fiborin (SF) filters and TiO$_2$ coated silk fibroin (SF) filters

Preparation of *Bombyx mori* silk fibroin

Silk cocoons were dried in sunlight and then cut into small lengths. Then they were de-gummed by boiling with with 2500 ml of 0.5% (w/w) in sunlight soap solution at 90^{0}C for 60 mins and washed with distilled water. Then the fibroin was separated from silk sericin. After that, SF fiber was uniformly reformed into rectangular-shaped filters and dried at 80^{0}C for 3 hrs in a vacuum oven. Finally, the SF filters was coated with TiO$_2$ dissolved in commercial grade polyvinyl acetate (PVA) and Tween 80 solution using the paint brushing technique.

The TiO$_2$ coating process can be performed as follows: first, dissolve TiO$_2$ in 132 ml polyvinyl acetate (PVA) solution to obtain the dosages of 1.0, 2.5, 5.0, and 7.5 % w/v of PVA. Then 1.125 ml of Tween 80 was added into the solution to enhance the dissolution of TiO$_2$ in the PVA solution and the adhesion of TiO$_2$ onto the surface of the SF filters, and left them until air dried. Finally, the 56.25 ml of PVA solution was coated onto the filters using the paint brushing technique to minimize loss of TiO$_2$ from the filters.

Study of morphological structure and physical properties

The flow chart for characterization studies of TiO_2 coated SF filters as show in Fig. 3.5
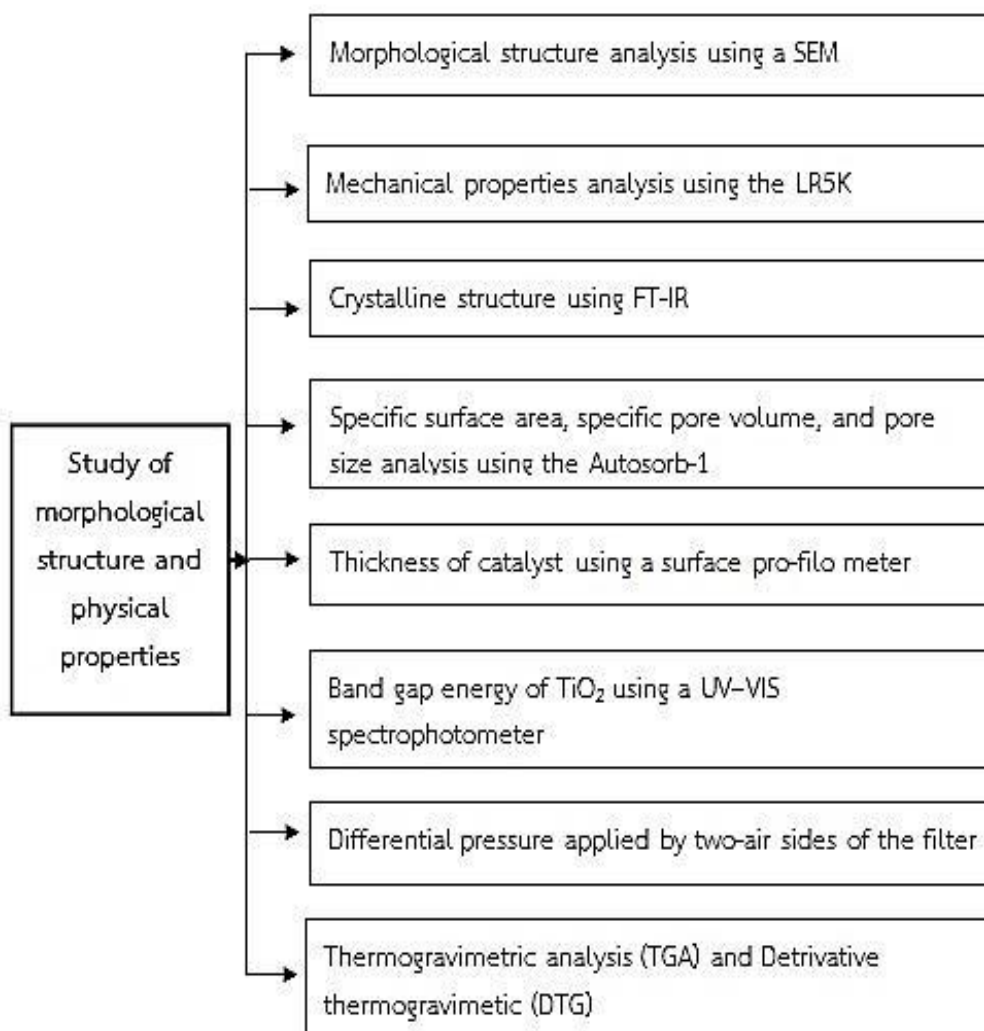
Fig. 3. 5 Diagrams of morphological structure, mechanical properties analysis

1) Study of morphological structure

Scanning electron microscope (SEM)

SEM characterization was performed by using a scanning electron microscope (SEM; JSM7000F, JEOL, U.S.A.), at an acceleration voltage of 5 kV as shown in Fig. 3.6. TiO_2 coated SF fiber samples for SEM was cryogenically fractured in liquid nitrogen and then mounted onto aluminum specimen stubs by means of double-sided adhesive tape and sputter-coated with a thin gold layer under rarefied Argon atmosphere.

Fig. 3. 6 Scanning electron microscope (SEM; JSM7000F, JEOL, U.S.A.)

2) Optical Properties of TiO$_2$-coated SF filters

UV-VIS spectrophotometer

The ban gap energy properties of the TiO$_2$ coated SF fiber were measured using the Lambda 35 for measurements on solid sample (Lambda 35, Perkin Elmer instrument, USA) equipped with an integrating sphere as shown in Fig. 3.7. All spectra was monitored in the absorbance mode and acquired under ambient conditions with using the scan ranges from 250 to 800 nm.

Fig. 3. 7 UV-VIS spectrophotometer (Lambda 35, Perkin Elmer instrument, USA)

The band gap energy of the catalyst

The ultraviolet-visible spectrum of the photo-catalysts was recorded by a UV/VIS/NIR spectrophotometer (Lambda 1050, Perkin Elmer instrument, USA) along with 150 mm sphere. TiO_2-coated SF filter sample was clamped on the external port of the integrating sphere. The scan wavelength ranges from 250 to 800 nm. All spectra was monitored in the absorbance mode and acquired under ambient conditions. The band-gap energy of the SF filters was calculated from absorbance results[133]. The optical absorbance spectra, the adsorption coefficient, and the band gap of the SF filters were evaluated.

The band gap engergy can be caculated using the following eqution;

$$\text{Band Gap Energy } (E) = h*c/\lambda \tag{3.1}$$

where: h = Planks constant = 6.626 $\times 10^{-34}$ (J.s),

c = Speed of light = 3.0 x 10^{8} (m/s)

λ = Cut off wave length (m)

and 1eV = 1.6 x10^{-19} J. [134]

3) Study of Differential Pressure (ΔP) of TiO$_2$-coated SF Filters

Differential pressure (ΔP) across the TiO$_2$-coated SF filters was conducted using a differential manometer method. The pressure exerted by a column of fluid of height h and density $\boldsymbol{\rho}$ is given by the hydrostatic pressure equation,

$$\Delta P = \boldsymbol{\rho} g \,(\Delta h) \qquad\qquad (3.2)$$

where: $\boldsymbol{\rho}$ is fluid density ($\boldsymbol{\rho}$= 998.816 kg/m^3 for water)

g is acceleration of gravity (g= 9.81 m/s^2)

3.5.4 Removal Efficiency of the TiO$_2$ coated SF Filters

For this part of experiment, three sets of experiment were conducted to investigate the effect of initial formaldehyde concentration, the effect of air flow rate, and the effect of catalyst dosage. There were three replications for each experiment.

4) Study of Mechanical properties of TiO$_2$-coated SF Filters

Mechanical testing

The mechanical properties of the TiO$_2$ coated SF fiber were measured. Static uniaxial tension tests was carried out at room temperature by using a universal material test machine LR5K (Lloyd instruments, USA) with pneumatic clamping as shown in Fig. 3.8. The load cell was set at 50 N. The crosshead speed at 100 mm/min, and the gauge length at 200 mm were used. Five specimens of each SF

fiber were measured at the same conditions. The force–displacement curves was displayed and then used to determine with stress and strain of the SF fiber.

The mechanical properties including tensile stress and strain of the synthesized TiO_2 coated SF fibers were measured. Static uni-axial tension tests was carried out at room temperature. The force-displacement curves were displayed and then used to determine the stress-strain of the SF filters.

Fig. 3. 8 Universal material test machine LR5K (Lloyd instruments, USA)

The stress and strain of the SF fiber can be calculated as follows:

$$\text{Stress } (\sigma) = \frac{F}{W} \qquad (1)$$

where σ = stress (N/mm^2)

   F = force (N)

   W = the specimen width of the SF fiber (mm)

$$\text{Strain } (\varepsilon) = \frac{L - L0}{L0} \qquad (2)$$

where ε = strain

   L_0 = the initial specimen length of the SF fiber (mm)

   L = the final specimen length of the SF fiber (mm)

5) Chemical struture of SF filters and TiO$_2$ coated SF Filters by Fourier transform infrared (FTIR) spectroscopy

FTIR analysis

The chemistry functional groups of the pure SF and TiO$_2$coated SF filters were studied by Fourier Transform Infrared (FTIR) spectroscopy in Fig 3.9 with ATR mode; the samples were measured with a PerkinElmar spectrum two apparatus. Spectra were recorded in transmittances mode using KBr pellets in the 2000-550 cm^{-1} range with 2 cm^{-1} resolution [135].

Fig. 3. 9 Fourier transform infrared (FTIR) spectroscopy

6). Thermogravimetric analysis

Thermogravimetric analysis was conducted to measure the thermal weight loss of the pure SF and SF coated TiO_2 filters was characterized using a Thermo plus TG 8120 instrument (Fig. 3.10) at a heating rate of 10 °C per minute in nitrogen atmosphere. The weight losses at different stages were analyzed [135].

Fig. 3. 10 Thermo Plus TG8120 instrument

7) Isotherm of adsorption and desorption of nitrogen gas by Barrett Joyner Halenda (BJH) nitrogen adsorption technique

Physical properties of TiO_2 coated SF fiber samples were examined using the Autosorb-1(AS1Win Version 1.50) as shown in Fig. 3.10. Nitrogen gas was utilized as an adsorbate gas. The sample was degassed by setting the desired temperature at 60 ℃. The saturated vapor pressure of the adsorbate (P_0) is 760 mmHg. The BJH method was applied for specific surface area, specific pore volume, and pore size analysis. The BJH method was applied for a specific surface area, specific pore volume, and pore size analysis [31].

Fig. 3. 11 Autosorb-1(AS1Win Version 1.50)

3.3.3 Treatment of formaldehyde in a small reactor using the synthesized SF filters and commercial filter

Fig. 3.12 shows the schematic of the small reactor. As seen from the figure, a mixing fan was installed to ensure an adequate mixing of HCHO in the small reactor. Removal efficiency of HCHO concentration using the TiO_2-coated SF filters was tested with the dimensions of 40 cm × 45cm × 50cm. Two small fans were installed in the reactor to ensure adequate mixing of formaldehyde in the reactor. Gaseous formaldehyde in the room was pumped through the SF filters held by an air filter holder using the personal pump. Formaldehyde concentration was continuously measured every 5 min. for 3 hrs with the HCHO meter (HAL-HFX205). There were two replications for each experiment. Formaldehyde source was placed in the small reactor and allowed to reach equilibrium.

1. A small fan
2. HCHO meter
   (HAL-HFX205)
3. Air flow direction
4. TiO_2 coated SF filter
5. UV lamp
6. Aerosol personal
   pump
7 source of
   formaldehyde (HCHO)
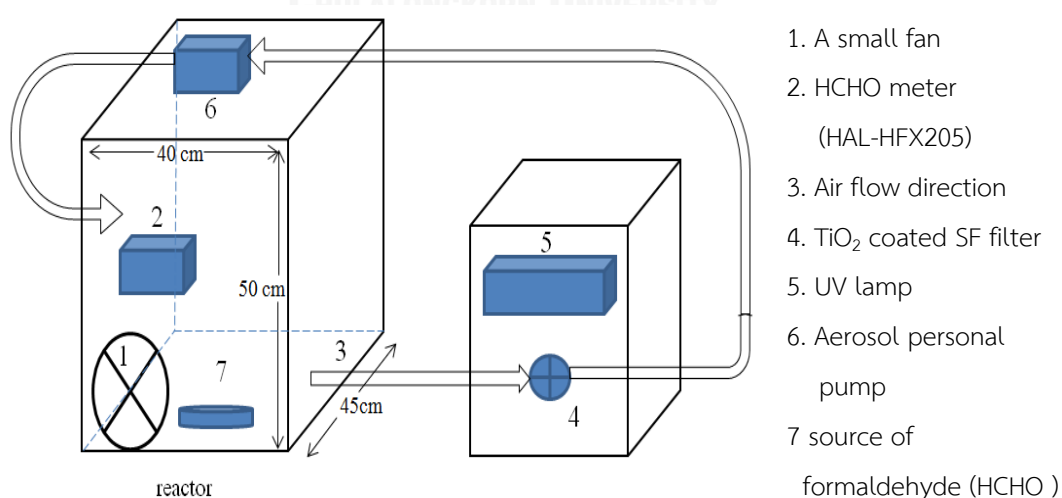
Fig. 3. 12 Schematic diagram of the small reactor

1) Impact of initial formaldehyde concentration

For this set of experiment, Initial concentration of HCHO at 2.5 ± 0.50 ppm, 5.0± 0.50 ppm, 7.5 ± 0.50 ppm, and 10 ± 0.50 ppm were used to study HCHO treatment via photocatalytic oxidation process of the TiO_2 coated SF filters. Two small fans were used to allow well mixing of indoor air. Gaseous formaldehyde concentration in small reactor was measured using the Handheld Formaldehyde Meter (HAL-HFX205) until the steady state was reach. The steady state formaldehyde concentration was reported as an initial concentration. Then the formaldehyde concentration was continuously measured every 5 minutes until it reaches steady state.

2) Impact of catalyst (TiO_2) dosage

For this set of experiment, four different amounts of TiO_2 was used to investigate the effect of catalyst dosage. Catalyst dosage was varied as 2.5%, 5.0%, 7.5%, and 10.0% wt.TiO_2/vol. sol. The optimal initial formaldehyde concentration from sections 1) of impact of initial formaldehyde concentration was set constantly.

3) Impact of air flow rate

This set of experiment was conducted in the similar manner as described above in section 1) tree different of air flow rate was varied from 3, 4, and 5 L/min. The optimal initial concentration obtained from section 1) while the catalyst dosage was kept constant at the same amount as in section 2) of impact of catalyst (TiO_2) dosage was used for this set.

Small fan

In this study, the small fans (220V) were used to ensure the well mix of HCHO in the small reactor as shown in Fig. 3.13.

Fig. 3. 13 Small fan

Aerosol personal pump

The aerosol personal pump was used to pump the HCHO into the small reactor. Air flow rate through personal pump can be controlled in this work, flow rate of air was varied at 3, 4, and 5 L/min as shown in Fig. 3.14

Fig. 3. 14 Aerosol personal pump

3.3.4 Application of the TiO$_2$ coated SF filters for photocatalytic oxidation (PCO) of formaldehyde in a large modeling room

1) The modeling room

For this phase, three sets of experiment were conducted to study the effects of initial concentration of HCHO, catalyst dosage, and air flow rate on the removal of HCHO concentration using synthesized SF filters.

The efficiency for HCHO removal in large modeling room was studied. Removal efficiency of the TiO$_2$-coated SF filters was tested in a closed modeling room with the dimensions of 1.20 m × 1.20 m × 1.85 m as shown in Fig.3.11. The temperature and relative humidity were continuously monitored by the Humidity and temperature data logger (HT 10). For all sets of experiment, temperature and

relative humidity ranged from 25-30 °C and 65-70 %, respectively. The TiO$_2$-coated

SF filter was constructed with the commercial air purifier equipped with two UV-C

lamps. The modified air purifier was then placed inside the modeling room (Fig.3.13).

Formaldehyde source was placed in the middle of the modeling room and allowed

to reach equilibrium. A mixing electrical fan was installed in the room to ensure

adequate mixing of formaldehyde in the room. Gaseous formaldehyde in the room

was sucked through the air purifier at an air flow rate of 84.40 ft^3/min. Formaldehyde

concentration was continuously measured every 5 min. for 8 hrs .

Fig. 3. 15 Schematic diagram of the reactor
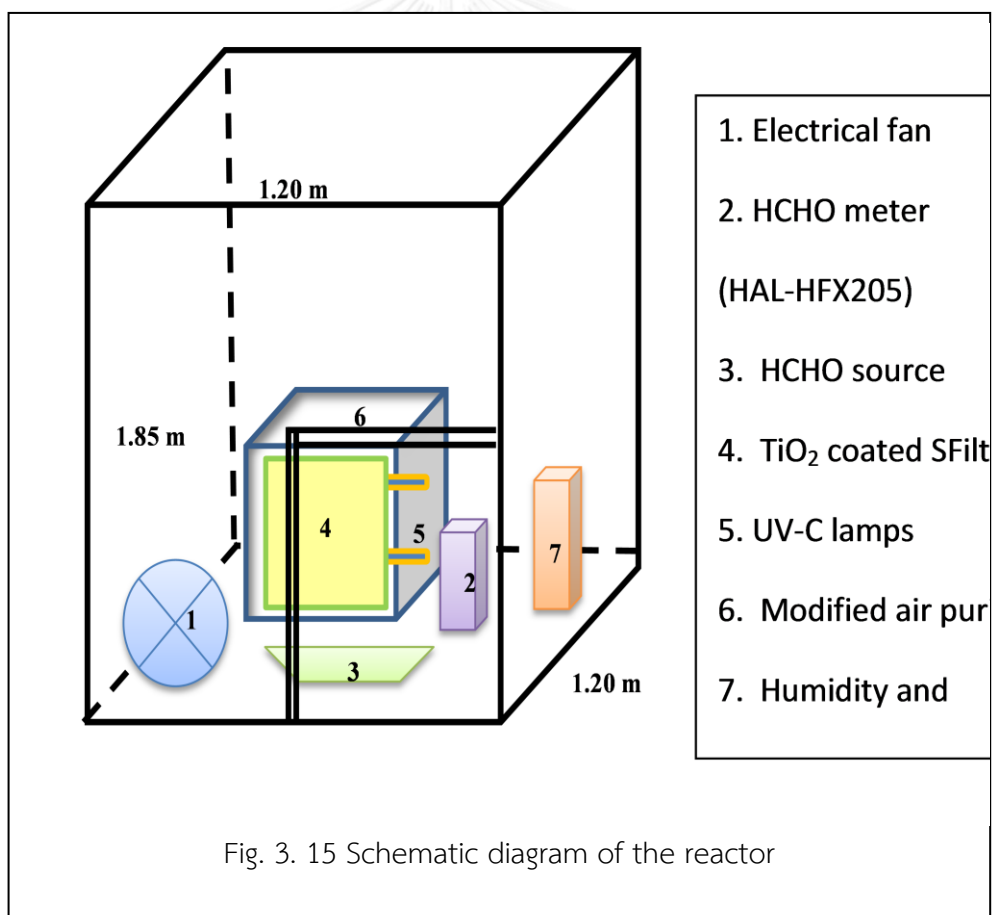
2) Modified commercial air cleaner

The modified commercial air cleaner (HATARI model HA-1244) in Fig 3.14 was installed in a large modeling room. It was designed to be able to operation at high performance continuously. The commercial air purifier was equipped with two UV-C lamps and included with the TiO_2 coated SF filer. Air flow rate was fixed at 84.40 ft^3/min.

Fig. 3. 16 The modified commercial air cleaner (HATARI model HA-1244)

Calculation of HCHO removal efficiency

To estimate the removal efficiency of HCHO in indoor air using TiO_2 coated SF

filters in this study, the following equation was used:

Formaldehyde (HCHO) removal efficiency (%)

$$\%RE = \frac{Co - C}{Co} \; x \; 100 \qquad (3.6)$$

where;   % RE is precent removal efficiency

C_0 is initial HCHO concentration (mg/m^3 or ppm)

C is final HCHO concentration (mg/m^3 or ppm)

3.4 Cost comparison between the SF filters and the commercial air filter

The last past of the study is to compare the cost of a commercial air filter

and synthesized of TiO_2 coated SF filters. Cost of synthesised SF filter was estimated

as explained in Appendix C. Cost of typical commercial air filter (Polyester class Eu 2)

was compared with synthesized SF filter.

CHAPTER IV

RESULTS AND DISCUSSION

4.1 Monitoring of Formaldehyde Concentrations in A Gross Anatomy Laboratory and General Health Survey

Gaseous formaldehyde (HCHO) concentrations in the gross anatomy laboratory (GAL) at the Division of Anatomy, College of Medicine and Public health, Ubon Ratchathani University, Thailand, were measured by the Handheld Formaldehyde Meter (HAL-HFX205). The duration time was every 20 min from 9 am to 4 pm, three days a week during October to December 2012. This period covered the on and off school time. Total area of the GAL is approximately 161.6 m^2 as shown in Fig 4.1. The GAL consists of eighteen tables of the cadavers. Table no. 1-14 are equipped with the exhausted pipes. While table no. 15 and the rest are not equipped with the exhausted pipes. Two air conditioners are installed in the room as labeled no. 1. Inside the room there are two ventilating fans as labeled no. 2, one electrical fan as labeled no. 3, six lavatories as labeled no. 4, and fifty two windows as shown in Fig. 4.1.
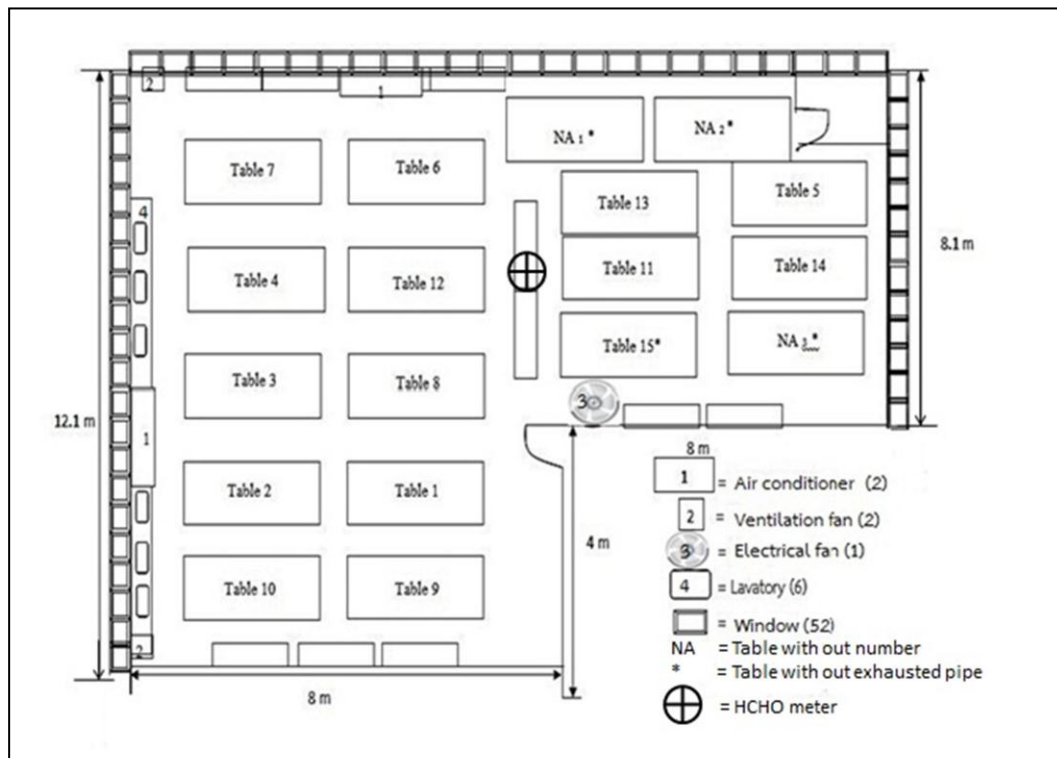
Fig. 4. 1Schematic diagram of the gross anatomy laboratory

Formaldehyde concentrations in the gross anatomy laboratory were measured under three case studies 1) no practical activity 2) the laboratory practice for the 2nd year medical student class 3) the laboratory practice for the 3rd year medical student class. The average formaldehyde concentrations were 1.580 ± 0.284 ppm, $\geq 15.66 \pm 0.000$ ppm, and 2.160 ± 0.386 ppm for the first, second, and third cases, respectively. Number of data samplings for each case is presented in Table 4.1. The average formaldehyde concentration for the second case was statistically significant higher than that of the third case (p-value = 0.001). For the second case,

the autopsy study was done for the whole cadaver whereas for the third case, the study was done for only head and brain section. Moreover, the cadavers used to study for the third case were kept in the laboratory longer than those of the second case. Thus formaldehyde concentration was likely to be lower due to the evaporation. However, formaldehyde concentrations in the room were relative high as compare to other works (IARC, 2006). These high concentrations may be caused by poor ventilation in the room. Since all the windows were kept closed for most of the time and there are only two small ventilating fans installed in the room. Moreover the laboratory room is located in basement therefore good air exchange could hardly be obtained.

Table 4. 1 Means and Standard Deviations of Gaseous Formaldehyde Concentrations of Three Case Studies (n = data collection of air sampling)

Case study (n)	Formaldehyde	
	Concentration, Mean ± SD (ppm)	p-value
No practical activity (8)	1.580 ± 0.284	
2nd year medical student class (21)	≥15.66 ± 0.000*	
3rd year medical student class (21)	2.160 ± 0.386	0.001

Note.

* Upper limit formaldehyde concentration of the Hand-held Formaldehyde Meter (HAL-HFX205) = 15.66 ppm,

General Information

Totally, there were forty people who answered the general health questionnaires (GHQ). Results from the GHQ reveal that most of the volunteers were women (65.0 %). Among these, twenty three persons (57.5 %) are at the age of under 19 years. Ninety five percent of these people were born in the place out of town. Most of them (92.5 %) stay in the dormitory. Half of them are the second year medical students while the rest are the third year medical students. The more details from the GHQ are displayed in Table 4.2. Moreover, the study showed that information of the period and frequency of each individual spending in the anatomy laboratory. Results found that 90% of the group (40 students) spending their time in anatomy laboratory less than 2 years. Results on frequency indicated that 87.5 % of the group was practiced in anatomy laboratory less than 3 day per week and 57.5 % spending less than 4 hours per day in anatomy laboratory. Table 3 displays health information of the sampling group. A symptom of allergies inducing from dust, mold spores, and animal feathers was mainly found (35%) among the sampling group. In 2012, five medical symptoms have been diagnosed and cured among the sampling group including irregular heart beat; throat irritation, cough and sore throat, phlegm, eye irritation, headache, and dizziness as 65.0%, 62.5 %, 45.0 %, 30.0 %, and 25.0 %, respectively.

Table 4. 2 General Information Practice Anatomy Laboratory

General information	Amount	Percent (%)
1. Age		
under 19 year old	23	57.5
20 - 25 year old	17	42.5
over 26 year old	0	0.0
2. Gender		
Male	14	35.0
Female	26	65.0
4. Birth place		
Bangkok	2	5.0
Out of town	38	95.0
5. Present address		
Flat	1	2.5
Private house	2	5.0
Dorm	37	92.5
6. Levels of education		
Second year medical student	20	50.0
Third year medical student	20	50.

7. How long have you been working in

the anatomy laboratory?

under 2 year	36	90.0
among 3 - 4 year	4	10.0

8. How many hours a day for working in

anatomy laboratory?

under 4 hours per day	23	57.5
among 5 - 8 hours per day	17	42.5

9. How many days a week working in

anatomy laboratory?

under 3 day per week	35	87.5
among 4 - 7 day per week	5	12.5

Table 4. 3 General Health Information

General information	Amount (n) (Percent (%))	
	Been a disease	Never been a disease
Have you ever had anyone of the following diseases?		
1. Have you ever had an operation on the breasts (Which is not the result of an accident).	0(0)	40 (100)
2. Heart disease	1(2.5)	39(97.5)
3. Bronchitis	1(2.5)	39(97.5)
4. Pneumonia	3(7.5)	37(92.5)
5. Pleurisy	0(0.0)	40 (100)
6. Pulmonary tuberculosis	0(0.0)	40 (100)
7. Asthma	1(2.5)	39(97.5)
8. Sinus	0(0.0)	40 (100)
9. Migraines	4(10.0)	36(90.0)
10. Dermatitis	3(7.5)	37(92.5)
11. Fever from pollen grain	3(7.5)	37(92.5)
12. Allergies from dust, mold spores,	14(35.0)	26(65.0)

animal feathers

Have you been treated a variety of

medical symptom during the year 2012.

(after studying in anatomy laboratory)

1. Throat irritation, cough, sore throat	25(62.5)	15(37.5)
2. Phlegm	18(45.0)	22(55.0)
3. Eye irritation	12(30.0)	28(70.0)
4. Skin irritation	9(22.5)	31(77.5)
5. Nasal Irritation, shortness of Breath	7(17.5)	33(82.5)
6. Asthma, breathing difficulty	3(7.5)	37(92.5)
7. Headache, dizziness	10(25.0)	30(75.0)
8. Diarrhea, severe abdominal pain	8(20.0)	32(80.0)
9. Nausea and vomiting	4(10.0)	36(90.0)
10.Chest pain	2(5.0)	38(95.0)
11. Irregular heart beat	26(65.0)	13(32.5)

Gaseous formaldehyde concentrations in the gross anatomy laboratory at the Division of Anatomy, College of Medicine and Public health, Ubon Ratchathani University, Thailand were measured by the Handheld Formaldehyde Meter (HAL-HFX205). For the second case of the 2nd year medical student class, the result showed the highest formaldehyde concentration (15.66 ppm), in which the autopsy

study was done for the whole cadaver. Whereas, for the third case, the study was done for only head and brain section. Moreover, the cadavers used to study for the third case were kept in the laboratory longer than those of the second case. Thus formaldehyde concentration was likely to be lower due to the evaporation. These high concentrations may be caused by poor ventilation in the room. Since all the windows were kept closed for most of the time and there are only 2 small ventilating fans installed in the room. Moreover the laboratory room is located in basement therefore good air exchange could hardly be obtained. However, formaldehyde concentrations in indoor air during the period with no practical activity (1.580 ± 0.284 ppm) were lower than during the period with practical activities of 3rd year medical student class (2.160 ± 0.386 ppm). Comparing with the declaration of Ministry of Interior, the maximum formaldehyde concentrations for eight hours should not exceed 3 ppm [6].

The clinical symptoms induced by gaseous formaldehyde exposure of medical students during working in gross anatomy laboratory were analyzed. The most common clinical symptom was irregular heartbeat (65.0%). Followed by throat irritation; cough, sore throat (62.5%). The third one was phlegm (42.5%). These results agreed to several previous studies which reported that the students had throat irritation, eyes irritation, and skin irritation [136, 137]. Anyone working in gross anatomy should use deodorant and wear activated carbon mask. This is also

confirmed by Ikaharu et. al., (2003)[138] that wearing mask can decrease the clinical symptoms by gaseous formaldehyde exposure in medical students.

Formaldehyde concentrations in the gross anatomy laboratory of the three case studies as shown in Table 4.1 are relatively high as compared with levels set by the declaration of the Ministry of Interior of Thailand in 1977 which stated that formaldehyde concentrations for eight hours should not exceed 3 ppm (Ministry of Interior, 1977). The analyzed data from GHQ revealed that the sampling group had been treated for medical symptom such as irregular heartbeat, throat irritation, phlegm, eye irritation, and headache. It is anticipated that the results of the study could be used in the planning for protection of medical students, instructors, and cadaver-related workers against the toxicity of formaldehyde, the improvement of ventilation systems, and the achievement of effective formaldehyde treatment systems [139]. Medical students, instructors, and cadavers-related workers should wear personal protective devices such as activated carbon masks, goggles, and rubber gloves when working in the gross anatomy laboratory.

4.2 Synthesis of SF filters

4.2.1 Silk fiborin (SF) filters

The SF filters synthesized from the *Bombyx mori* silkworm have a yellowish color and thin sheet. They were reformed into rectangles with dimensions of 25 cm x 36 cm as shown in Fig. 4.2.

Fig. 4. 2 Silk fibroin (SF) filter

Silk fibroin filters were coated with TiO_2 at different dosages as shown in Figure. 4.3: A) 1.0% wt.TiO_2/vol. sol, B) 2.5% wt.TiO_2/vol. sol, C) 5.0% wt.TiO_2/vol. sol, and D) 7.5% wt.TiO_2/vol. sol on surface of the synthesized filters. The color of SF filters are light yellow. In order to, the color of SF filters is ivory white when increasing dosages of TiO_2 as seen in Fig. 4.4. Moreover, Fig. 4.4 shows characteristics of silk fibroin filters coated with TiO_2 over different lengths of time. UV irradiation

changed color of silk fibroin filters at long length (336 hr) to intense yellow color as compared to those of SF filters at other lengths.

4.2.2 TiO$_2$-coated silk fibroin (SF) filters
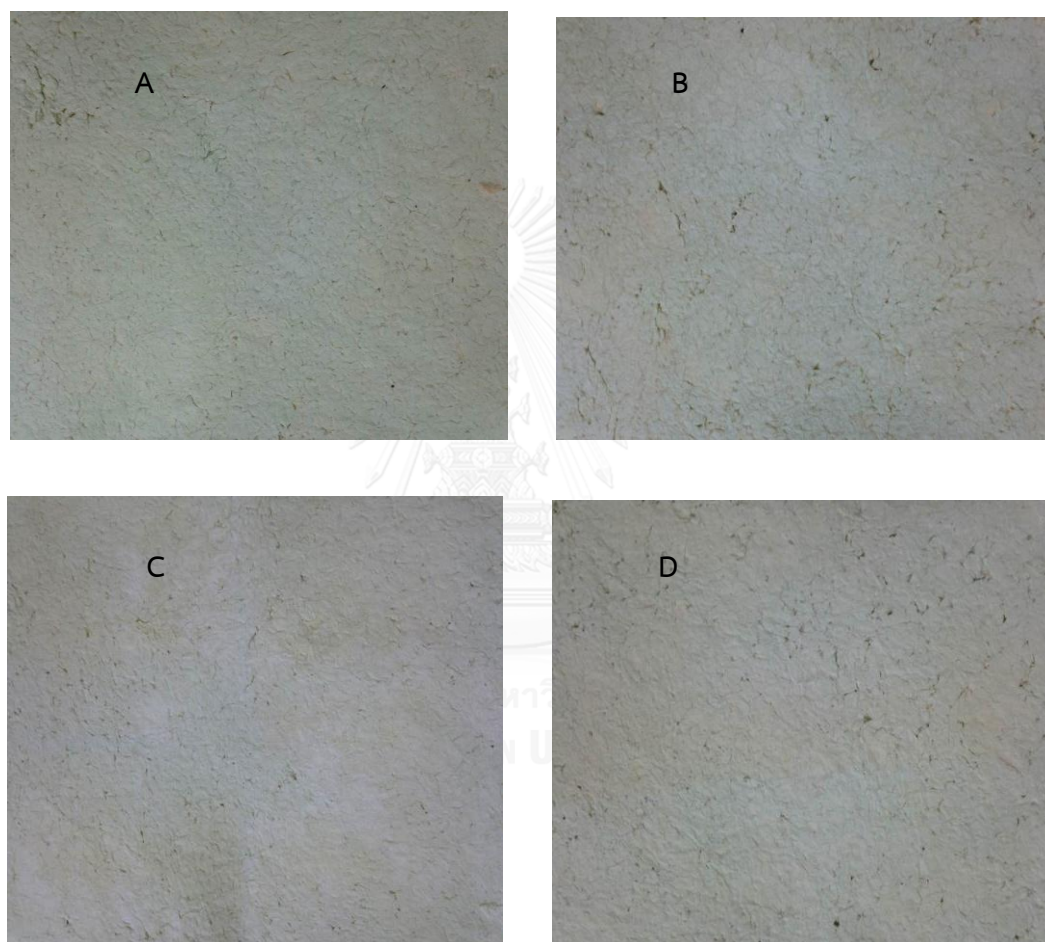
Fig. 4. 3 Silk fibroin filter coated with TiO$_2$ at different dosage before treatment of A) 1.0% wt.TiO$_2$/vol.sol, B) 2.5% wt.TiO$_2$/vol.sol, C) 5.0% wt.TiO$_2$/vol.sol, and D) 7.5% wt.TiO$_2$/vol.sol
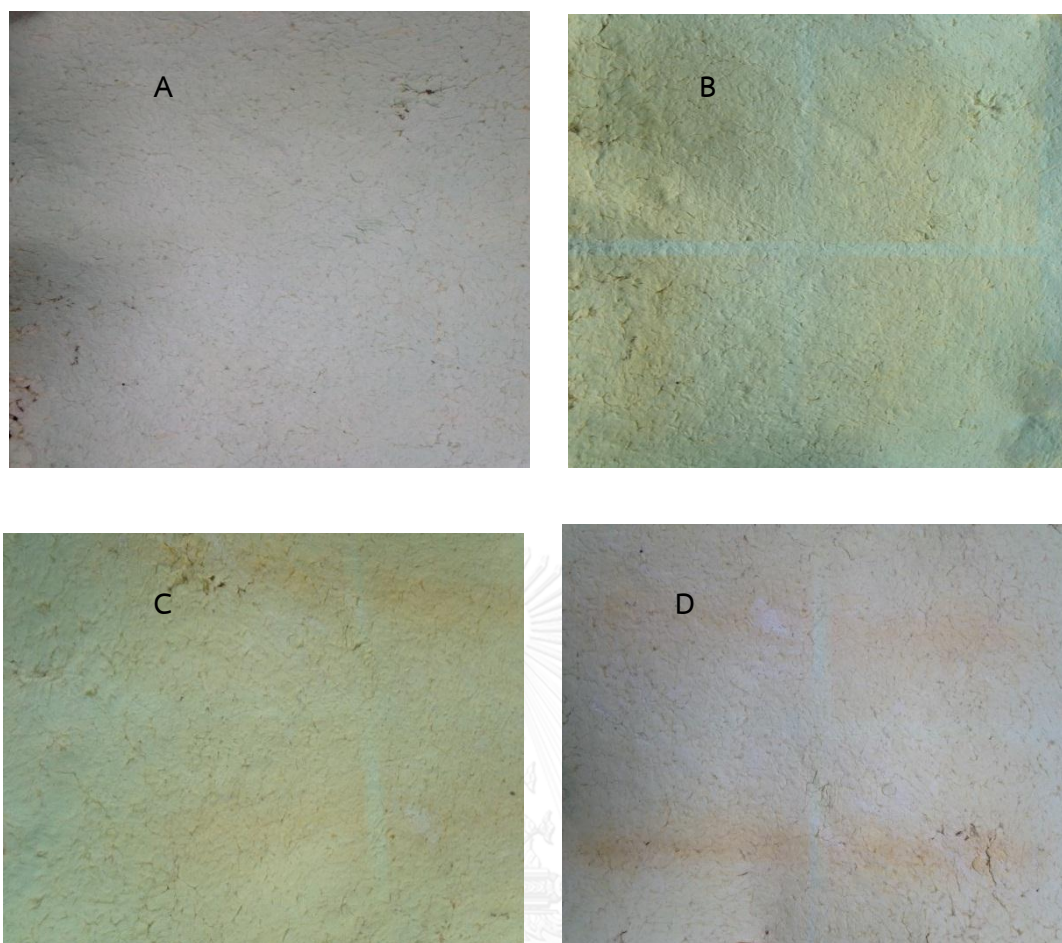
Fig. 4. 4 General physical property of TiO_2-coated with silk fibroin filters under UV irradiation at different period of time A) 0 hr, B) 72 hr, C) 120 hr, and D) 336 hr

4.2.3 Study of morphological structure and physical properties

    1) Study of morphological structure

    Scanning electron microscopy (SEM)

Scanning electron microscopy (SEM) images of TiO_2 were examined as shown in Fig 4.5 TiO_2 powder was granular shape with particle size (50-75 nm) at magnification of 10,000X and 20,000X, respectively. SEM images of the pure silk fibroin and silk fibroin filter coated TiO_2 at different dosages were displayed in Fig. 4.6-4.10.
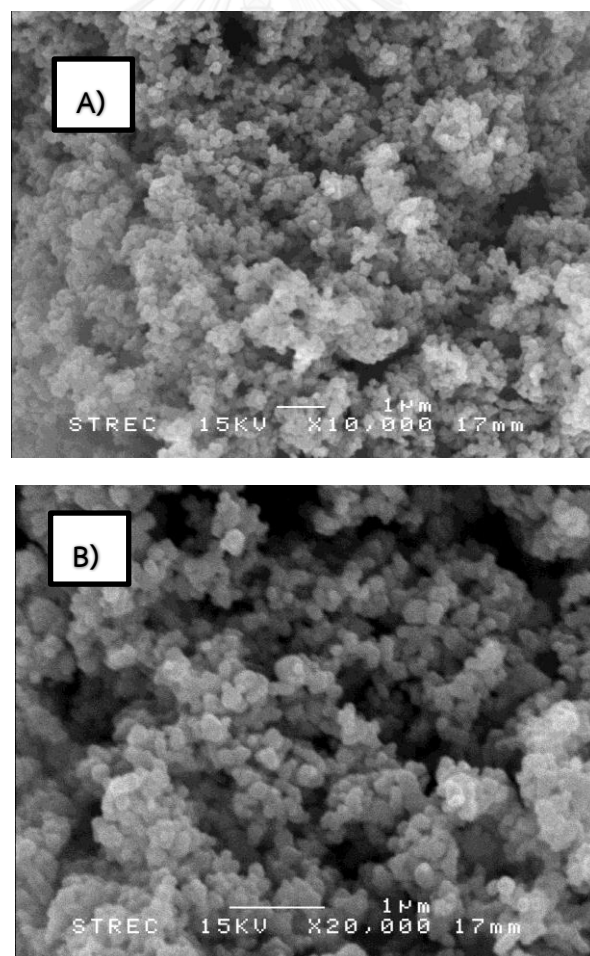
Fig. 4. 5 SEM micrographs of TiO_2 powder magnification of A) 10,000X and B) 20,000X

The pure SF filters displayed in figure 4.6 and SF filters coated with TiO_2 different dosage were displayed in figure 4.7 to 4.10. As seen in the figures, the magnification was obtained with 50X, 100X, 500X, and 2,000X, respectively. SEM micrographs revealed the fibrous morphology of the SF fiber. It was found that at different dosages, TiO_2 was well dispersed onto the surface of SF filter. However, a few clumps of TiO_2 particles onto the surface of the SF filters at the high dosages of TiO_2 are also noticed. An average diameter of the SF fiber was estimated to be approximately 10 μm. The thickness of the SF filters and SF filters coated with TiO_2 were approximately 4.10 and 4.75 mm, respectively.
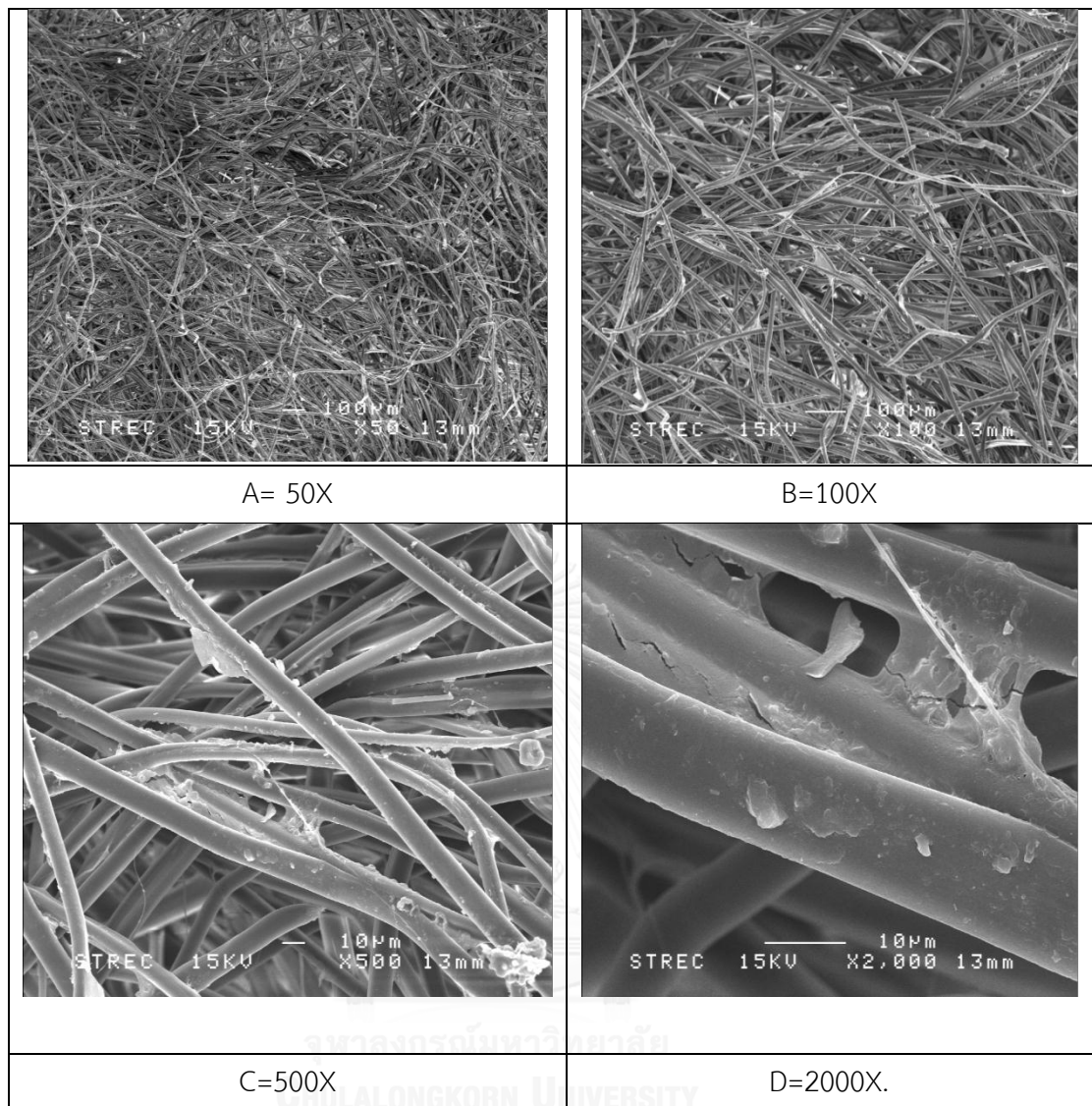
Fig. 4. 6 SEM micrographs of pure silk fibroin filter at different magnifications of A) 50X, B) 100X, C) 500X and D) 2,000X
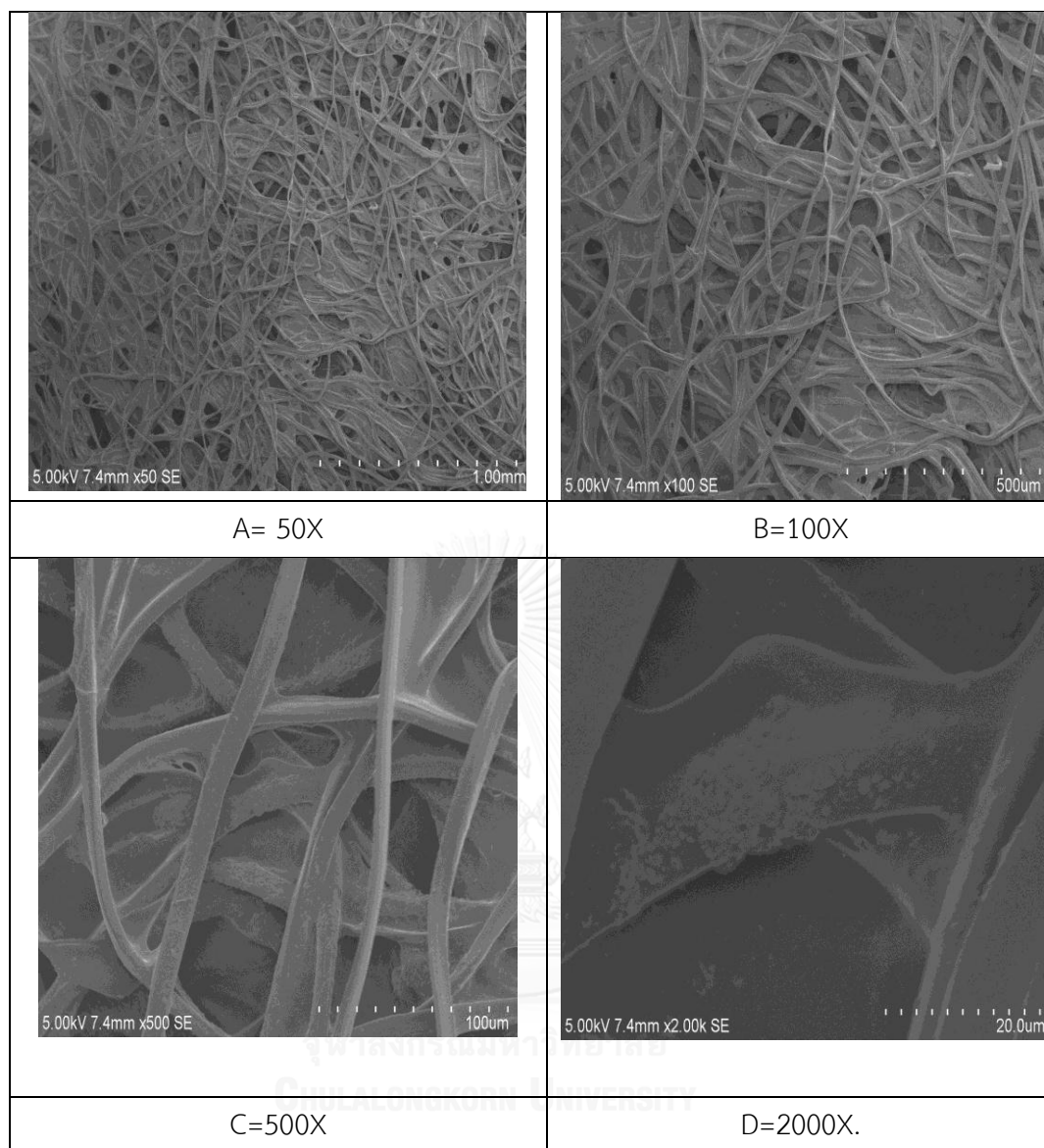
Fig. 4. 7 SEM micrographs of 1.0 % wt.TiO$_2$/vol.sol of TiO$_2$-coated SF filters at different magnification of A) 50X, B) 100X, C) 500X and D) 2,000X
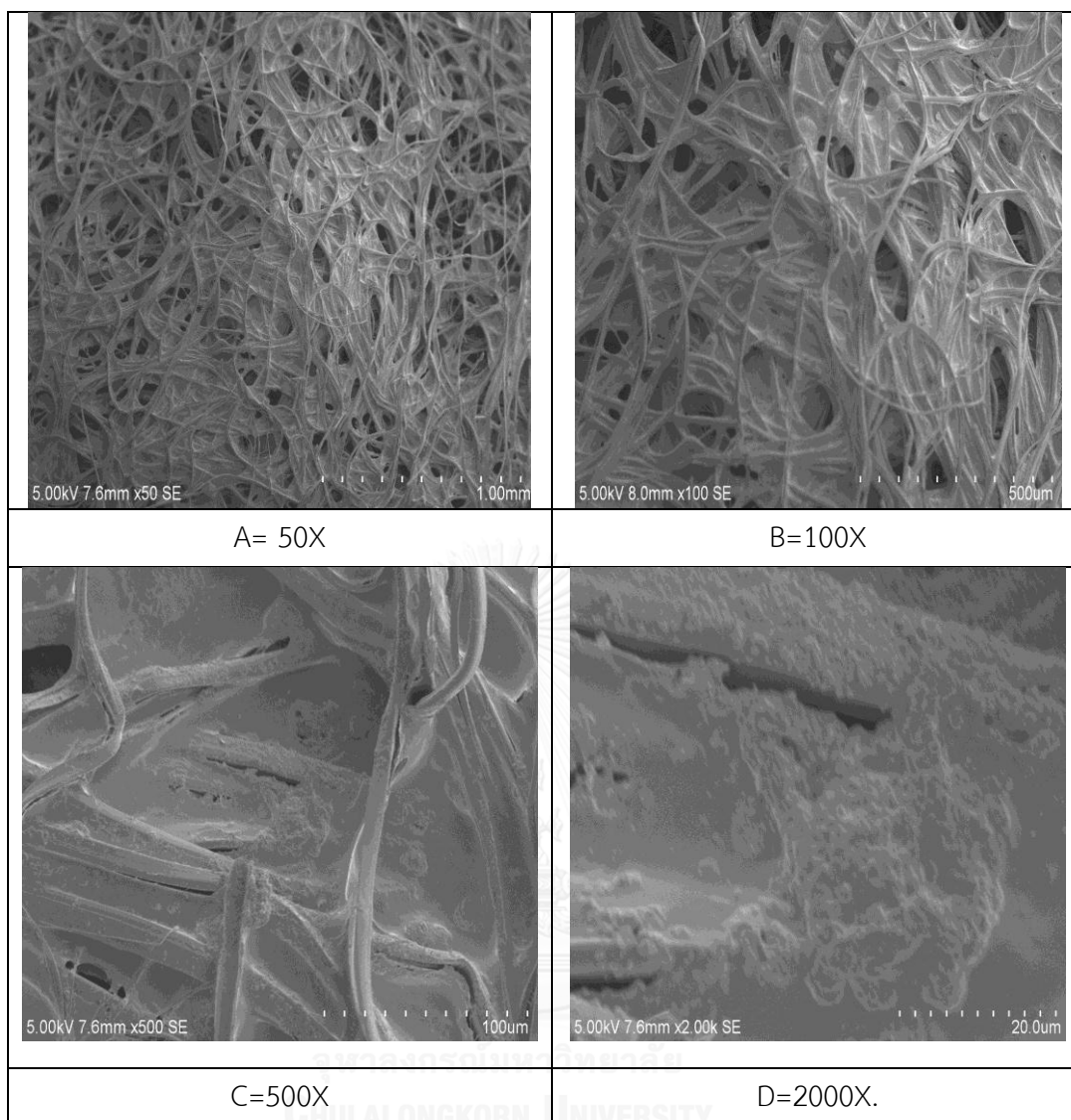
Fig. 4. 8 SEM micrographs of 2.5 % wt.TiO$_2$/vol.sol of TiO$_2$-coated SF filters at different magnification of A) 50X, B) 100X, C) 500X and D) 2,000X

A= 50X	B=100X
C=500X	D=2000X.
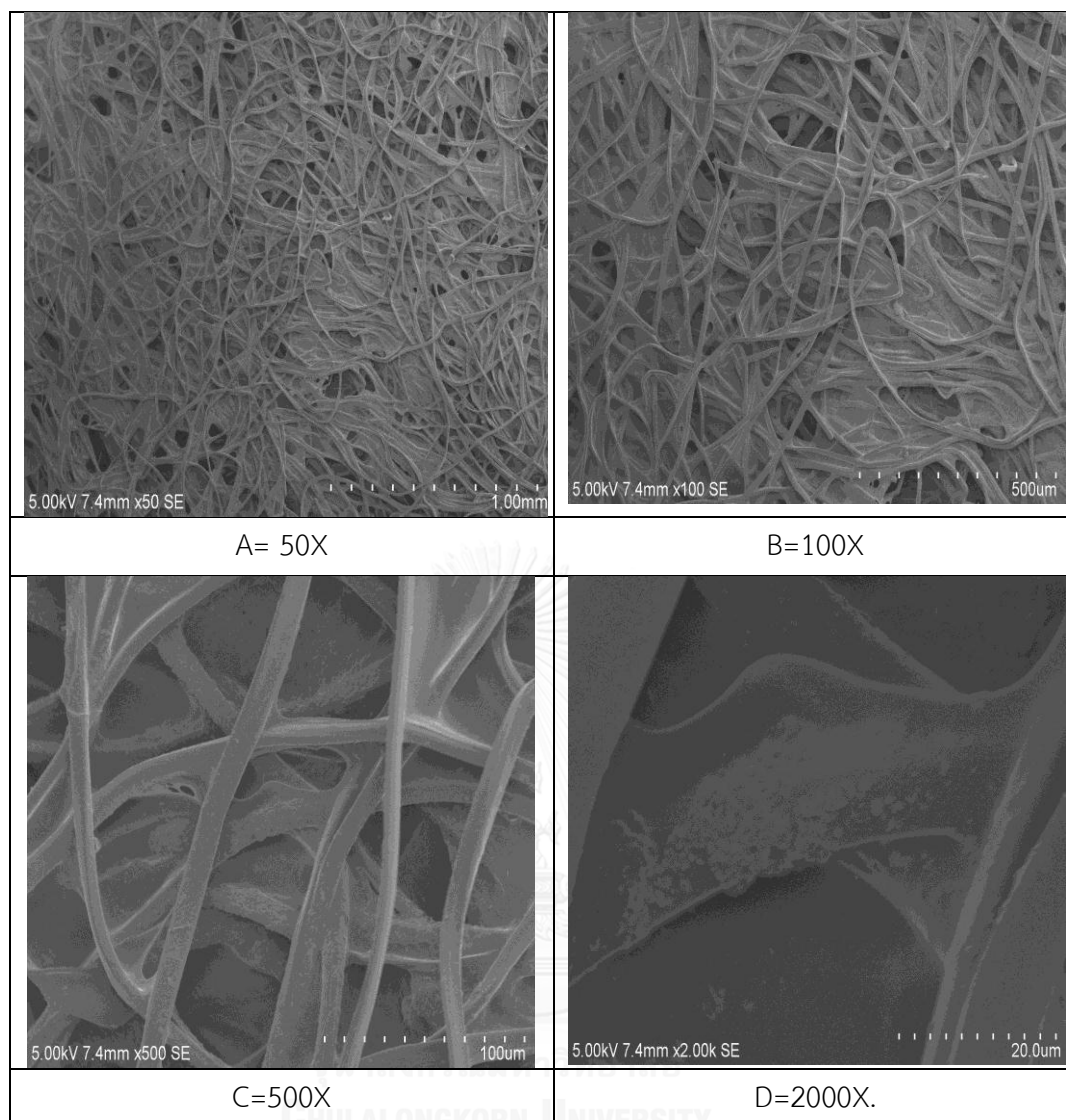
Fig. 4. 9 SEM micrographs of 5.0 % wt.TiO_2/vol.sol of TiO_2-coated SF filters at different magnification of A) 50X, B) 100X, C) 500X and D) 2,000X
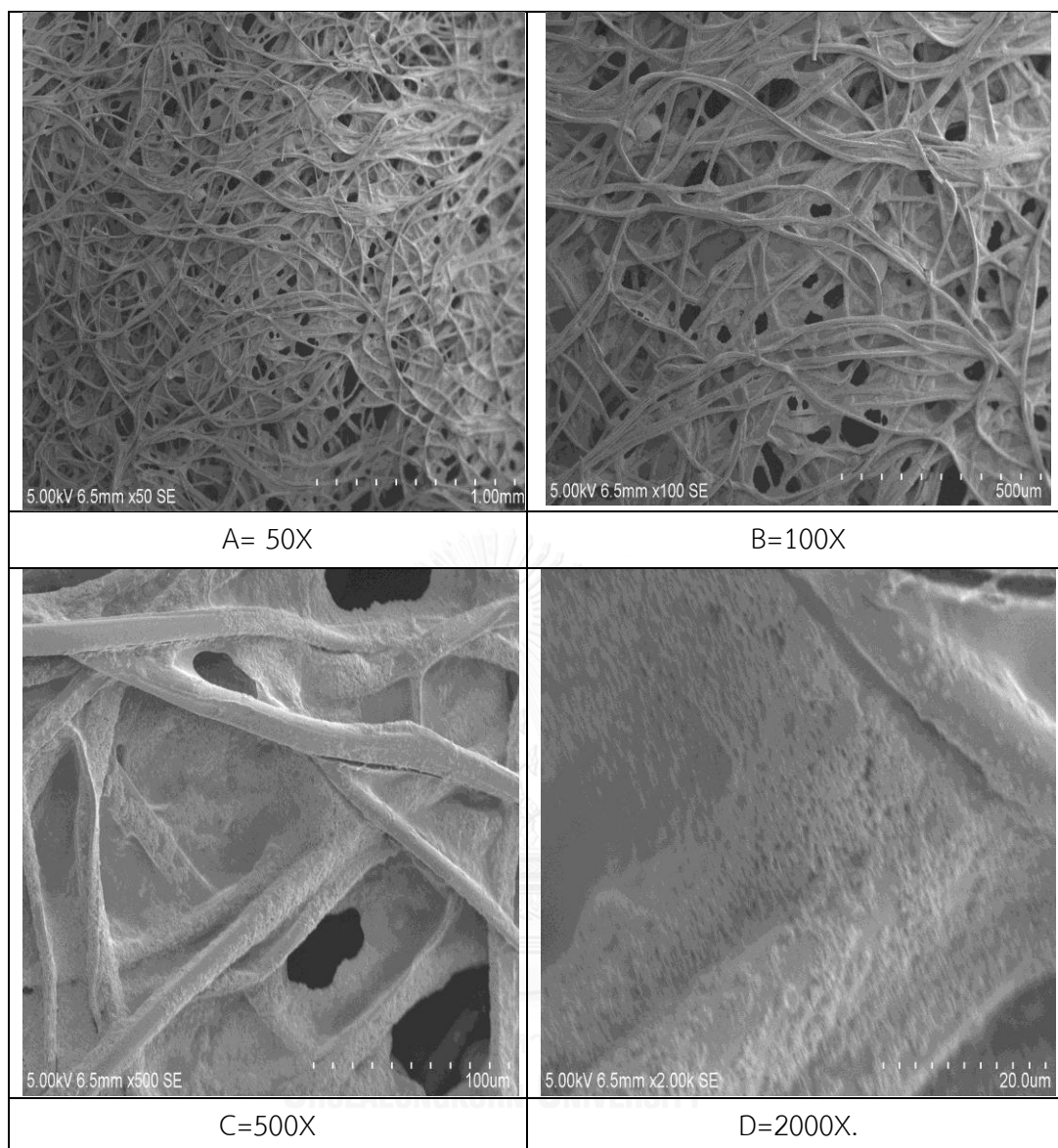
Fig. 4. 10 SEM micrographs of 7.5 % wt.TiO$_2$/vol.sol of TiO$_2$-coated SF filters at different magnification of A) 50X, B) 100X, C) 500X and D) 2,000X

2). Energy disperse spectroscopy (EDS) micrographs

The chemical composition of the TiO_2-coated SF filters were studied by Energy disperse spectroscopy (EDS) micrographs. An EDS scanning electron microscope was used to separate characteristic X-rays of different elements from an energy spectrum. EDS was used to analyse the chemical compositions of the SF TiO_2-coated filters. Fig. 4.11 shows EDS micrographs of the TiO_2-coated SF filters at dosages of 1.0, 2.5, 5.0, and 7.5% wt. TiO_2/vol.sol. The results show analyses of the test samples in which characteristics X-ray frequencies of carbon (C), oxygen (O), gold (Au), and the last two peaks of titanium (Ti) were detected as distinct peaks, respectively. The stronger peak from Ti was observed upon the addition of higher amounts of TiO_2.
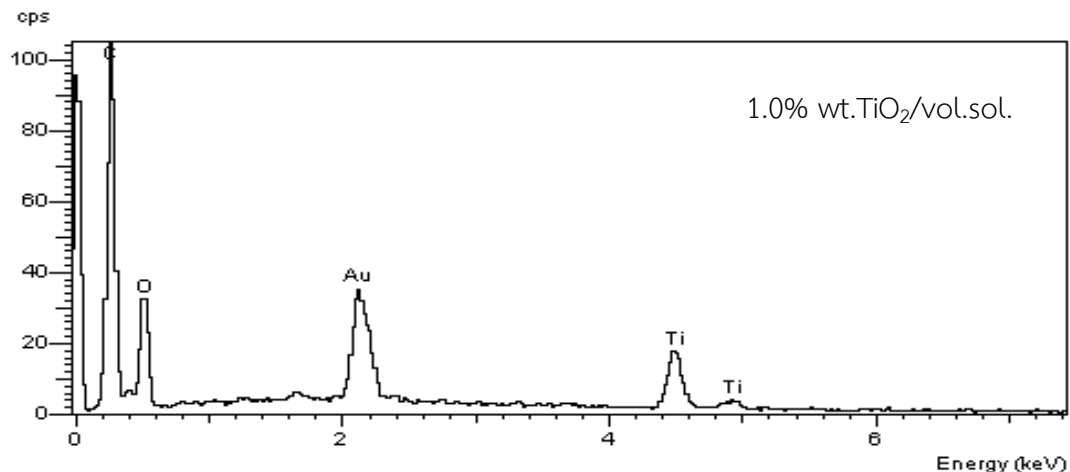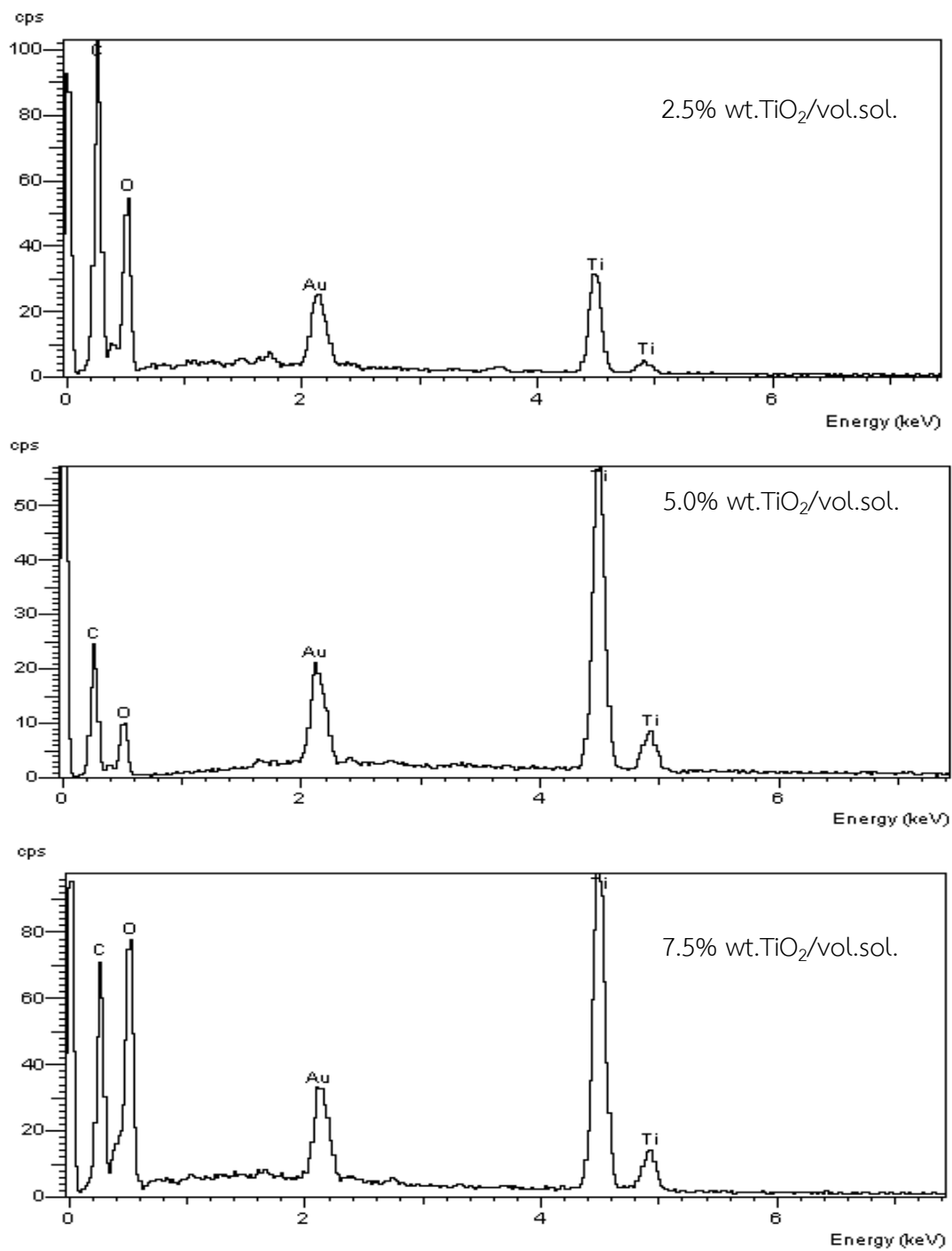
Fig. 4. 11 EDS micrographs of silk fibroin filters coated with 1.0, 2.5, 5.0, and 7.5 % wt.TiO$_2$/vol.sol

3). Optical Properties of TiO$_2$-coated SF filters

The UV absorption of SF filter and SF filters coated TiO$_2$ at different dosage 1.0, 2.5, 5.0, 7.5% wt.TiO$_2$/vol.sol. were shown in Fig 4.12. As can be seen from spectra, the SF filters coated TiO$_2$ tranmits UV litght in ranged of 200-800 nm. All spectra was monitored in the absorbance mode and acquired under ambient conditions. The optical absorbance spectra, the adsorption coefficient, and the band gap of the SF filters will be evaluated. The band gap engergy can be caculated using the following eqution; Band Gap Energy $(E) = h*c/\lambda$; where h = Planks constant = 6.626 x 10^{-34} (J.s), c = Speed of light = 3.0 x 10^{8} (m/s) , λ = Cut off walength (m), and 1eV = 1.6 x10^{-19} J. [140]. The spectral data recorded showed the strong cut off at 390 nm.

The ultraviolet-visible spectrum of the photo-catalysts was recorded by a UV-VIS spectrophotometer as shown in Table 4.4. The resulting spectrum was obtained for TiO$_2$. The spectral data recorded showed the strong cut off at 390 nm. Therefore, the band gap engergy can be caculated as 3.185576 eV. This result agrees with other results [141].
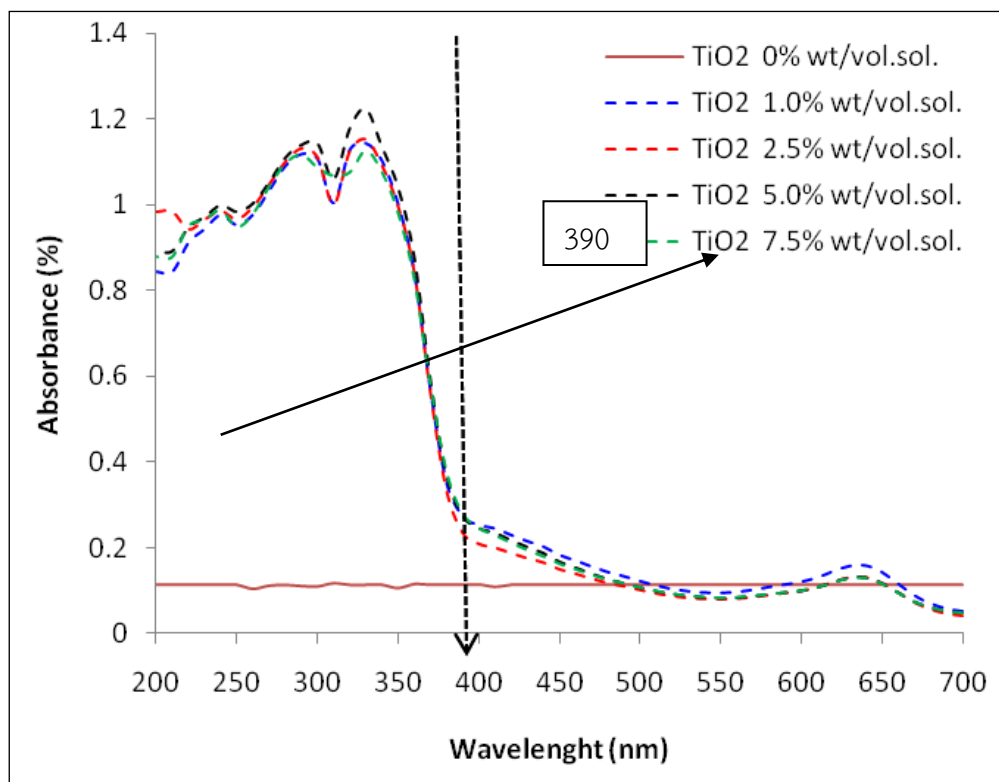
Fig. 4. 12 UV absorbance spectra of the silk fibroin filters coated TiO_2 different dosage.

Table 4. 4 The spectral data for band-gap energy of TiO_2-coated SF filters

h (J.s)	c (m/s)	λ (m)	E (J)	E (eV)
6.63×10^{-34}	3.00×10^{8}	390×10^{-9}	5.10×10^{-19}	3.18556

4). Study of Differential Pressure (ΔP) of TiO$_2$-coated SF Filters

The investigation of differential pressure (ΔP) across the TiO$_2$-coated SF filters was conducted using a differential manometer method. This measurement is the key indicator for filter performance and the most important factor to consider preventing the filter from blocking due to the system. Differential pressures of the TiO$_2$-coated SF Filters are displayed in Table 4.5. For the SF filter without catalyst, the differential pressure was very small, and it was relatively increased with percent TiO$_2$ coated on the SF filters. However, the differential pressures of the SF filter are higher than that of the commercial air filter. The differential pressure of commercial filter (Polyester class Eu 2) was 680±6.90

Table 4. 5 The differential pressure of the TiO$_2$-coated SF Filters

ΔP (kg/m·s or Pa) Mean ± SD	Percent TiO$_2$ dosages					
	0	1.0	2.5	5.0	7.5	Commer-cial filter
	872 ±20	1,293±7	2,224±34	2,635±20	3,321±13	680±90

5). Study of Mechanical properties of TiO$_2$-coated SF Filters

The resistance to mechanical compression of pure SF filters and TiO$_2$-coated SF filters were measured by the Dumbbell method ASTM D638, Type V test with a universal tensile testing machine (UTM) by loading cell 50 N crosshead speed 10 mm/min and gauge length 50 mm. Five specimens of each SF filters were measured at the same condition. The stress and strain of the SF filters were reported in Table 4.6. The results show that the maximum value of average stress (0.440±0.080 N/mm^2) and that of average strain (0.028±0.073) were obtained for the TiO$_2$ coated SF filter with 7.5% wt. TiO$_2$/vol.sol. While the minimum stress was received for the pure SF filter. The higher values of these properties when increasing the amount of TiO$_2$ might be resulted from the quantity of TiO$_2$ filled in the pure of SF filters making them denser. There for the strength of the filters could be enhanced.

Table 4. 6 Mechanical properties of silk fibroin filter

Samples (%TiO_2wt/ vol.sol.)	Maximum load (N)	Elastic value (stress,σ) (N/mm^2)	Strain (ε)
0 (pure SF)	3.020±0.094	0.088±0.002	0.184±0.039
1.0	6.093±1.106	0.140±0.022	0.085±0.185
2.5	9.155±4.138	0.206±0.080	0.029±0.089
5.0	9.673±0.046	0.245±0.001	0.021±0.075
7.5	17.314±3.401	0.440±0.080	0.028±0.073

6). Chemical struture of SF filters and TiO_2 coated SF Filters by Fourier transform infrared (FTIR) spectroscopy

To investigate the conformational characteristics of the SF and TiO_2-coated SF filters, samples were examined using FTIR spectroscopy. The chemical structures of the filters is shown in Fig. 4.13 The infrared spectra of the filters showed fingerprints of the samples with absorption peaks corresponding to the following amide bands: amide I, amide II, and amide III. Amide I vibrations represent CO stretching, while amide II vibrations represent the bending of NH bonds associated with CN stretching [142]. Amide III vibrations are associated with the combination of NH deformation and CN stretching vibrations [143].

From the figure, the characteristic bands corresponding to the amide groups were found in the region between 1700 - 1200 cm^{-1} [144]. Narrow absorption bands at 1622 cm^{-1} (amide I), 1533 cm^{-1} (amide II), and 1225 cm^{-1} (amide III) attributed to the amide groups were due to the crystalline structures of the filters. These results indicated that the band at 1700 cm^{-1} could be indicative of an antiparallel arrangement of the fibroin chains in the Silk II β-sheet domains [145]. A wide absorption band between 550 and 750 cm^{-1} should have been due to the envelope of the Ti-O bands [146]. As seen in Fig 4.13, the smaller peaks were observed with higher amounts of TiO$_2$ coated on the SF filters. The smaller peaks observed in this study may have been caused by TiO$_2$ covering the filter surfaces, which would have reduced light transmittance.
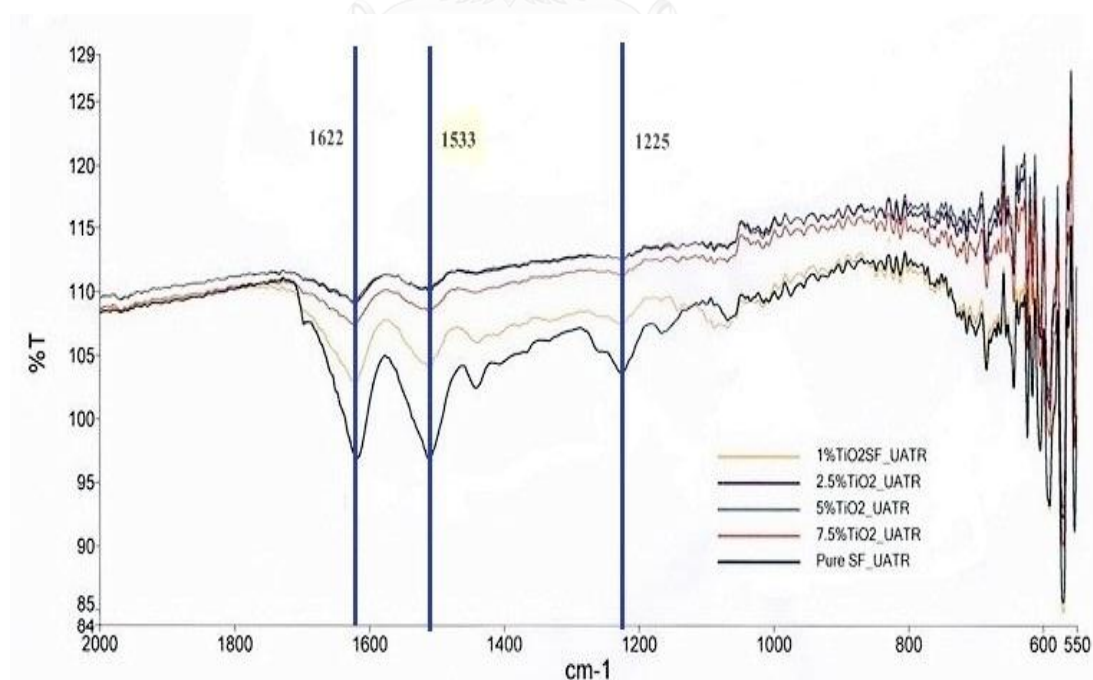
Fig. 4. 13 FTIR transmittance spectra of pure SF and TiO$_2$-coated SF filters

7). Thermogravimetric analysis

The thermal behavior of the silk fibroin and TiO_2 coated silk fibroin filters was investigated by thermogravimatric analysis (Thermo plus TG 8120). The degradation temperature, known as a criterion of thermal degradation, was calculated based on differential TGA curves. Additionally, the location of peaks observed in the detrivative thermogravimetic (DTG) curve also provided information on the component and the effect of the composite components on the temperature scale.

Thermogravimetric curves of pure SF and TiO_2 coated SF filters are shown in Fig. 4.14. From TGA curves, the determination of the mass decrement during the heating process was performed. All samples showed similar curves with peak temperatures and stages of weight loss. For their regions of mass loss: the first one was presented near 100℃ and is attributed to the loss of unbound water, while the second stage in the range of 270–500 °C and the third one was presented in the range of 500 – 630 °C are associated with the breakdown of side chain groups of amino acid residues as well the cleavage of peptide bonds.

As shown in picture, the initial weight loss of the pure SF and TiO_2 coated SF was about 7 and 6 %, respectively, till 200 °C. These weight changes could be attributed to the elimination of adsorbed water, as reported previously.

Since the SF filters was hydrophilic, it was subject to a dehydration process, in which absorbed or crystal water was released. The second stage of decomposition, which is a major step for each sample because weight loss is about 50%, occurred in

the temperature range of 270 - 500 °C compared to the initial mass sample. Another

strong weight loss of about 15% was observed in the range of 500 – 630 °C range, for

both the pure SF and TiO_2 coated SF filters. This is associated with the breakdown of

side chain groups of amino acid residues as well as the cleavage of peptide bonds

[147].
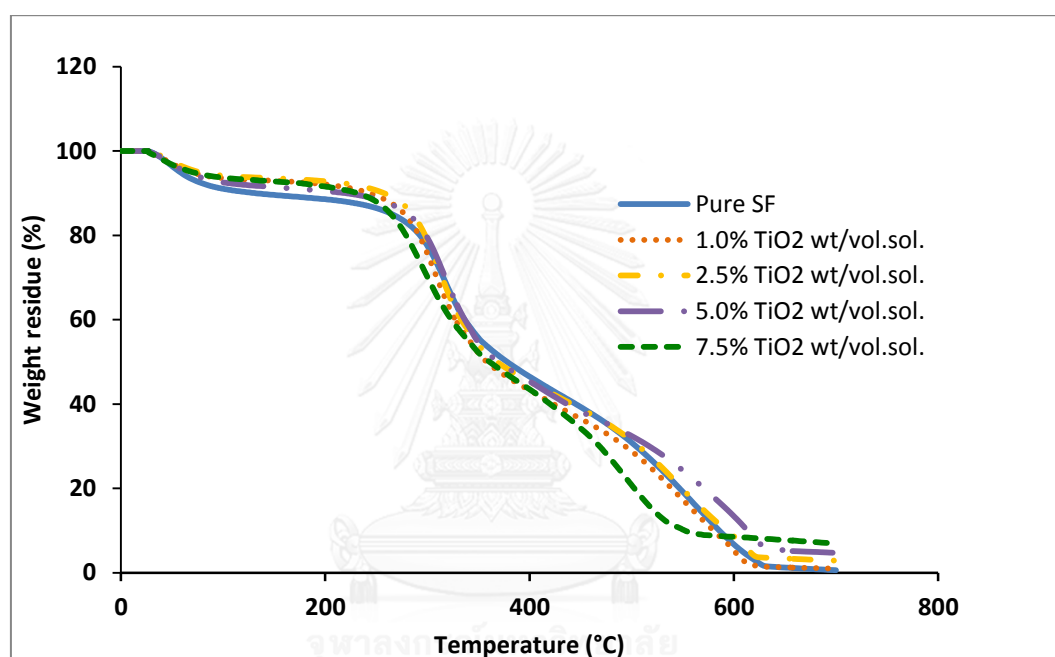
Fig. 4. 14 Thermogravimetric analysis of pure silk fibroin and silk fibroin coated with TiO_2 filters

DTG thermograms of pure SF and TiO_2-coated SF filters are shown in Fig. 4.15.

Endothermic peaks below 100 °C are associated with water loss during heating.

Thermal degradation peaks present two distinguishable weight losses for the pure SF

and TiO_2 coated SF filters. The presence of double degradation peaks indicates that

endothermic reactions of different structures occurred. The decomposition behavior

of silk is influenced by the intrinsic morphological and physical properties of the sample, with the degree of molecular orientation being one of the most important parameters [148]. The pure SF filters began to degrade near 250 °C showing the fastest weight change with a peak temperature at 310 °C. The TiO_2 coated SF filters began significantly loosing weight near 250 °C but the fastest weight loss was observed at about 315 °C.

The pure SF showed the other peak temperature at 590 °C, while the other peak temperature for the TiO_2 coated SF filters occurred at about 610°C. By comparison, the peak temperatures of TiO_2 coated SF filters were higher than that of the pure SF filters. The increase of the peak temperature may be associated with the crystalline structural transition from Silk I to Silk II, which is also consistent with FI-IR results.
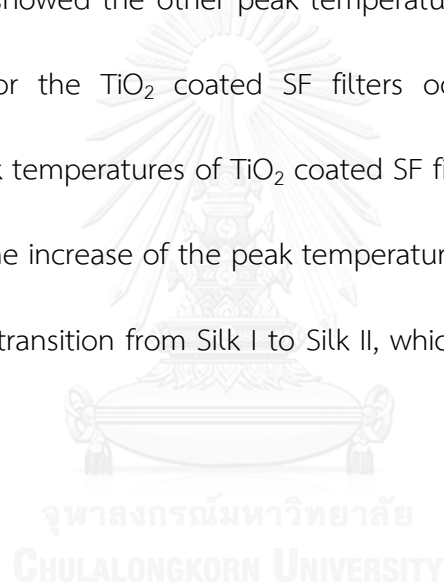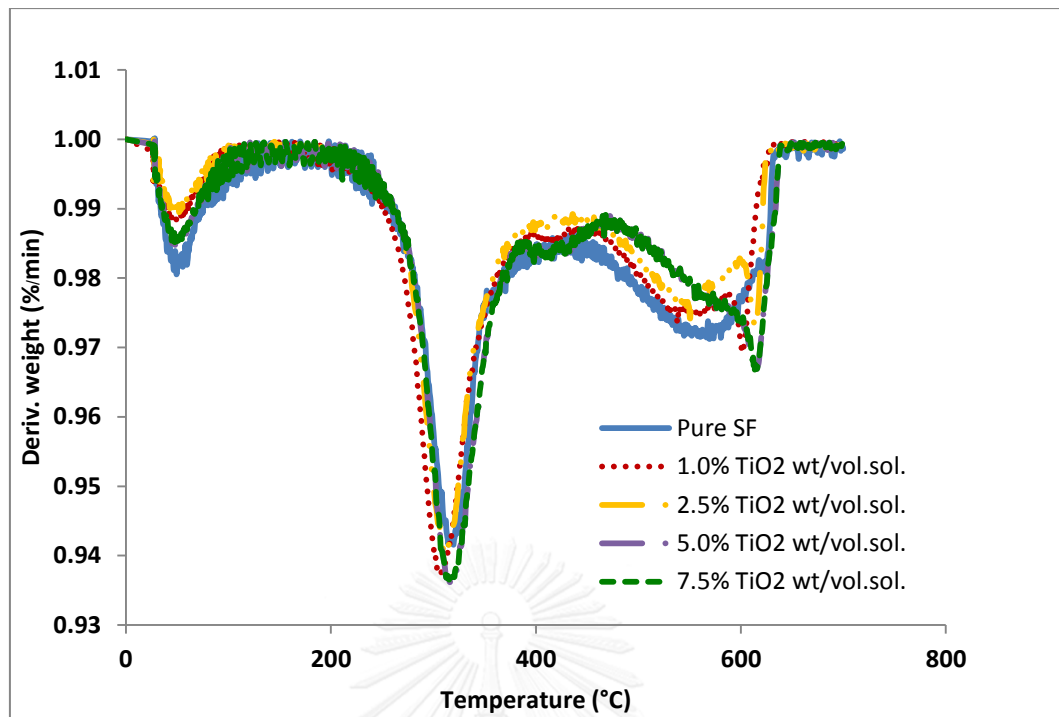
Fig. 4. 15 Detrivative thermogravimetic of pure silk fibroin and TiO_2 coated silk fibroin filters

8). Physical characteristics of silk fibroin filters

N_2 - adsorption analysis was applied to characterize specific surface area, specific pore volume, and pore size distribution of pure SF filter and TiO_2-coated SF filters as shown in Table 4.7. The specific surface area, specific pore volume, and pore size distribution were analyzed with isotherm of adsorption and desorption of nitrogen gas on the SF filter by the Barret–Joyner–Halender (BJH) method. The results were displayed of specific surface areas of the pure SF filter and those of TiO_{2-} coated SF filters at 1.0 and 5.0 % TiO_2 wt./vol.sol. were approximately 57.87, 63.69, and 114.75 m^2/g, respectively. It can be noted that the higher the dosage of

TiO_2, the higher the specific surface area. Moreover, the pore volumes were determined to be 0.031, 0.035, and 0.061cm^3/g, respectively. The average pore sizes were calculated on the basis of pore size distribution data to be 25.33 Å for all sample filters. The average pore sizes obtained in this study are similar to the ones obtained from the previous study [31]. The results indicated that these pores can be classified as mesopore [149].

Table 4. 7 Physical properties of silk fibroin filters

Samples (%TiO_2wt./ vol.sol.)	Physical properties		
	Specific surface area (m^2/g)	Specific pore volume (cm^3/g)	Pore size (Å)
0 (pure SF)	57.87	0.031	25.33
1.0	63.69	0.035	25.33
5.0	114.75	0.061	25.33

4.3 Treatment of formaldehyde in a small reactor using the synthesized SF filters and commercial filter

Removal efficiency of the synthesized SF filters was tested in a closed reactor with the dimensions of 40 cm × 45 cm × 50 cm. Two small fans were installed in the reactor to ensure adequate mixing of formaldehyde in the reactor. Gaseous formaldehyde in the room was pumped through the SF filters held by an air filter

holder at using the personal pump. Formaldehyde concentration was continuously measured every 5 min. for 3 hrs with the HCHO meter (HAL-HFX205). There were two replications for each experiment.

4.3.1 Photocatalytic Oxidation (PCO) of formaldehyde using the TiO$_2$ coated SF filters

Three sets of experiments were conducted to study impact of initial HCHO concentration, TiO$_2$ dosage, and air flow rate. For all sets of experiment, the UV light intensity and the temperature in the reactor were keep constant at around 0.125 mW/cm^2 at wavelength of 254 nm and ambient air temperature, respectively. For the first set, the initial HCHO concentration was varied from 2.5 ± 0.50 ppm, 5.0± 0.50 ppm, 7.5 ± 0.50 ppm, and 10 ± 0.50 ppm. Whereas the air flow rate and the TiO$_2$ dosage were fixed at around 5 L/min and 5% wt.TiO$_2$/vol. sol., respectively. For the second set, dosage of TiO$_2$ was varied from 1.0, 2.5, 5.0, and 7.5% wt.TiO$_2$ /vol.sol. While the air flow rate and the initial HCHO concentration were set at about 5 L/min and 5 ppm, respectively. For the last set, air flow rate was varied from 3, 4, and 5 L/min. While the initial HCHO concentration and catalyst dosages were maintained at about 5 ppm and 5% wt.TiO$_2$/vol. sol., respectively.

1) Impact of initial formaldehyde concentration

Initial concentration of HCHO at 2.5 ± 0.50 ppm, 5.0± 0.50 ppm, 7.5 ± 0.50 ppm, and 10 ± 0.50 ppm were used to study HCHO treatment via photocatalytic oxidation process of the TiO_2 coated SF filters. From the results, the HCHO concentration decreased rapidly during the initial period of treatment as shown in Fig. 4.16. The highest HCHO removal efficiency was 57.15 ± 1.65 % at initial concentration of 5.0± 0.50 ppm followed by 45.30 ± 0.18 %, 41.19 ± 0.69%, and 32.92 ± 0.39 % at initial concentration of HCHO of 7.5 ± 0.50 ppm, 10 ± 0.50 ppm, and 2.5 ± 0.50 ppm, respectively as displayed in Table 4.8. As seen from Fig. 4.17, formaldehyde concentration decreased rapidly for the first 120 min of treatment time. Then it tended to reach equilibrium for all experiments. The results showed that the removal efficiency of HCHO was relatively increased when increasing initial concentration of HCHO from 2.5 ± 0.50 ppm, 5.0± 0.50 ppm. However, further increase of initial HCHO concentration from 7.5 ± 0.50 ppm to 10.0± 0.50 ppm resulted in the reduction of removal efficiency. This may be due to the higher the initial concentrations, the more mass of formaldehyde pumped through the filter. Consequently, there are not enough reactive sites for such a relatively high formaldehyde concentration to be adsorbed onto them and reacted with hydroxyl radicals at this low catalyst dosage.

Fig. 4. 16 Photocatalytic oxidation of gaseous formaldehyde at different initial concentrations: 2.5, 5.0, 7.5, and 10.0 ppm

Table 4. 8 Effect of initial formaldehyde concentration on removal efficiencies

	Initial HCHO concentrations (ppm)			
	2.5 ± 0.50	5.00 ± 0.50	7.50 ± 0.50	10.00 ± 0.50
Percent formaldehyde removal efficiency	32.92 ± 0.39	57.15 ± 1.65	45.30 ± 0.18	41.19 ± 0.69

2) Impact of catalyst (TiO$_2$) dosage

Photocatalytic destruction of formaldehyde affected by catalyst dosage was investigated. Catalyst dosage was varied as 2.5%, 5.0%, 7.5%, and 10.0% wt.TiO$_2$/vol. sol. Results in Fig. 4.17 shows that HCHO concentration decreased rapidly during the initial period of treatment. The highest HCHO removal efficiency was 68.21 ± 0.48 % at dosage of 5.0% wt.TiO$_2$ /vol. sol. followed by 61.95 ± 1.68%, 57.37 ± 1.49%, and 44.00 ± 2.20 % at catalyst dosages of 2.5, 1.0, and 7.5% wt.TiO$_2$/vol. sol, respectively as displayed in Table 4.9. HCHO concentration decreased rapidly for the first 100 min of treatment time. Then it tended to reach equilibrium for all experiments. The results showed that the removal efficiency of HCHO was relatively increased when increasing TiO$_2$ dosage from 1.0% to 5.0% wt.TiO$_2$/vol. sol. However, further addition of TiO$_2$ from 5.0% to 7.5% resulted in the reduction of removal efficiency. This may be caused by the limitation of light penetration through the thickness of catalyst. The degradation rate was started to decline caused by the mass transfer and light penetration limitation[70, 150].
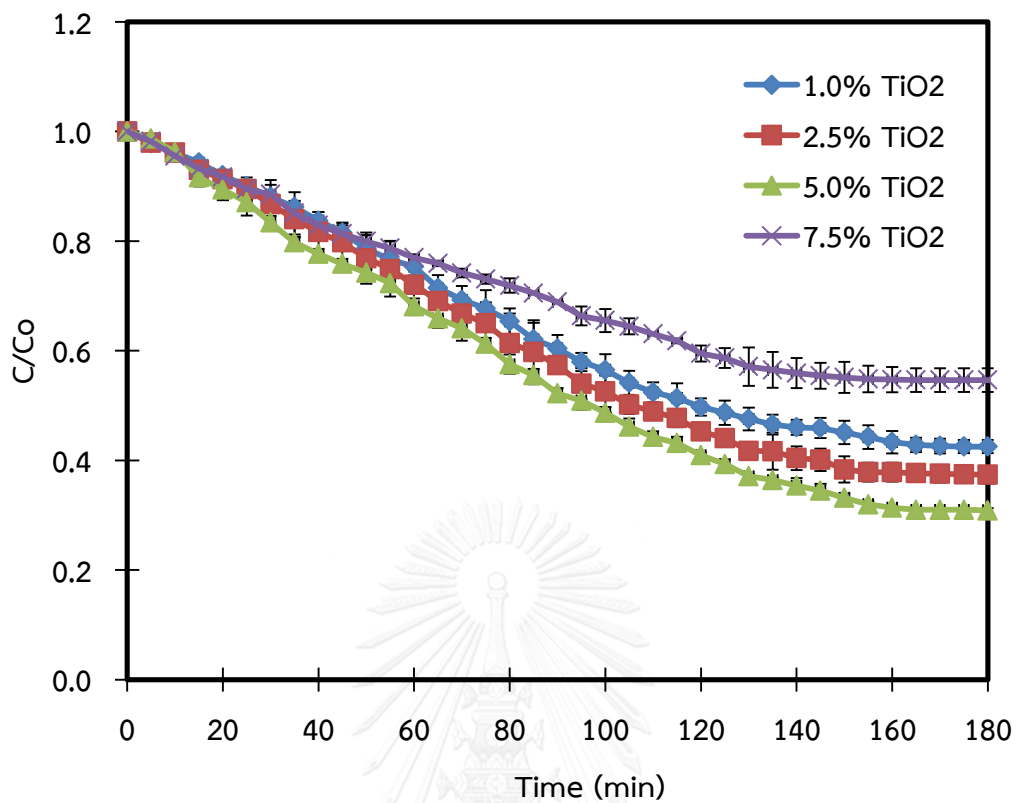
Fig. 4. 17 Photocatalytic oxidation of gaseous formaldehyde at different catalyst
(TiO_2) dosages: 1.0, 2.5, 5.0, and 7.5 % wt. /vol. sol.

Table 4. 9 Effect of TiO_2 dosage on formaldehyde removal efficiencies

	TiO_2 Dosage (% wt /vol. sol.)			
	1.0	2.5	5.0	7.5
Percent formaldehyde removal efficiency	57.37 ± 1.49	61.95 ± 1.68	68.21±0.48	44.00 ± 2.20

3) Impact of air flow rate

Effect of air flow rate on treatment of HCHO was studied for this set. Air flow rate was varied from 3, 4, and 5 L/min. The correlation between HCHO concentration and time was plotted as shown in Fig 4.18. As seen from the figure, HCHO concentration decreased rapidly during the initial period of treatment. The result showed that HCHO removal efficiencies for these set of experiments ranged from 31.35-68.23%. The highest HCHO removal efficiency of 68.23 ± 0.44 % was obtained when using the air flow rate of 5 L/min followed by 49.98 ± 0.13% and 31.35 ± 1.01% at air flow rate of 4 L/min and 3 L/min, respectively as displayed in Table 4.10. For a certain amount of formaldehyde, the higher air flow rate, the greater chance of formaldehyde to be adsorbed and reacted on the catalyst surface. Thus the higher removal efficiency might be obtained.
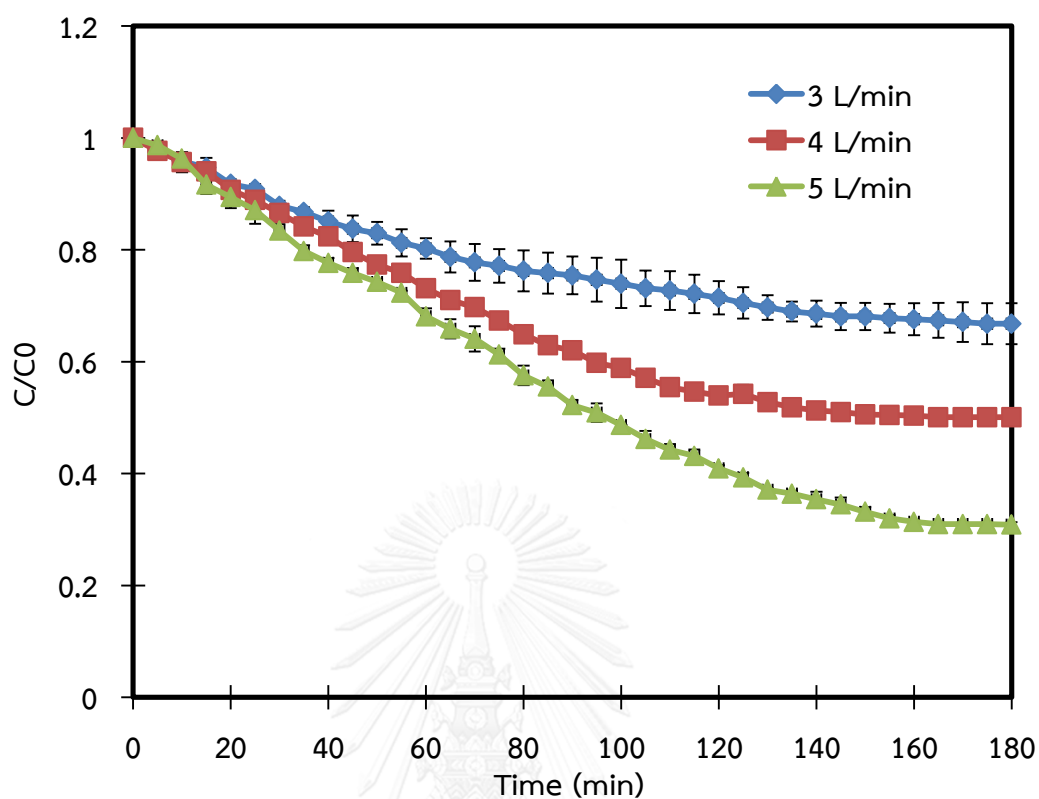
Fig. 4. 18 Photocatalytic oxidation of gaseous formaldehyde at different air flow rates: 3, 4, and 5 L/min

Table 4. 10 Effect of air flow rate on formaldehyde removal efficiencies

	Air flow rate (L/min)		
	3	4	5
Percent formaldehyde removal efficiency	31.35 ± 1.01	49.98 ± 0.13	68.23 ± 0.44

4.3.2 Treatment of HCHO using pure silk fibroin (SF) filters

Treatment of HCHO using pure silk fibroin (SF) filters in a small reactor was also investigated. Two sets of experiment were conducted to study adsorption and photolysis of formaldehyde using pure silk fibroin filters. For all set, air flow rate, air temperature, and initial HCHO concentration were set at around 5 L/min, ambient air temperature, and 5.00 ± 0.50 ppm, respectively. For the photolysis experiments, the UV light intensity at approximately 0.125 mW/cm^2 (wavelength of 254 nm) was applied.

Study of adsorption and photolysis of HCHO

The correlation between HCHO concentration and time was plotted in Fig 4.19. The initial HCHO concentration reached equilibrium at around 120 min after treatment. Formaldehyde concentration decreased slightly during the initial period of treatment. The results show that the highest HCHO removal efficiencies of 44.23 ± 0.13 % and 42.20 ± 0.4 were obtained for photolysis process and adsorption process, respectively as displayed in Table 4.11.
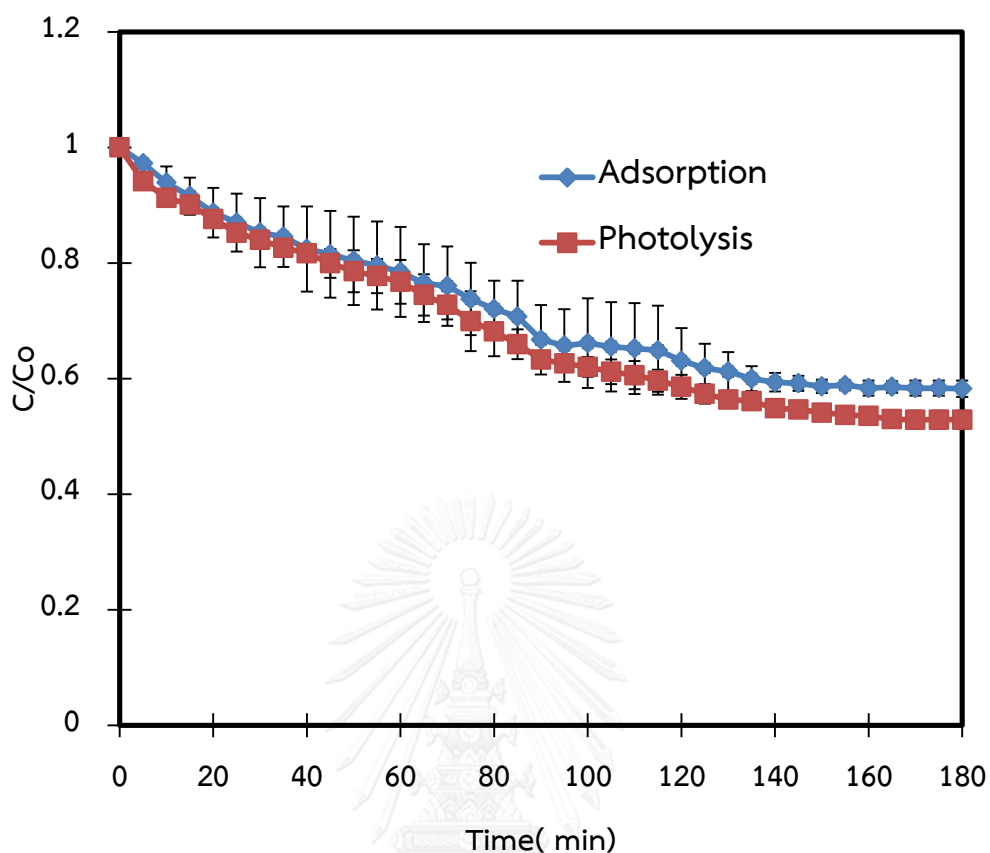
Fig. 4. 19 Adsorption and photolysis of HCHO using pure silk fibroin (SF) filters

Table 4. 11 Removal efficiency of formaldehyde via photolysis and adsorption processes

	adsorption	photolysis
Percent formaldehyde Removal efficiency	42.20 ± 0.43	44.23 ± 0.13

4.3.3 Treatment of HCHO using commercial air filters (Polyester class Eu 2)

Treatment of HCHO using commercial air filters (Polyester Eu 2 with thickness of 0.5 mm) was studied and compared with the SF filters. Set of experiments was conducted under the same conditions as described in section 4.3.2.

Study of adsorption and photolysis of HCHO

The correlation between HCHO concentration and time was plotted in Fig 4.20. The initial HCHO concentration reached equilibrium after 140 min of treatment. Formaldehyde concentration decreased slightly during the initial period of treatment. The result showed that the highest HCHO removal efficiencies of 43.49 ± 0.13 % and 35.50 ± 2.42 % were obtained for photolysis and adsorption processes, respectively as displayed in Table 4.12.
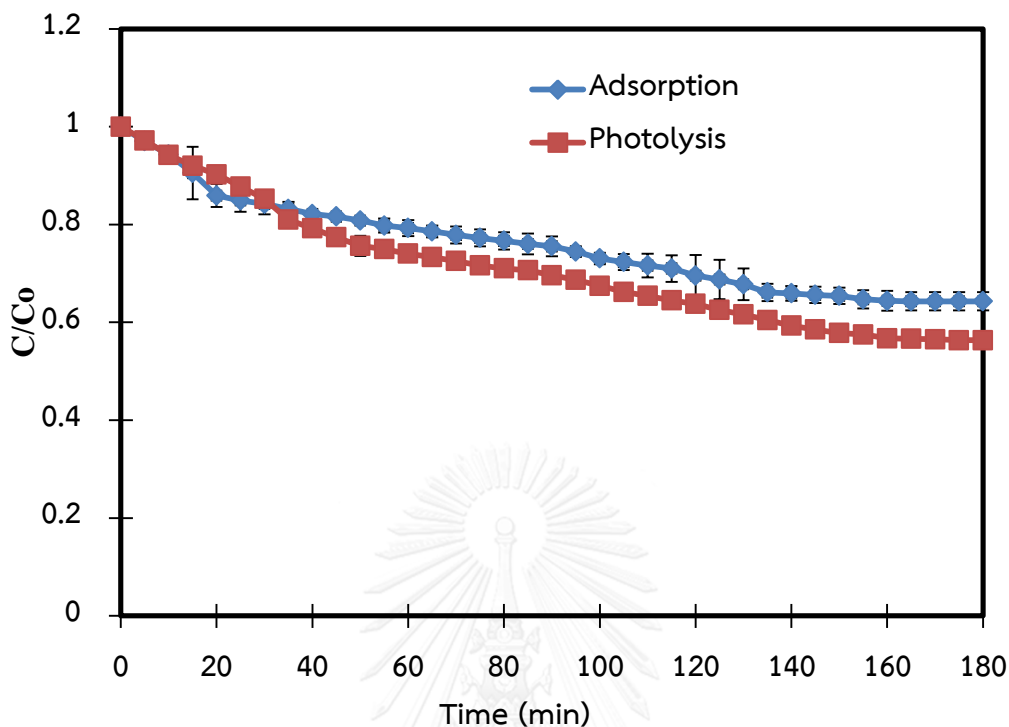
Fig. 4. 20 Adsorption and photolysis of HCHO using commercial air filters (Polyester Eu 2)

Table 4. 12 Formaldehyde removal efficiency using commercial air filters (Polyester Eu 2) via photolysis and adsorption processes

	adsorption	photolysis
Percent formaldehyde Removal efficiency	35.50 ± 2.42	43.49 ± 0.13

In comparison, results from sections 3.4.1-3.4.3 reveal that the highest removal efficiency was received when using the TiO2 coated SF filters followed by the pure SF filters and the air commercial filters.

4.4 Kinetics study of HCHO treatment

Chemical kinetics is the study of the rate and mechanism by which one chemical species is converted to another. The rate is the mass, in moles, of a product produced or reactant consumed per unit time. The mechanism is the sequence of individual chemical events whose overall result produces the observed reaction. To analyze kinetically this experimental data of formaldehyde decomposition, the Langmuir–Hinshelwood (L-H), the widely used equation for describing the mechanism of the destruction of organic compounds, was applied. The LH kinetics is the most commonly used kinetic expression to explain the kinetics of the heterogeneous catalytic processes. It has been widely investigated to successfully describe the photocatalytic oxidation rate with different pollutants.

The relation of photocatalytic oxidation rate was studied. The HCHO degradation rate constants were obtained by fitting the experimental data using first order reaction kinetics and rate constant. The plots indicate that the slopes of fitted straight line using least square method followed the first order reaction [151].

1) Impact of initial formaldehyde concentration

Fig.4.21 shows the correlation between ln(C/Co) and treatment time at different initial HCHO concentrations. The plot indicates that the slopes of fitted straight line using the least square method followed the first order reaction. The simplified L-H reaction rate constants were calculated to be 0.0029, 0.0055, 0.0046 and 0.0033 min^{-1}, at initial concentration of 2.5, 5.0, 7.5, and 10.0 ppm, respectivly. The Simplified Langmuir-Hinshelwood forms, ln(C/Co) = -kKt = -K't, at different initial concentration are displayed in Table 4.13.
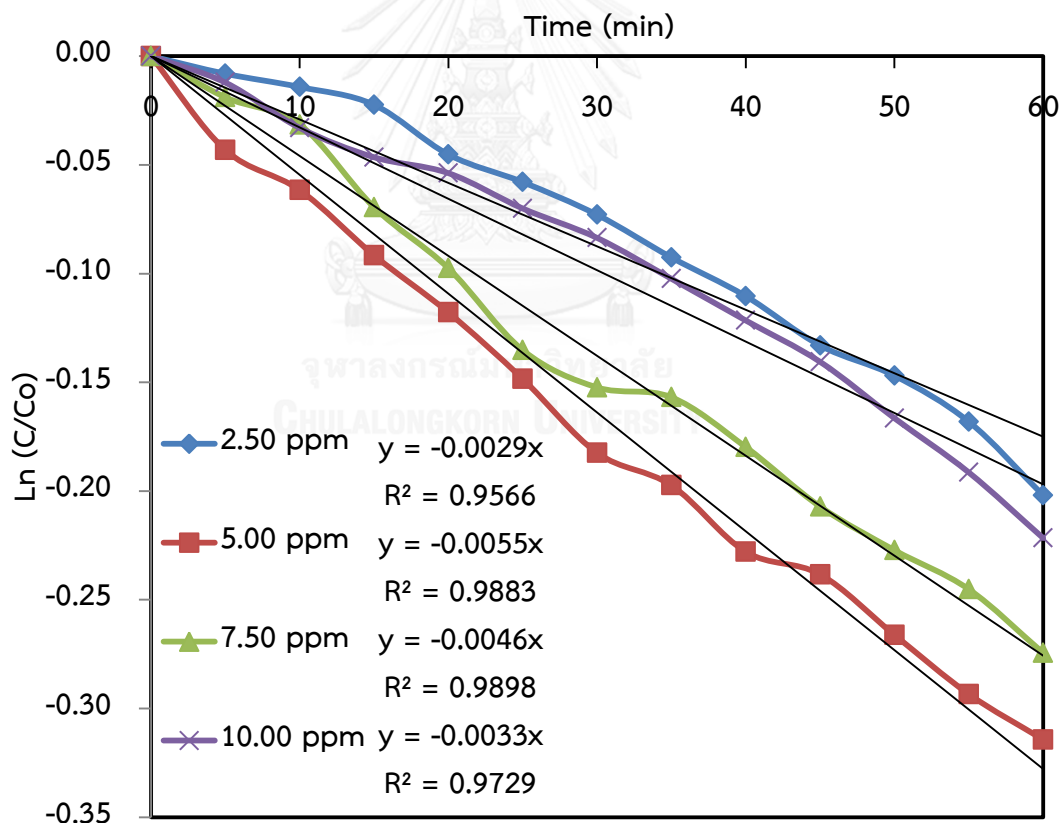
Fig. 4. 21 Correlation between ln (C/C_0) and time at different initial concentration of HCHO: 2.5, 5.0, 7.5, and 10 ppm

Table 4. 13 Simplified Langmuir-Hinshelwood form, $\ln(C_0/C) = kKt = K't$, at different initial concentration of HCHO

Initial HCHO concentration (ppm)	Simplified Langmuir-Hinshelwood form	$K'(min^{-1})$	R^2
2.5 ± 0.50	y = -0.0029x	0.0029	0.9566
5.0 ± 0.50	y = -0.0055x	0.0055	0.9883
7.5 ± 0.50	y = -0.0046x	0.0046	0.9898
10.0 ± 0.50	y = -0.0033x	0.0033	0.9729

2) Impact of the catalyst (TiO$_2$) dosage

Fig. 4.22 shows the correlation between $\ln(C/C_o)$ and treatment time at different catalyst dosages. The plot indicates that the slopes of fitted straight line using the least square method followed the first order reaction. for the The simplified L-H reaction rate constants were calculated to be 0.0052, 0.0049, 0.0065, and 0.0049 min^{-1}, at catalyst dosage of 1.0%, 2.5%, 5.0%, and 7.5 % (wt.TiO$_2$/ vol. sol.), respectivly. The Simplified Langmuir-Hinshelwood forms at different dosages of TiO$_2$ are displayed in Table 4.14.
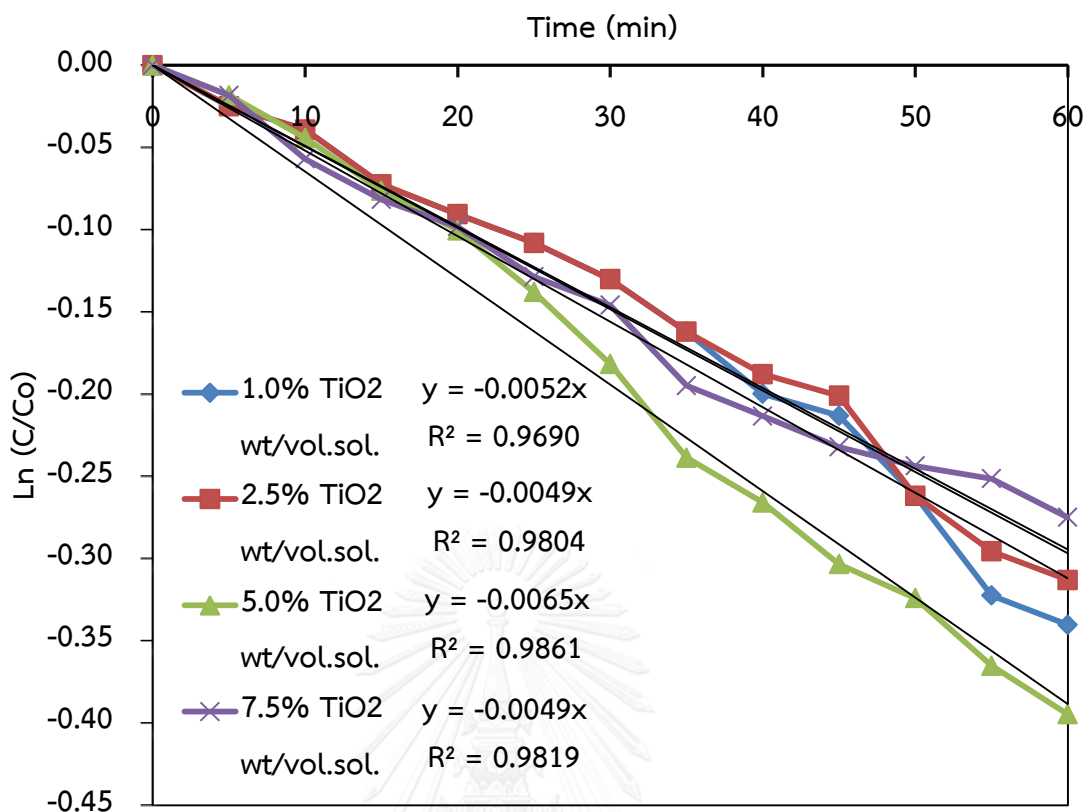
Fig. 4. 22 Correlation between ln (C/C$_0$) and time at different catalyst (TiO$_2$) dosages: 1.0, 2.5, 5.0, and 7.5 % wt. /vol.sol.

Table 4. 14 Simplified Langmuir-Hinshelwood form, ln(C$_0$/C) = kKt = K't, at different dosages of TiO$_2$.

Dosage of TiO$_2$ (%TiO$_2$wt/ vol.sol.)	Simplified Langmuir-Hinshelwood form	K'(min^{-1})	R^2
1.0	y = -0.0052x	0.0052	0.9690
2.5	y = -0.0049x	0.0049	0.9804
5.0	y = -0.0065x	0.0065	0.9861
7.5	y = -0.0049x	0.0049	0.9819

3) Impact of air flow rate

Fig. 4.23 shows the correlation between ln(C/Co) and treatment time at different air flow rate. The plot indicates that the slopes of fitted straight line using the least square method followed the first order reaction. The simplified L-H reaction rate constants were calculated to be 0.0037, 0.0053, and 0.0061 min^{-1} at the air flow rate of 3, 4, and 5 L/min, respectivly. The Simplified Langmuir-Hinshelwood forms at different air flow rate are displayed in Table 4.15.
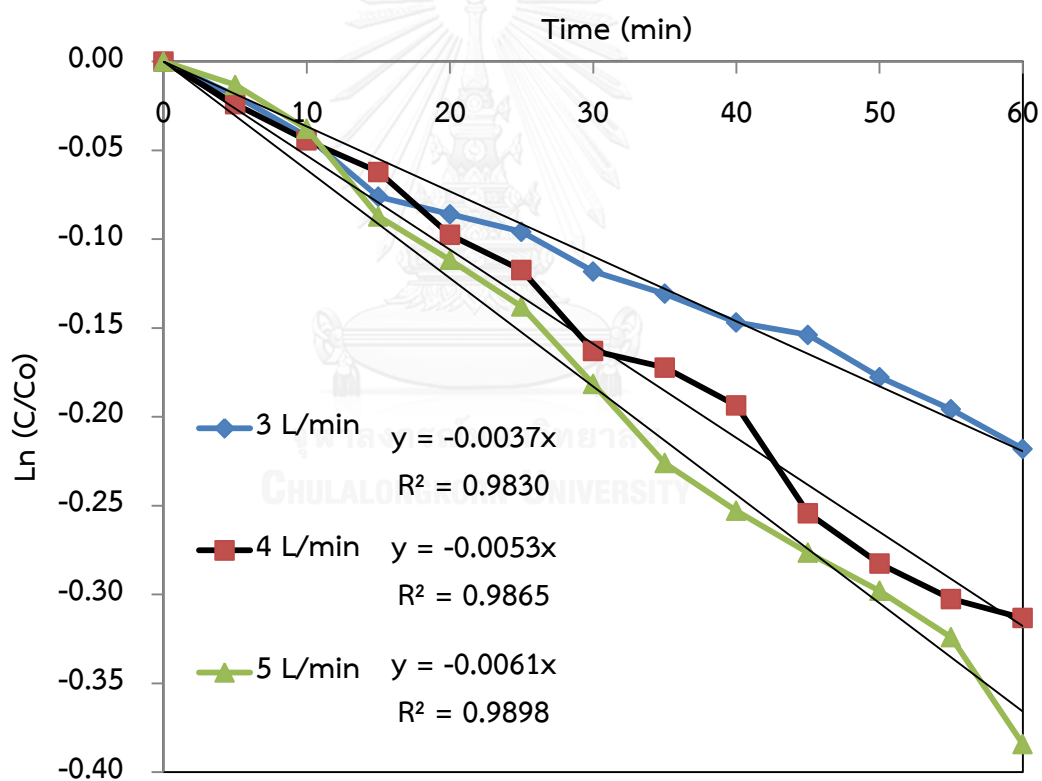
Fig. 4. 23 Correlation between ln (C/C$_0$) and time at different air flow rate: 3, 4, and 5 L/min

Table 4. 15 Simplified Langmuir-Hinshelwood form, $\ln(C_0/C) = kKt = K't$, at different air flow rate

Air flow rate (L/min)	Simplified Langmuir-Hinshelwood form	K'(min^{-1})	R^2
3	y = -0.0037x	0.0037	0.9830
4	y = -0.0053x	0.0053	0.9865
5	y = -0.0061x	0.0061	0.9898

4.5 Application of the TiO$_2$ coated SF filters for photocatalytic oxidation (PCO) of formaldehyde in a large modeling room

Photocatalytic oxidation of TiO$_2$ coated SF filters for treatment of HCHO was tested in the large modeling room with the dimensions of 1.20 m × 1.20 m × 1.85 m. The temperature and relative humidity were continuously monitored by the Humidity and temperature data logger (HT 10). For all sets of experiment, temperature and relative humidity ranged from 25-30 °C and 65-70 %, respectively. The TiO$_2$-coated SF filter was incorporated with the commercial air purifier equipped with two UV-C lamps. The modified air purifier was then placed inside the modeling room. Formaldehyde source was placed in the middle of the modeling room and allowed to reach equilibrium. A mixing electrical fan was installed in the room to ensure adequate mixing of formaldehyde in the room. Gaseous formaldehyde in the

room was sucked through the air purifier at an air flow rate of 84.40 ft^3/min. Formaldehyde concentration was continuously measured every 5 min. for 8 hrs.

Set of experiments was conducted to investigate the effect of initial formaldehyde concentrations on removal efficiency of the filters. There were two replications for each experiment. Experimental conditions were set as follows: the catalyst dosage of 2.50 % (wt./vol. sol.), UV light intensity at approximately 0.85 mW/cm^2 at wavelength of 254 nm. While, the initial formaldehyde concentration was varied as 5.00 ± 0.50 ppm, 7.50 ± 0.50 ppm, and 10.00 ± 0.50 ppm. The Gaseous formaldehyde concentrations in the room were measured using the Hand-held Formaldehyde Meter (HAL-HFX205) until a steady state is reached. The steady state of formaldehyde concentration was reported as the initial concentration. Then the modified air purifier was turned on and the formaldehyde concentrations were continuously measured every 5 minutes until a steady state is reached again.

As seen from Fig. 4.24, the photocatalytic degradation rate of formaldehyde at the initial concentration of 7.50 ppm was faster as compared to those of formaldehyde at other concentrations. While the highest removal efficiency (54.72 ± 1.75 %) was obtained at the initial concentration of 5.00 ppm and TiO_2 dosage of as 2.50 % (wt./vol. sol.) displayed in Table 4.16. Photocatalytic degradation of HCHO has demonstrated the potential use of the TiO_2-coated SF filter as an alternative photocatalytic oxidation process and economic indoor air purification.
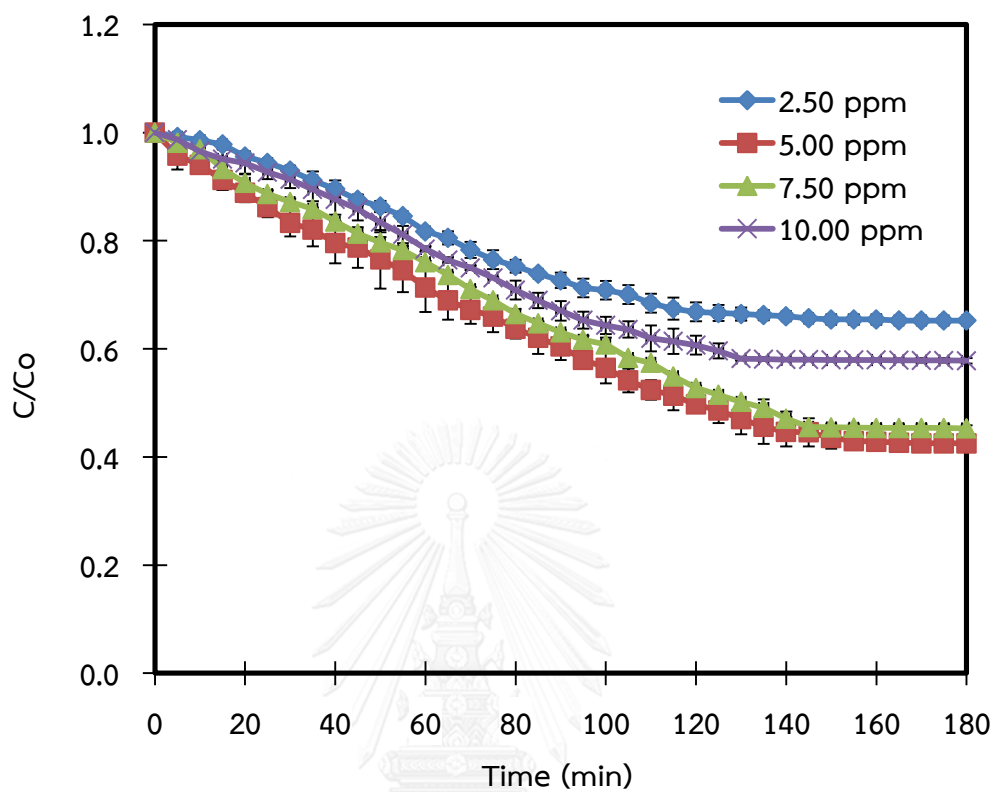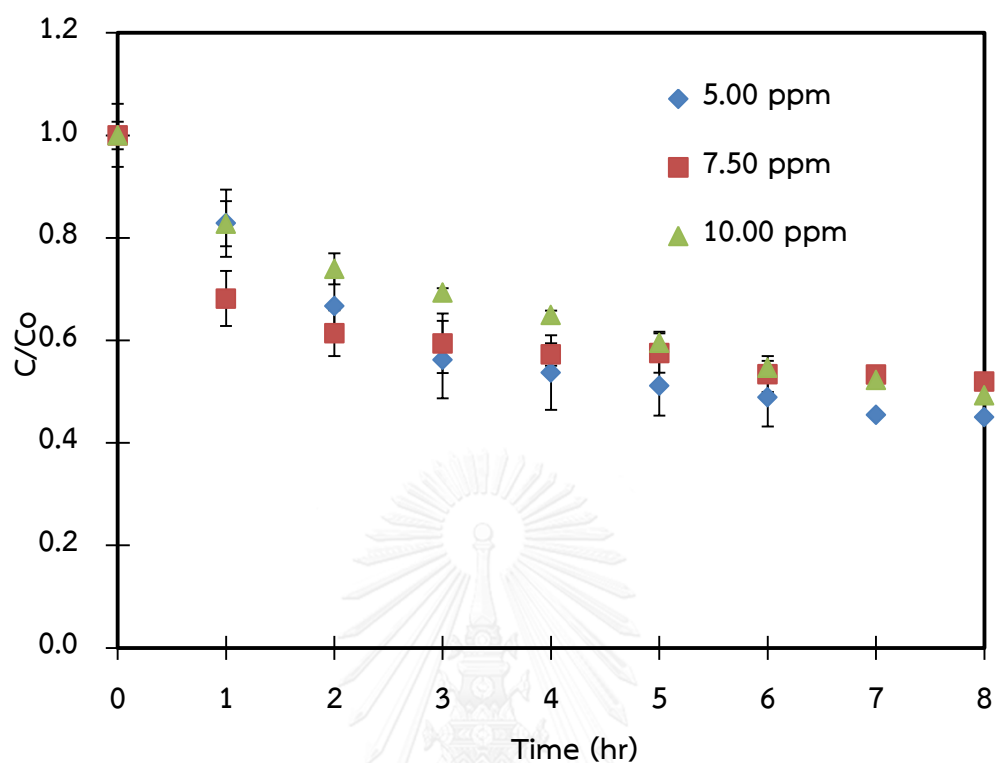
Fig. 4. 24 Photocatalytic oxidation of gaseous formaldehyde at different initial concentrations

Table 4. 16 Effect of initial concentration on formaldehyde removal efficiencies

	Initial Concentrations of Formaldehyde (ppm)		
	5.00 ± 0.50	7.50 ± 0.50	10.00 ± 0.50
Percent formaldehyde removal efficiency	54.72 ± 1.75	47.09 ± 2.23	46.56 ± 1.51

4.6 Cost comparison between the SF filters and the commercial air filter

Cost comparation of the commercial and synthesized filters were performed as shown in Table 4.17. The results suggested that the pure SF filter was much less expensive than the TiO_2 coated SF filter and the commercial air filter (Polyester class Eu 2 thickness 0.5 mm, 720 cm^2). Total cost for synthesis of pure SF filter and SF coated with TiO_2 is approximately 15.41 baht/piece and 51.41 bath/piece, resectivery (the detail for culculation is described in appendix C). While the cost of commercial filters is around 259 bath/piece.

Table 4. 17 Cost comparison between the SF filters and the commercial air filter

Commercial filter (Polyester Eu 2)	SF filter	TiO_2-coated SF filter
259 bath/piece	15.41 bath/piece	51.41 bath/piece
RE = 43 %	RE = 42 %	RE = 68 %

CHAPTER V

CONCLUSION AND RECOMMENDATIONS

5.1 Conclusion

This research was divided into 4 phases. Phase 1 was the measurement of gaseous formaldehyde concentrations in indoor air of the gross anatomy laboratory (GAL) in the Division of Anatomy, College of Medicine and Public health, Ubonratchathani University, Thailand. The results of gaseous formaldehyde concentrations during the three classes of GAL were relatively high as compared to other works (IARC, 2006). The general health questionnaires (GHQ) were studied with volunteers as medical students who spending time in GAL. The result showed that five medical symptoms have been diagnosed and cured among the sampling group including irregular heart beat; throat irritation, cough and sore throat, phlegm, eye irritation, headache, and dizziness. This information could be used as a fundamental data for planning to protect medical students, instructors, and cadaver related workers from the toxicity of formaldehyde.

In phase two, synthesis of SF and TiO_2-coated SF filters and study of their morphological structure and physical properties were performed. In Phase 3, treatment of formaldehyde in a small reactor using the synthesized SF filters and commercial filter were investigated. Three impacts affecting the removal efficiency of HCHO including intial HCHO concentration, catalyst dosage, and air flow rate were

studied. The study showed the feasibility of using SF filter as efficient air purifier for HCHO. The highest removal efficiency was approximately 68.21 ± 0.48 % at the initial concentration of 5.0 ± 0.5 ppm, catalysis dosage of 5.0 wt.TiO_2/vol. sol., and air flow rate of 5 L/min. Phase 4 focused on the application of the TiO_2 coated SF filters for formaldehyde removal in a large modeling room via photocatalytic oxidation process. The highest removal efficiency of approximately 57.15 ± 1.65 % was obtained at the initial concentration of 5.00 ppm. Finally, cost comparison between the SF filters and the commercial air filter was studied. The results revealed that the TiO_2 coated SF filter is much cheaper than the commercial air filter. This new integrating material has demonstrated the potential use of the TiO_2 coated SF filters as an alternative and economic indoor air purifier.

5.2 Recommendations

The gaseous formaldehyde concentrations in indoor air of the gross anatomy laboratory (GAL) should be measured for every semester. The health effect should be concerned with medical students or lab worker who spending time in GAL. For the application of TiO_2-coated SF filters as an air purifier, different air pollutants and ranges of air flow rate should be further studied.

Form this study, it can be seen clearly that TiO_2-coated SF filters can enhance the formaldehyde removal efficiency by photocatalytic oxidation, however, there are some issues arising such as pressure drop of air flow through the filter and the actual amount of TiO_2 coated on SF filters. Dosage of TiO_2 has an effect on

formaldehyde removal efficiency, in which increasing TiO_2 up to 5.0% wt.TiO_2/vol. sol. resulting in higher removal efficiency. However, when TiO_2 was increased up to 7.5 and 10.0 % wt.TiO_2/vol. sol., removal efficiency decreased. This may be caused by the limitation of UV light penetration through filters, and higher pressure drop occurrence as the TiO_2 dosage increased. Therefore, future work should study the effect of TiO_2 dosage in range between 1.0-5.0% wt.TiO_2/vol. sol..

In treatment process of formaldehyde removal, there are several mechanisms occur which is consisted of: mass transfer of reactants, adsorption of reactants on the catalyst surface, photochemical reaction on the surface, desorption of products from the surface, and mass transfer of products from the surface into the bulk of the fluid (air). From this study, formaldehyde removal in a small reactor using the synthesized SF filters was dominated by adsorption mechanism. The pollutant was adsorbed on the surface (mostly the internal surface) of SF filter material. The enhancement of removal efficiency by photocatalytic oxidation reaction can be found for the maximum of approximately 20%. This may be due to the limitation of relatively low UV light intensity and relative humidity in the reactor. Therefore, the recommendation for future work for this aspect would be to study the effect of UV light intensity and relative humidity more inclusively.

REFERENCES

1. EPA., U.S., An Introduction to Indoor Air Quality-Organic Gases (Volatile Organic Compounds – VOCs). 2009.

2. Osawa, H. and M. Hayashi, Status of the indoor air chemical pollution in Japanese houses based on the nationwide field survey from 2000 to 2005. Building and Environment, 44, (7):1330-1336. 2009.

3. US.EPA., Health and environmental effects profile for formaldehyde. EPA/600/x-85/362. Environmental Criteria and Assessment Office, Office of Health and Environmental Assessment, Office of Research and Development, Cincinnati, OH. 1988.

4. IARC., IARC Monographs on the Evaluation of Carcinogenic Risks to Humans, Wood Dust and Formaldehyde, Lyon, 62: 217-362. 1995.

5. Belanger, P.L. and K.H. Kilburn, California Society for Histotechnology, Los Angeles, CA,Health Hazard Evaluation Report (NIOSH Report No. HETA 81-422-1387), Cincinnati, OH,US Department of Health and Human Services, Public Health Service, Centers for Disease Control, National Institute for Occupational Safety and Health. 1981.

6. T, M.o.I., he Notification of the Ministry of Interior, issued under the Announcement of Revolutionary Party No. 103, dated March 16, B.E. 2515 (1972), published in the Royal Government Gazette Vol. 94, Part 64, dated July 12, B.E. 2520 (1977). 1977.

7. (ACGIH), A.C.o.G.I.H., Notice of intended changeformaldehyde. Appl Occup Environ Hyg, 7: 852-74. 1992.

8. Japan Ministry of Health, L.a.W., Guidelines for reducing formaldehyde concentrations in indoor air of workplaces. Tokyo: Ministry of Health, Labour and Welfare. . 2002.

9. Ohmichi, K., et al., Formaldehyde exposure in a gross anatomy laboratory-personal exposure level is higher than indoor concentration. Environ Sci Pollut Res Int, 13: 120-124. 2006.

10. EPA., U., Characterizing air emissions from indoor sources, EPA report: EPA/600/F-95/005, US Environmental Protection Agency, Washington, DC. 1995.

11. (ATSDR), A.f.T.S.a.D.R., Toxicological Profi le for Formaldehyde (Draft). Public Health Service, U.S. Department of Health and Human Services, Atlanta, GA. 1997.

12. (WHO), W.H.O., Environmental Health Criteria for Formaldehyde. Vol 89. World Health Organization, Geneva, Switzerland. 1989.

13. (NIOSH), N.I.f.O.S.a.H., Criteria for a recommended standard: occupational occupational exposure to formaldehyde. (DHEW publication no. (NIOSH) 77-126). Cincinnati, Ohio: National Institute for Occupational Safety and Health. 1997.

14. Thongsri, T. and S. Petkasem, Health risk from exposure to formaldehyde dispersed in anatomy class. Journal of Department of Science Service, 55: 9-15. 2007.

15. Hoffmann, M.R., et al., Chem. Rev. 95., 1995.

16. Jardim, W.F. and R.M. Alberici, Photocatalytic destruction of VOCs in the gasphase using titanium dioxide, Appl. Catal. B: Environ. 14: 55–68. 1997.

17. Zhao, J. and X.D. Yang, Photocatalytic oxidation for indoor air purification: a literature review, Build. Environ. 38: 645–654. 2003.

18. Fujishima, A. and K. Honda, Electrochemical photolysis of water at a semiconductor electrode. Nature, 238: 37-38. 1972.

19. Formenti, M., et al., Heterogeneous photocatalysis for partial oxidation of paraHns. Chem. Tech. 680-681. 1971.

20. Hager, S., R. Bauer, and G. Kudielka, Photocatalytic oxidation of gaseous chlorinated organics over titanium oxide. Chemosphere, 41: 1219-1225. 2000.

21. Perez-Rigueiro, J., Mechanical properties of silkworm silk in liquid media. Polymer. 41(23). 8433-8439. 2000.

22. Chen, C., et al., Preparation of non-woven mats from all-aqueous silk fibroin solution with electrospinning method, J. Polymer, vol.4: 6322- 6327. 2006.

23. Jingxin, Z., et al., Electrospinning and rheology of regenerated Bombyx mori silk fibroin aqueous solutions:The effects of pH and concentration, Polymer, vol.49: 2880 – 2885. 2008.

24. Li, G.Y., et al., The natural silk spinning process, Eur J Biochem., vol. 268: 6600-6606. 2001.

25. Wang, X., et al., Controlled release from multilayer silk biomaterial coatings to modulate vascular cell responses. Biomaterials, vol.29: 894 - 903. 2008.

26. Karageorgiou, V., et al., Porous silk fibroin 3-D scaffolds for delivery of bone morphogenic protein-2 in vitro and in – vivo, J Biomed Mater Res,vol.78A,: 324- 334. 2006.

27. Altman, G.H., et al., Silk-based Biomaterials, Biomaterials, vol.24: 401-416. 2003.

28. Wang, Y.Z., et al., Cartilage tissue engineering with silks caffolds and human articular chondrocytes, Biomaterials, vol.27: 4434- 4442. 2006.

29. Vachairoroj, N., et al., Int. J. Biol. Macromol. 45: 470–477, 2009.

30. Chamchongkaset, J., et al., Adv. Mater. Res. 8: 685–688, 2008.

31. Triped, J., et al., Synthesis of silk fibroin fiber for indoor air particulate removal. International Journal of Environmental Science and Engineering 2:3. 2010.

32. Jones, A.P., Indoor air quality and health. J. Atmosp. Environ. 33:4535-4564. 1999.

33. Robinson, J. and W.C. Nelson, National Human Activity Pattern Survey Data Base, United States Environmental Protection Agency, Research Triangle Park, NC. 1995.

34. US.EPA., Characterizing air emissions from indoor sources. EPA Report EPA/600/F-95/005, UnitedStates Environmental Protection Agency, Washingtion, DC. 1995.

35. Niu, J.L., Some significant environmental issues in high-rise residential building design in urban areas. J. Energy Build. 36: 1259-1263. 2004.

36. Gao, Z.S., Review of indoor emission source models. Part 1: overview. J. Environ. Pollut., 120: 533-549. 2002

37. Panel, C.I.R.E., Final report on the safety assessment of formaldehyde. J. Am. Coll. Toxicol., 3: 157-184. 1984.

38. Reuss, G., et al., Formaldehyde. In: Ullmann's Encyclopedia of Industrial Chemistry, 6th rev. Ed., Vol. 15, Weinheim, Wiley-VCH Verlag GmbH and Co.: 1-34. 2003.

39. Gerberich, H.R. and G.C. Seaman, Formaldehyde. In: Kroschwitz, J.I. and Howe-Grant, M.,eds, Kirk-Othmer Encyclopedia of Chemical Technology, 5th Ed., Vol. 11, New York, John Wiley and Sons. 929-951. 2004.

40. Lewis, B., Formaldehyde in dentistry: A review for the millennium. J. clin. pediatr. Dent. 22: 167-177. 1998.

41. Kilburn, K.H., B.C. Seidman, and R. Warshaw, Neurobehavioral and respiratory symptoms of formaldehyde and xylene exposure in histology technicians. Arch. environ Health, 40: 229-233. 1985.

42. Shaham, J., et al., DNA-protein crosslinks and p53 protein expression in relation to occupational exposure to formaldehyde. Occup. environ. Med., 60: 403-409. 2003.

43. Williams, T.M., R.J. Levine, and P.B. Blunden, Exposure of embalmers to formaldehyde and other chemicals. Am. ind. Hyg. Assoc. J., 45: 172-176. 1984.

44. Stewart, P.A., et al., Study design for assessing exposures of embalmers for a case control study. Part I. Monitoring results. Appl. occup. environ. Hyg., 7: 532-540. 1992.

45. Ying, C.J., et al., Micronuclei in nasal mucosa, oral mucosa and lymphocytes in students exposed to formaldehyde vapor in anatomy class. Biomed. environ. Sci., 10: 451-455. 1997.

46. He, J.L., L.F. Jin, and H.Y. Jin, Detection of cytogenetic effects in peripheral Lymphocytes of students exposed to formaldehyde with cytokinesis-blocked micronucleus assay. Biomed. environ. Sci., 11: 87-92. 1998.

47. Burgaz, S., et al., Micronuclei frequencies in exfoliated nasal mucosa cells from pathology and anatomy laboratory workers exposed to formaldehyde. Neoplasma, 48: 144-147. 2001.

48. Spirtas, R., et al., TLV carcinogenicity categories: recent modifications. Appl. Occup. Environ. Hyg. 16: 875-883. 2001.

49. IARC., IARC Monographs on the Evaluation of Carcinogenic Risks to Humans, Vol. 83, Tobacco Smoke and Involuntary Smoking, Lyon. 2004.

50. Hao, G., L. Liu, and J. Wu, Clinical analysis on 17 cases of acute poisoning caused by the inhalation of formaldehyde. Hebei Med, 4(6):58-9. 1998.

51. Liu, W.J. and J.L. Song, Analysis on a case of formaldehyde poisoning. J Chin People's Public Secur Univ. 24(4): 22-23. 2001.

52. Hao, Y.A., Case of death caused by inadvertently drinking formaldehyde. Chin J Forensic Med, 19(S1): 65. 2004.

53. Li, S. and Z. Song, An incident of food poisoning in students caused by formaldehyde. Chin. J. Sch. Health, 27(4): 341. 2006

54. Wilhelmsson, B. and M. Holmstrom, Possible mechanisms of formaldehyde-induced discomfort in the upper airways. Scand J. Work Environ. Health, 18(6):403–407. 1992.

55. Yuan, C.H. and B. Dong, Health effect on anatomy teachers exposed to formaldehyde. Chin. J. Clin. Anat. 25(3):105. 2007.

56. Weisskopf, M.G., et al., Prospective study of chemical exposures and amyotrophic lateral sclerosis. J Neurol Neurosurg Psychiatry, 80(5): 558-561. 2009.

57. Armon, C., An evidence-based medicine approach to the evaluation of the role of exogenous risk factors in sporadic amyotrophic lateral sclerosis. Neuroepidemiology 22(4): 217-28. 2003.

58. ATSDR., Toxicological profile for formaldehyde: Agency for Toxic Substances and Disease Registry & Health and Human Services. 1999.

59. US.EPA., US Environmental Protection Agency. Indoor Air Quality (IAQ). www.epa.gov/indoor-air-quality-iaq. 2014.

60. Kim, K.J., Adsorption–desorption characteristics of VOCs over impregnated activated carbons. Catalysis Today. 111(3-4): 223–228. 2006.

61. Wittmann, G., K. . , Preparation, structural characterization and photocatalytic activity of mesoporous Ti-silicates", Applied Catalysis B: Environmental. 61(1-2). 47-57. 2005.

62. William, J.C. and P.E. Lead, VOC Control strategies in plant design. In Chemical Processing: Project Engineering Annual. 1997.

63. Marks, J.R. and T. Rhoads, Planning saves time and money,when installing VOC controls.Chemical Processing, 5, 42. 1991.

64. Ottenger, S.P.P. and A.H.C. van den Oever, Kinetics of organic compound removal from waste gases with a biological fil-ter. Biotechnology and Bioengineering, 12(25). 1983.

65. Leson, G. and A.M. Winer, Bio-filtration: an innovative air pollution control technology for VOC emissions.Journal of the Air and Waste Management Association, 41(8), 1045. 1991.

66. Kiared, K., et al., Biological elimination of VOCs in bio-filter.Environmental Pro-gress, 15(3), 148. 1996

67. Webster, T.S., et al., Bio-filtration of odours, toxics and volatile organic compoundsfrom publicly owned treatment works.Environmental Progress, 15(3), 141. 1996.

68. Li, G.Y., et al., Pollution profiles, health risk of VOCs and biohazards emitted from municipal solid waste transfer station and elimination by an integrated biological-photocatalytic flow system: a pilot-scale investigation, J. Hazard. Mater. 250. 147-154. 2013.

69. An, T.C., et al., Comparison of the removal of ethanethiol in twin-biotrickling filters inoculated with strain RG-1 and B350 mixed microorganisms, J. Hazard. Mater. 183. 372-380. 2010.

70.   Destaillats, H., et al., Key parameters influencing the performance of photocatalytic oxidation (PCO) air purification under realistic indoor conditions. Applied Catalysis B: Environmental, 2012. 128: p. 159-170.

71.   Ravelli, D., D. Dondi, and A.M. Fagnoni, Albini, Photocatalysis. A multi-faceted concept for green chemistry, Chem. Soc. Rev. 38. 1999-2011. 2009.

72.   Wang, S.B., H.M. Ang, and M.O. Tade, Volatile organic compounds in indoor environment and photocatalytic oxidation: state of the art, Environ. Int. 33. 694-705. 2007.

73.   An, T.C., et al., Photocatalytic degradation and detoxification of o-chloroaniline in the gas phase: mechanistic consideration and mutagenicity assessment of its decomposed gaseous intermediate mixture, Appl. Catal. B: Environ. 102. 140-146. . 2011.

74.   Sun, L., et al., Mechanistic study and mutagenicity assessment of intermediates in photocatalytic degradation of gaseous toluene, Chemosphere 78. 313-318. . 2010.

75.   Chen, J.Y., et al., Adsorption and degradation of model volatile organic compounds by a combined titania-montmorillonite-silica photocatalyst, J. Hazard. Mater. 190. 416-423. 2011.

76.   Cao, L., photocatalytic oxidation of toluene on nanoscale TiO2 catalysts: studies of deactivation and regeneration", Journal of catalysis. 196(2). 253-261. 2000.

77.   Zhao, J. and X. Yang, Photocatalytic oxidation for indoor air purification: a literature review. Building and Environmetal. 38(5). 645-654. 2003.

78.   Radwan, A. and Al-Rasheed, Water treatment by heterogeneous photocatalysis an overview in 4th Saline Water Desalination Research Institute Conversion Corporation (SWCC).Saudi Arabia: Jeddah. . 2005.

79.   Fox, M.A. and M.T. Dulay, Heterogeneous photocatalysis. Chemical Reviews. 93(0). 341-357. 1993. .

80.   Tompkins, D.T., Evaluation of photocatalytic air cleaning capability: a literature review and engineering analysis. ASHARE Research Project RP-1134. 2001.

81.   Ohtani, B., Preparing articles on photocatalysis beyond the illusions, misconceptions, and speculation. Chemistry Letters 37, 217-229. 2008.

82.   Jinhan, M., et al., Photocatalytic purification of volatile organic compounds in indoor air: A literature review. Atmos. Environ. 43: 2229-2246. 2009.

83. Ollis, D.F., Photocatalytic purification and remediation of contaminated air and water. Comptes Rendus De L Academie Des Sciences Serie Ii Fasci-cule C-Chimie 3: 405-411. 2000.

84. Chen, D.H., X.J. Ye, and K.Y. Li, Oxidation of PCE with a UV LED photocatalytic reactor. Chem. Eng. Tech. 28: 95-97. 2005.

85. Attwood, A.L., et al., Identification of a surface alkylperoxy radical in the photocatalytic oxidation of acetone/O^{-2} over TiO_2. J. Phy. Chem. A, 107: 1779-1782. 2003.

86. Shie, J.L., et al., Photodegradation kinetics of formaldehyde using light sources of UVA, UVC and UVLED in the presence of composed silver titanium oxide photocatalyst. J. Hazard. Materials, 155: 164-172. 2008.

87. Wang, K.H., et al., The study of the photocatalytic degradation kinetics for dichloroethylene in vapor phase. Chemosphere, 39:1371-1384. 1999.

88. Egerton, T.A. and C.J. King, The influence of light intensity on photoactivity on TiO_2 pigmented systems. J. Oil and Colour Chem. Assoc., 62: 386-391. 1979.

89. Zhong, L., et al., Modeling and physical interpretation of photocatalytic oxidation efficiency in indoor air applications. Building and Environment, 2010. 45(12): p. 2689-2697.

90. Al-Ekabi, H. and N. Serpone, Kinetic-studies in heterogeneous photocatalysis .1.Photocatalytic degradation of chlorinated phenols in aerated aqueous-solutions over TiO2 supported on a glass matrix. J. Phys. Chem. 92: 5726-5731. 1988. .

91. Chen, D. and A.K. Ray, Removal of toxic metal ions from wastewater by semiconductor photocatalysis. Chem. Eng. Sci. 56. 1561-1570. 2001

92. Yang, J., et al., A study of the photocatalytic oxidation of formaldehyde on $Pt/Fe_2O_3/TiO_2$ Journal of Photochemistry and Photobiology A: Chemistry 137. 197-202. 2000.

93. Bodaghi, H.Y., Evaluation of the photocatalytic antimicrobial effects of a TiO2 nanocomposite food packaging film by in vitro and in vivo tests. LWT - Food Science and Technology. 50 (2). 702-706. . 2013.

94. Strehlow, W.H. and E.L. Cook, Compilation of energy band gaps in elemental and binary compound semiconductors and insulators. Journal of Physical and Chemical Reference Data. 2(1). 163–200. 1973.

95. Lim, T.H. and S.D. Kim, Trichloroethylene degradation by photocatalysis in annular flow and annulus fluidized bed photoreactors," Chemosphere. 54 (3). 305-312. 2004.

96.   Farhanian, D., et al., Impact of design parameters on the performance of ultraviolet photocatalytic oxidation air cleaner. Building and Environment, 2013. 66: p. 148-157.

97.   Kim, J.H., Control of the dispersion properties of a TiO2 nano powder for electronic paper. Journal of the Korean Physical Society. 48(8). 1329-1333. 2006.

98.   Behnajady, M.A., et al., Investigation of the effect of heat attachment method parameters at photocatalytic activity of immobilized ZnO nanoparticles on glass plate. Desalination, 2009. 249(3): p. 1371-1376.

99.   Bhatkhande, D.S., Pangarkar, V.G., Beenackers, A.A.C.M. , Photocatalytic degradation for environmental applications a review. Journal of Chemical Technology and Biotechnology. 77(1). 102-116. . 2001.

100.   Bickley, R.I., A structural investigation of titanium dioxide photocatalysts. Journal of Solid State Chemistry. 92(1). 178-190. 1991.

101.   Smyth, J.R. and D.L. Bish, Crystal Structures and Cation Sites of the Rock-Forming Minerals.Boston: ALLEN & UNWIN. 1988.

102.   Moy, R.L., L. A., and A. Zalka, Commonly used suture materials in skin surgery. J. Am Fam. Physician. 44(6): 2123–2128. 1991.

103.   Zhou, C.Z., Fine organization of B. mori fibroin heavy chain gene. J. Nuc. Acids Res. 28(12): 2413-2419. 2000.

104.   Tanaka, K., S. Inoue, and S. Mizuno, Hydrophobic interaction of P25, containing Asn-linked oligosaccharide chains, with the H-L complex of silk fibroin produced by B. mori. J. Insect Biochem Mol Biol. 29(3): 269-276. 1999.

105.   Kaplan, D.L., et al., Protein based materials. Boston: Birkhauser. 103–131. 1998.

106.   Zhou, C.Z., et al., Silk fibroin: structural implications of a remarkable amino acid sequence. J. Proteins. 44(2): 119–122. 2001.

107.   Vollrath, F. and D.P. Knight, Liquid crystalline spinning of spider silk. J. Nature. 410(6828): 541–548. 2001.

108.   Gosline, J., The structure and properties of spider silk. J. Endeavour.10: 37-44. 1986.

109.   Magoshi, J., et al., Mechanism of Fibre Formation of Silkworm. J. Amer. Chem. Society: 292-310. 1994.

110.   Vepari, C. and D.L. Kaplan, Silk as a biomaterial. Prog Polym Sci. 32. 991-1007. 2007.

111. Inoue, S., et al., Silk fibroin of Bombyx mori is secreted, assembling a high molecular mass elementary unit consisting of H-chain, L-chain, and P25, with a 6:6:1 molar ratio. J Biol Chem. 275. 40517–28. 2000.

112. Takahashi, Y., M. Gehoh, and K. Yuzuriha, Structure refinement and dif-fuse streak scattering of silk (Bombyx mori). Int J Biol Macromol24. 127–138. 1999.

113. Vollrath, F. and D. Porter, Silks as ancient models for modern polymers.Polymer. 50. 5623-5632. 2009.

114. Zhou, C.Z., et al., Silk fibroin: structural implications of a remarkable amino acidsequence. Protein Struct Funct Genet. 44. 119–122. 2001.

115. Foo, C.W.P., et al., Role of pH and charge on silk protein assembly in insects and spiders.Appl Phys A Mater Sci Process. 82. 223–233. 2006.

116. Jin, H.J. and D.L. Kaplan, Mechanism of silk processing in insects and spi-ders. Nature. 424. 1057–1061. 2003.

117. Marsh, R., R.B. Corey, and L. Pauling, An investigation of the structure ofsilk fibroin. Biochim Biophys Acta. 16. 1-34. 1995.

118. Bourne, P.E. and H. Weissig, Structural bioinformatics. 1st ed. Chichester: John Wiley & Sons Inc.; p. 649. 2003.

119. Garrett, R.H., Grisham, C.M. , Biochemistry. 3rd ed. Belmont: BrooksCole. p. 108. 2007.

120. Asakura, T., et al., The role of irregular unit, GAAS, on the secondary structure of Bombyx mori silk fibroin studied with13C CP/MAS NMR and wide-angle X-ray scattering.Protein Sci. 11. 1873–1877. 2002.

121. Kameda, T., et al., Hydrogen-bonding structure of serine side chains in Bombyx mori and Samia cynthia ricini silk fibroin determined by solid-state.2H.

122. Koh, L.-D., et al., Structures, mechanical properties and applications of silk fibroin materials. Progress in Polymer Science, 2015. 46: p. 86-110.

123. Rammensee, S., Huemmerich, D., Hermanson, K. D., Scheibel, T., Bausch, A. R. Rheological Characterization of hydrogels formed by recombinantly produced spider silk. J. Appl Phys A: 82261-82264. 2006.

124. Solheim, E., Sudmann, B., Bang, G., Sudmann, E. , Biocompatibility and effect on osteogenesis of poly (ortho ester) compared to poly (D, L-lactic acid). J. Biomed Mater Res. 49(2): 257-263. 2000

125. Meinel, L., Hofmann, S., Karageorgiou, V., Kirker-Head, C., McCool, J., Gronowicz ,G. et al., , The inflammatory responses to silk films in vitro and in vivo. J. Biomat. 26: 147-155. 2005.

126. Putthanarat, S., Stribeck, N., Fossey, S. A., Eby, R. K., Adams, W. W. , Investigation of the nanofibrils of silk fibers. J. Polymer. 41.7735-7747. 2000.

127. Gopal, R., et al., Electrospun nanofibrous filtration membrane. Journal of Membrane Science, 2006. 281(1): p. 581-586.

128. Chen, W.X., et al., Copper (II)-silk fibroin complex fibers as air-purifying materials for removing ammonia. Textile research journal, 2005. 75(4): p. 326-330.

129. Timothy, N.O., Photooxidation of sub-parts-per-million toluene and formaldehyde levels on titania using a glass-plate reactor. Environ. Sci. Technol. 30, 3578-3584. 1996. .

130. Obuchi, E., Sakamoto, T., Nsalsno, K., , Photocatalytic decomposition of acetaldehyde over TiO2/SiO2 catalyst.Chem. Eng. Sci. 54, 1525-1530. 1999. .

131. Coronado, J.M., Zorn1, M.E., Tejedor, I., Anderson, M.A., and Photocatalytic oxidation of ketones in the gas phase over TiO2 thin films: a kinetic study on the influence of water vapor. Appl. Catal. B Environ. 43, 329-344. 2003.

132. Sanongraj, W., Chemical Engineering on Kinetics and Reactor Design. [online] https://www.google.co.th [March 3, 2014]. 2014.

133. Shinde, P., et al., Properties of spray deposited titanium dioxide thin films and their application in photoelectrocatalysis. Solar Energy Materials and Solar Cells, 2008. 92(3): p. 283-290.

134. Andronic, L. and A. Duta, TiO 2 thin films for dyes photodegradation. Thin Solid Films, 2007. 515(16): p. 6294-6297.

135. Feng, X.-X., et al., Preparation and characterization of novel nanocomposite films formed from silk fibroin and nano-TiO 2. International journal of biological macromolecules, 2007. 40(2): p. 105-111.

136. Mizuki, M. and T. Tsuda, Relationship between atopic factors and physical symptoms induced by gaseous formaldehyde exposure during an anatomy dissection course. Arerugi. 50: 21-28. 2001.

137. Kunugita, N., et al., Exposure to formaldehyde during an anatomy dissection course. J UOEH. 26: 337-348. . 2004.

138. Ikuharu, M., et al., Formaldehyde concentrations in breathing zone in an anatomy Laboratory. Part 2. Effect of deodorization agent and mask. J of the Wakayama Med Soci, 54: 121-132. 2003.

139. Kunugita N, N.T., Kikuta A, Kawamoto T, Arashidani K. , Exposure to formaldehyde during an anatomy dissection course. J UOEH. 26: 337-348. . 2004.

140. Dharma, J., Simple method of measuring the band gap energy value of TiO_2 in the powder form using a UV/Vis/NIR spectrometer, Perkin Elmer. 2012.

141. Andronic, L. and A. Duta, TiO2 thin films for dyes photodegradation. Thin Solid Films. 55(3). 6294-6297. 2007.

142. Franks, F., Protein Biotechnology: Isolation, Characterization and Stabilization. The Humana Press Inc., Totowa. 1993.

143. Magnani, A., M.C. Roncolini, and R. Barbucci, Advantages and problems using FT-IR spectroscopy to study blood-surface interactions by monitoring the protein adsorption process. Mod. Aspects Protein Adsorpt. Biomater., 81. 1991.

144. Brame, E.G. and J.G. Grasselli, Infrared and Raman Spectroscopy; Part C, Marcel Dekker, New York.   . 1977.

145. Lu, Q., et al., Water-Insoluble Silk Films with Silk I Structure Acta Biomater, 6, 1380-1387. . 2010

146. Simi, C.K. and A.T. E., Nanocomposite based on modified TiO2-BSA for functional applications. Colloids and Surfaces B: Biointerfaces 71, 319-324. 2009.

147. Feng, X.X., Preparation and characterization of novel nanocomposite films formed silk fibroin and nano-TiO 2. International journal of biological macromolecusles. 40(2). 105-111. 2007.

148. Tsukada, M., et al., Structure and dyeability of Bombyx mori silk fibers with different filament sizes. Appl. Polym. Sci. 60 (10). 1619-1627. 1996.

149. Ishizaki, K., S. Komarneni, and M. Nanko, Porous materials, process technology and application. The Netherlands: Kluwer Academic Publisher. 1998.

150. Zhao, J. and X. Yang, Photocatalytic oxidation for indoor air purification: a literature review. Building and Environment, 2003. 38(5): p. 645-654.

151. Liu, H., et al., Kinetic analysis of photocatalytic oxidation of gas-phase formaldehyde over titanium dioxide. Chemosphere, 2005. 60(5): p. 630-635.

APPENDIX

APPENDIX A

Measurement of gaseous formaldehyde concentration

Fig. A. 1 Outside of the gross anatomy laboratory in the Division of Anatomy,

College of Medicine and Public health, Ubon Ratchathani University

APPENDIX B

General health questionnaires (GHQ)

No. ....

Questionnaire for air quality and the environment

The exposure to chemical risk to health and safety

The purpose of questionnaire is designed to collect data. The report attributed the thesis's doctoral student of program in Hazardous Substance and Environmental Management. The questionnaire was concerned with environment and the impact of exposure to chemicals at risk on health and safety. Therefore ask that you please fill out the questionnaire to meet the most true to the integrity of the findings.

In completing this questionnaire will not be offered individually. Comments or suggestions, it is particularly useful for research. Thank you for taking the time to answer the questionnaire.

Part 1 General Information Practice Anatomy Laboratory

Please: Check √ in box ❏

1. Age

   ❏ under 19 year old   ❏ 20 - 25 year old   ❏ over 26 year old

2. Gender

   ❏ Male   ❏ Female

3. Birth place

☐ Bangkok   ☐ Out of town

4. Present address

☐ Flat   ☐ Private house   ☐ Dorm

5. Levels of education

☐ Second year medical student   ☐ Third year medical student

6. How long have you been working in the anatomy laboratory?

☐ under 2 year   ☐ among 3 - 4 year

7. How many hours a day for working in anatomy laboratory?

☐ under 4 hours per day   ☐ among 5 - 8 hours per day

8. How many days a week working in anatomy laboratory?

☐ under 3 day per week   ☐ among 4 - 7 day per week

Part 2 General Health Information

Please: Check √ in box ☐ (answered choose more than 1 choice) and fill in the

blanks to complete the questionnaire

Have you ever had anyone of the following deseases?

☐ 1. Have you ever had an operation on the breasts (Which is not the result of an

accident).

☐ 2. Heart disease

☐ 3. Bronchitis

❏ 4. Pneumonia

❏ 5. Pleurisy

❏ 6. Pulmonary tuberculosis

❏ 7. Asthma

❏ 8. Sinus

❏ 9. Migraines

❏ 10. Dermatitis

❏ 11. Fever from pollen grain

❏ 12. Allergies from dust, mold spores, animal feathers

Have you been treated a variety of medical symptom during the year 2012 (after studying in anatomy laboratory).

	Been a disease	Never been a disease
1. Throat irritation, cough, sore throat	❏	❏
2. Phlegm	❏	❏
3. Eye irritation	❏	❏
4. Skin irritation	❏	❏
5. Nasal Irritation, shortness of Breath	❏	❏
6. Asthma, breathing difficulty	❏	❏
7. Headache, dizziness	❏	❏
8. Diarrhea, severe abdominal pain	❏	❏

9. Nausea and vomiting	❏	❏
10. Chest pain	❏	❏
11. Irregular heart beat	❏	❏

Additional comments:

....

....

....

....

....

....

....

APPENDIX C

Caculation

Band gap energy of TiO_2 using a UV–VIS spectrophotometer

The band gap engergy can be caculations by this eqution

Band Gap Energy $(E) = h * c / \lambda$ (Luminita, 2008) (1.1)

h = Planks constant = 6.626 x 10^{-34} Joules.sec

c = Speed of light = 3.0 x 10^{8} meter/sec

λ = Cut off walength = 390 x10^{-9} meter

Where 1eV = 1.6 x10^{-19} Joules

$$E = \frac{(6.626 \times 10^{-3} \, J.\sec) \times (3 \times 10^8 \, m/sec)}{390 \times 10^{-9} \, m}$$

$$E = 5.09692 \times 10^{-19}$$

$$ev = \frac{5.09692 \times 10^{-19} J \times 1ev}{1.6 \times 10^{-19} J}$$

$$ev = 3.185576$$

Claculate of cost of silk fibroin filter

Silk cocoons from waste slik cocoons

Silk fibroin filter in dimention 25 cm x 36 cm = 900 cm^2

Sunlight soap 70 g	= 12.5 bath	used 12.5 g	= 2.25 bath
Distilled water 1000 ml	= 3.30 bath	used 5 L	= 16.50 bath
TiO$_2$ 1000 g	= 200 bath	used 5 g	= 1.00 bath
Tween 80 500 ml	= 1,000 bath	used 2 ml	= 4.00 bath
PVA 1000 ml	= 200 bath	used 200 ml	= 40.00 bath

Electrical Energy Charge

1) Use electric pan 1,090 W for 1 hr = 1.09 kWh = 1.09 Unit

2) Use hot air oven 4,500 W for 3 hr = 0.67 kWh = 1.50 Unit

Total = 2.59 Unit

Energy charge of the first 15 kWh (1st –15th) = 2.35 bath

* Metropolitan Electricity Authority

Total = 66.10 bath

Cost of TiO$_2$-coted silk fibroin filter of 900 cm^2 = 66.10 bath

Cost of pure silk fibroin filter of 900 cm^2 = 21.10 bath

Claculate of cost in area 720 cm^2 (bath/ piece)

Cost of TiO$_2$-coted silk fibroin filter of 720 cm^2 = 51.41 bath/ piece

Cost of pure silk fibroin filter of 720 cm^2 = 16.41 bath/ piece

Commercial air filter

(Polyester class Eu 2 thickness 0.5 mm, 720 cm^2) = 259 bath/ piece

APPENDIX D

Efficiency of the HCHO removal in small modeling room

Table D. 1 Efficiency removal of PCO of effect initial HCHO concentration about 2.50 ± 0.50 ppm in a small modeling room

Time (min)	Test 1st	C_{CO} Test 1st	$C_{CO}/C_{CO,0}$	Test 2nd	C_{CO} Test 2nd	$C_{CO}/C_{CO,0}$	Average $C_{CO}/C_{CO,0}$	error
0	2.47	2.47	1	2.51	2.51	1.000003991	1.000001995	2.82199E-06
5	2.44	2.47	0.987854251	2.50	2.51	0.99601309	0.991933671	0.00576917
10	2.43	2.47	0.983805668	2.48	2.51	0.988031289	0.985918478	0.002987965
15	2.42	2.47	0.979757085	2.45	2.51	0.976058586	0.977907836	0.002615233
20	2.36	2.47	0.955465587	2.40	2.51	0.956104083	0.955784835	0.000451485
25	2.34	2.47	0.947368421	2.36	2.51	0.94014048	0.94375445	0.005110926
30	2.31	2.47	0.935222672	2.32	2.51	0.924176877	0.929699774	0.007810557
35	2.28	2.47	0.923076923	2.26	2.51	0.900231472	0.911654198	0.016154173
40	2.24	2.47	0.906882591	2.22	2.51	0.884267869	0.89557523	0.015991023
45	2.18	2.47	0.882591093	2.18	2.51	0.868304266	0.87544768	0.010102312
50	2.15	2.47	0.870445344	2.15	2.51	0.856331564	0.863388454	0.00997995
55	2.09	2.47	0.846153846	2.12	2.51	0.844358862	0.845256354	0.001269246
60	2.02	2.47	0.817813765	2.05	2.51	0.816422557	0.817118161	0.000983733
65	2.01	2.47	0.813765182	2.00	2.51	0.796468053	0.805116618	0.012230917
70	1.96	2.47	0.793522267	1.94	2.51	0.772522648	0.783022458	0.014848973
75	1.92	2.47	0.777327935	1.89	2.51	0.752568145	0.76494804	0.017507816
80	1.88	2.47	0.761133603	1.87	2.51	0.744586343	0.752859973	0.01170068
85	1.83	2.47	0.740890688	1.85	2.51	0.736604542	0.738747615	0.003030763
90	1.77	2.47	0.71659919	1.85	2.51	0.736604542	0.726601866	0.01414592
95	1.73	2.47	0.700404858	1.82	2.51	0.724631839	0.712518349	0.017131063
100	1.72	2.47	0.696356275	1.81	2.51	0.720640939	0.708498607	0.01717185
105	1.7	2.47	0.688259109	1.79	2.51	0.712659137	0.700459123	0.017253425
110	1.66	2.47	0.672064777	1.75	2.51	0.696695534	0.684380156	0.017416575
115	1.63	2.47	0.659919028	1.73	2.51	0.688713733	0.674316381	0.020360931
120	1.62	2.47	0.655870445	1.71	2.51	0.680731931	0.668301188	0.017579725
125	1.62	2.47	0.655870445	1.70	2.51	0.67674103	0.666305738	0.014757732
130	1.62	2.47	0.655870445	1.69	2.51	0.67275013	0.664310288	0.011935739
135	1.62	2.47	0.655870445	1.68	2.51	0.668759229	0.662314837	0.009113746
140	1.62	2.47	0.655870445	1.67	2.51	0.664768328	0.660319387	0.006291753
145	1.61	2.47	0.651821862	1.66	2.51	0.660777427	0.656299645	0.006332541
150	1.6	2.47	0.647773279	1.66	2.51	0.660777427	0.654275353	0.009195321
155	1.6	2.47	0.647773279	1.66	2.51	0.660777427	0.654275353	0.009195321
160	1.6	2.47	0.647773279	1.66	2.51	0.660777427	0.654275353	0.009195321
165	1.6	2.47	0.647773279	1.65	2.51	0.656786527	0.652279903	0.006373328
170	1.6	2.47	0.647773279	1.65	2.51	0.656786527	0.652279903	0.006373328
175	1.6	2.47	0.647773279	1.65	2.51	0.656786527	0.652279903	0.006373328
180	1.6	2.47	0.647773279	1.65	2.51	0.656786527	0.652279903	0.006373328

Table D. 2 Efficiency removal of PCO of effect initial HCHO concentration about 5.00 ± 0.50 ppm in a small modeling room

Time (min)	Test 1st	C_{CO} Test 1st	$C_{CO}/C_{CO,0}$	Test 2nd	C_{CO} Test 2nd	$C_{CO}/C_{CO,0}$	Average $C_{CO}/C_{CO,0}$	error
0	4.77	4.77	0.999993706	4.94	4.94	1	0.999996853	4.45029E-06
5	4.48	4.77	0.939154971	4.82	4.94	0.975724718	0.957439845	0.025858716
10	4.43	4.77	0.928665534	4.70	4.94	0.951449437	0.940057485	0.016110652
15	4.29	4.77	0.89929511	4.57	4.94	0.925151215	0.912223162	0.018283027
20	4.18	4.77	0.876218348	4.45	4.94	0.900875933	0.888547141	0.017435546
25	4.05	4.77	0.848945812	4.32	4.94	0.874577711	0.861761761	0.01812449
30	3.89	4.77	0.815379613	4.20	4.94	0.85030243	0.832841021	0.024694161
35	3.81	4.77	0.798596513	4.16	4.94	0.842210669	0.820403591	0.030839865
40	3.67	4.77	0.769226089	4.06	4.94	0.821981268	0.795603678	0.037303544
45	3.63	4.77	0.76083454	4.02	4.94	0.813889507	0.787362023	0.037515527
50	3.47	4.77	0.727268341	3.97	4.94	0.803774806	0.765521574	0.054098241
55	3.42	4.77	0.716778904	3.82	4.94	0.773430704	0.745104804	0.040058872
60	3.25	4.77	0.681114817	3.68	4.94	0.745109542	0.71311218	0.045251104
65	3.17	4.77	0.664331718	3.53	4.94	0.71476544	0.689548579	0.035662027
70	3.12	4.77	0.653842281	3.41	4.94	0.690490158	0.67216622	0.025913963
75	3.05	4.77	0.639157069	3.36	4.94	0.680375458	0.659766263	0.029145802
80	2.98	4.77	0.624471857	3.21	4.94	0.650031356	0.637251606	0.018073295
85	2.86	4.77	0.599297208	3.17	4.94	0.641939595	0.620618401	0.030152721
90	2.80	4.77	0.586709883	3.07	4.94	0.621710194	0.604210038	0.024748957
95	2.71	4.77	0.567828896	2.92	4.94	0.591366091	0.579597494	0.01664331
100	2.60	4.77	0.544752135	2.89	4.94	0.585297271	0.565024703	0.028669741
105	2.51	4.77	0.525871148	2.75	4.94	0.556976109	0.541423628	0.021994529
110	2.44	4.77	0.511185936	2.65	4.94	0.536746708	0.523966322	0.018074195
115	2.36	4.77	0.494402836	2.63	4.94	0.532700827	0.513551832	0.027080769
120	2.32	4.77	0.486011287	2.51	4.94	0.508425546	0.497218416	0.015849275
125	2.24	4.77	0.469228187	2.48	4.94	0.502356725	0.485792456	0.023425414
130	2.15	4.77	0.4503472	2.42	4.94	0.490219084	0.470283142	0.02819368
135	2.07	4.77	0.433564101	2.36	4.94	0.478081444	0.455822772	0.031478515
140	2.04	4.77	0.427270439	2.30	4.94	0.465943803	0.446607121	0.027346198
145	2.04	4.77	0.427270439	2.29	4.94	0.463920863	0.445595651	0.025915763
150	2.01	4.77	0.420976776	2.22	4.94	0.449760282	0.435368529	0.020353012
155	2.01	4.77	0.420976776	2.16	4.94	0.437622641	0.429299709	0.011770404
160	2.00	4.77	0.418878889	2.16	4.94	0.437622641	0.428250765	0.013253834
165	2.00	4.77	0.418878889	2.14	4.94	0.43357676	0.426227825	0.010392965
170	1.99	4.77	0.416781002	2.14	4.94	0.43357676	0.425178881	0.011876395
175	1.99	4.77	0.416781002	2.14	4.94	0.43357676	0.425178881	0.011876395
180	1.99	4.77	0.416781002	2.14	4.94	0.43357676	0.425178881	0.011876395

Table D. 3 Efficiency removal of PCO of effect initial HCHO concentration about 7.50

± 0.50 ppm in a small modeling room

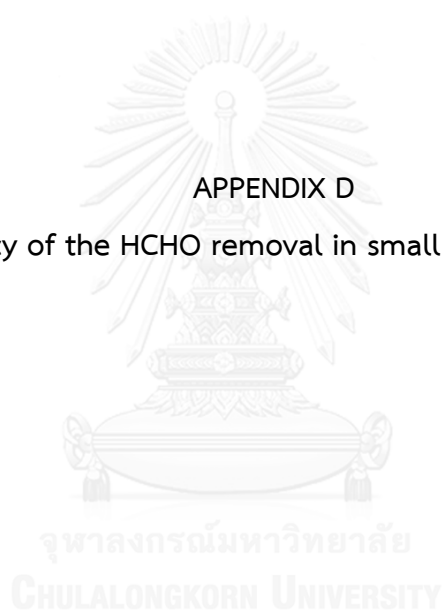| Time (min)	Test 1st	C_{CO} Test 1st	$C_{CO}/C_{CO,0}$	Test 2nd	C_{CO} Test 2nd	$C_{CO}/C_{CO,0}$	Average $C_{CO}/C_{CO,0}$	error
0	7.69	7.69	1	7.81	7.81	1	1	0
5	7.52	7.69	0.977893368	7.69	7.81	0.984633116	0.981263242	0.004765721
10	7.39	7.69	0.960988296	7.63	7.81	0.976949673	0.968968985	0.011286398
15	6.97	7.69	0.906371912	7.49	7.81	0.959021642	0.932696777	0.037228981
20	6.89	7.69	0.895968791	7.17	7.81	0.918043283	0.907006037	0.015609024
25	6.78	7.69	0.881664499	6.96	7.81	0.891151236	0.886407868	0.006708136
30	6.67	7.69	0.867360208	6.84	7.81	0.875784351	0.87157228	0.005956769
35	6.59	7.69	0.856957087	6.72	7.81	0.860417467	0.858687277	0.002446858
40	6.43	7.69	0.836150845	6.52	7.81	0.834805993	0.835478419	0.000950954
45	6.26	7.69	0.814044213	6.34	7.81	0.811755667	0.81289994	0.001618247
50	6.18	7.69	0.803641092	6.17	7.81	0.789985914	0.796813503	0.009655669
55	6.06	7.69	0.788036411	6.07	7.81	0.777180177	0.782608294	0.007676517
60	5.86	7.69	0.762028609	5.92	7.81	0.757971571	0.76000009	0.002868759
65	5.64	7.69	0.733420026	5.78	7.81	0.74004354	0.736731783	0.004683531
70	5.44	7.69	0.707412224	5.57	7.81	0.713151492	0.710281858	0.004058275
75	5.29	7.69	0.687906372	5.40	7.81	0.691381739	0.689644055	0.002457456
80	5.06	7.69	0.657997399	5.24	7.81	0.67089256	0.66444498	0.009118256
85	4.99	7.69	0.648894668	5.04	7.81	0.645281086	0.647087877	0.002555189
90	4.82	7.69	0.626788036	4.95	7.81	0.633755923	0.63027198	0.00492704
95	4.7	7.69	0.611183355	4.86	7.81	0.622230759	0.616707057	0.007811695
100	4.61	7.69	0.599479844	4.82	7.81	0.617108465	0.608294154	0.012465317
105	4.5	7.69	0.585175553	4.54	7.81	0.581252401	0.583213977	0.002774087
110	4.41	7.69	0.573472042	4.49	7.81	0.574849533	0.574160787	0.000974033
115	4.21	7.69	0.547464239	4.30	7.81	0.550518632	0.548991436	0.002159782
120	4.08	7.69	0.530559168	4.10	7.81	0.524907158	0.527733163	0.003996574
125	3.96	7.69	0.514954486	4.02	7.81	0.514662569	0.514808528	0.000206417
130	3.86	7.69	0.501950585	3.92	7.81	0.501856832	0.501903709	6.62936E-05
135	3.69	7.69	0.479843953	3.92	7.81	0.501856832	0.490850393	0.015565456
140	3.55	7.69	0.461638492	3.75	7.81	0.480087079	0.470862785	0.013045121
145	3.47	7.69	0.451235371	3.59	7.81	0.4595979	0.455416635	0.005913201
150	3.46	7.69	0.44993498	3.59	7.81	0.4595979	0.45476644	0.006832716
155	3.46	7.69	0.44993498	3.58	7.81	0.458317326	0.454126153	0.005927213
160	3.45	7.69	0.44863459	3.58	7.81	0.458317326	0.453475958	0.006846728
165	3.45	7.69	0.44863459	3.58	7.81	0.458317326	0.453475958	0.006846728
170	3.45	7.69	0.44863459	3.58	7.81	0.458317326	0.453475958	0.006846728
175	3.45	7.69	0.44863459	3.58	7.81	0.458317326	0.453475958	0.006846728
180	3.45	7.69	0.44863459	3.57	7.81	0.457036752	0.452835671	0.005941226

Table D. 4 Efficiency removal of PCO of effect initial HCHO concentration about 10.0 ± 0.50 ppm in a small modeling room

Time (min)	Test 1st	C_{CO} Test 1st	$C_{CO}/C_{CO,0}$	Test 2nd	C_{CO} Test 2nd	$C_{CO}/C_{CO,0}$	Average $C_{CO}/C_{CO,0}$	error
0	9.82	9.82	1	10.11	10.11	0.999971304	0.999985652	2.0291E-05
5	9.78	9.82	0.995925477	9.89	10.11	0.978202058	0.987063768	0.01253235
10	9.53	9.82	0.970459708	9.70	10.11	0.959401346	0.964930527	0.007819443
15	9.50	9.82	0.967403816	9.45	10.11	0.934663566	0.951033691	0.023150853
20	9.40	9.82	0.957217508	9.40	10.11	0.92971601	0.943466759	0.019446496
25	9.19	9.82	0.935826262	9.28	10.11	0.917841876	0.926834069	0.012716881
30	9.08	9.82	0.924621324	9.12	10.11	0.902009697	0.913315511	0.015988835
35	8.94	9.82	0.910360493	8.89	10.11	0.87925094	0.894805717	0.021997776
40	8.80	9.82	0.896099663	8.66	10.11	0.856492183	0.876295923	0.028006718
45	8.57	9.82	0.872671155	8.53	10.11	0.843628538	0.858149846	0.020536232
50	8.32	9.82	0.847205387	8.30	10.11	0.82086978	0.834037583	0.018622086
55	8.08	9.82	0.822758248	8.09	10.11	0.800090046	0.811424147	0.01602884
60	7.74	9.82	0.788124803	7.90	10.11	0.781289333	0.784707068	0.004833407
65	7.54	9.82	0.767752188	7.69	10.11	0.760509598	0.764130893	0.005121284
70	7.39	9.82	0.752472726	7.55	10.11	0.746656442	0.749564584	0.004112734
75	7.19	9.82	0.732100111	7.39	10.11	0.730824263	0.731462187	0.000902161
80	7.08	9.82	0.720895173	7.04	10.11	0.696191371	0.708543272	0.017468225
85	6.87	9.82	0.699503927	6.87	10.11	0.679369681	0.689436804	0.014237061
90	6.71	9.82	0.683205835	6.65	10.11	0.657600435	0.670403135	0.018105752
95	6.52	9.82	0.66385185	6.49	10.11	0.641768256	0.652810053	0.015615459
100	6.43	9.82	0.654684174	6.39	10.11	0.631873145	0.643278659	0.016129833
105	6.35	9.82	0.646535127	6.32	10.11	0.624946566	0.635740847	0.015265418
110	6.25	9.82	0.63634882	6.09	10.11	0.602187809	0.619268315	0.024155482
115	6.19	9.82	0.630237035	6.04	10.11	0.597240253	0.613738644	0.023332248
120	6.08	9.82	0.619032097	6.01	10.11	0.59427172	0.606651908	0.017508231
125	5.95	9.82	0.605789897	5.93	10.11	0.58635563	0.596072764	0.013742102
130	5.74	9.82	0.584398651	5.86	10.11	0.579429052	0.581913852	0.003514037
135	5.73	9.82	0.583380021	5.85	10.11	0.578439541	0.580909781	0.003493447
140	5.71	9.82	0.581342759	5.85	10.11	0.578439541	0.57989115	0.002052885
145	5.71	9.82	0.581342759	5.85	10.11	0.578439541	0.57989115	0.002052885
150	5.71	9.82	0.581342759	5.84	10.11	0.57745003	0.579396394	0.002752575
155	5.71	9.82	0.581342759	5.84	10.11	0.57745003	0.579396394	0.002752575
160	5.71	9.82	0.581342759	5.84	10.11	0.57745003	0.579396394	0.002752575
165	5.71	9.82	0.581342759	5.83	10.11	0.576460519	0.578901639	0.003452265
170	5.71	9.82	0.581342759	5.82	10.11	0.575471007	0.578406883	0.004151955
175	5.71	9.82	0.581342759	5.82	10.11	0.575471007	0.578406883	0.004151955
180	5.71	9.82	0.581342759	5.81	10.11	0.574481496	0.577912128	0.004851646

Table D. 5 Efficiency removal of PCO of effect catalyst (TiO$_2$) dosage (1.0%

wt.TiO$_2$/vol.sol.) in a small modeling room

Time (min)	Test 1st	C_{CO} Test 1st	$C_{CO}/C_{CO,0}$	Test 2nd	C_{CO} Test 2nd	$C_{CO}/C_{CO,0}$	Average $C_{CO}/C_{CO,0}$	error
0	4.77	4.77	0.999993706	4.94	4.94	1	0.999996853	4.45029E-06
5	4.68	4.77	0.981112719	4.82	4.94	0.975724718	0.978418719	0.003809892
10	4.63	4.77	0.970623282	4.70	4.94	0.951449437	0.961036359	0.013557956
15	4.49	4.77	0.941252858	4.67	4.94	0.945380616	0.943316737	0.002918766
20	4.38	4.77	0.918176097	4.55	4.94	0.921105334	0.919640716	0.002071284
25	4.32	4.77	0.905588772	4.42	4.94	0.894807113	0.900197942	0.007623785
30	4.19	4.77	0.878316236	4.36	4.94	0.882669472	0.880492854	0.003078203
35	4.11	4.77	0.861533136	4.26	4.94	0.86244007	0.861986603	0.000641299
40	3.97	4.77	0.832162712	4.16	4.94	0.842210669	0.837186691	0.007104978
45	3.83	4.77	0.802792288	4.09	4.94	0.828050088	0.815421188	0.017859962
50	3.67	4.77	0.769226089	3.97	4.94	0.803774806	0.786500448	0.024429632
55	3.62	4.77	0.758736652	3.82	4.94	0.773430704	0.766083678	0.010390264
60	3.54	4.77	0.741953553	3.78	4.94	0.765338944	0.753646248	0.016535968
65	3.33	4.77	0.697897917	3.61	4.94	0.730948961	0.714423439	0.023370618
70	3.22	4.77	0.674821155	3.51	4.94	0.71071956	0.692770357	0.025384005
75	3.12	4.77	0.653842281	3.46	4.94	0.700604859	0.67722357	0.033066136
80	3.04	4.77	0.637059181	3.31	4.94	0.670260757	0.653659969	0.023477059
85	2.86	4.77	0.599297208	3.17	4.94	0.641939595	0.620618401	0.030152721
90	2.80	4.77	0.586709883	3.07	4.94	0.621710194	0.604210038	0.024748957
95	2.71	4.77	0.567828896	2.92	4.94	0.591366091	0.579597494	0.01664331
100	2.60	4.77	0.544752135	2.89	4.94	0.585297271	0.565024703	0.028669741
105	2.51	4.77	0.525871148	2.75	4.94	0.556976109	0.541423628	0.021994529
110	2.44	4.77	0.511185936	2.65	4.94	0.536746708	0.523966322	0.018074195
115	2.36	4.77	0.494402836	2.63	4.94	0.532700827	0.513551832	0.027080769
120	2.32	4.77	0.486011287	2.51	4.94	0.508425546	0.497218416	0.015849275
125	2.25	4.77	0.471326075	2.48	4.94	0.502356725	0.4868414	0.021941983
130	2.20	4.77	0.460836638	2.42	4.94	0.490219084	0.475527861	0.020776527
135	2.16	4.77	0.452445088	2.36	4.94	0.478081444	0.465263266	0.018127641
140	2.15	4.77	0.4503472	2.32	4.94	0.469989683	0.460168442	0.013889333
145	2.13	4.77	0.446151426	2.33	4.94	0.472012623	0.459082024	0.018286628
150	2.08	4.77	0.435661988	2.30	4.94	0.465943803	0.450802896	0.021412476
155	2.04	4.77	0.427270439	2.26	4.94	0.457852042	0.44256124	0.021624459
160	2.00	4.77	0.418878889	2.21	4.94	0.447737341	0.433308115	0.020406007
165	2.00	4.77	0.418878889	2.16	4.94	0.437622641	0.428250765	0.013253834
170	1.99	4.77	0.416781002	2.15	4.94	0.435599701	0.426190351	0.01330683
175	1.99	4.77	0.416781002	2.14	4.94	0.43357676	0.425178881	0.011876395
180	1.99	4.77	0.416781002	2.14	4.94	0.43357676	0.425178881	0.011876395

Table D. 6 Efficiency removal of PCO of effect catalyst (TiO_2) dosage (2.5 % wt.TiO_2/vol.sol.) in a small modeling room

Time (min)	Test 1st	C_{CO} Test 1st	$C_{CO}/C_{CO,0}$	Test 2nd	C_{CO} Test 2nd	$C_{CO}/C_{CO,0}$	Average $C_{CO}/C_{CO,0}$	error
0	4.96	4.96	1	5.20	5.20	1	1	0
5	4.87	4.96	0.981839131	5.08	5.20	0.976929288	0.97938421	0.003471783
10	4.72	4.96	0.951571016	5.05	5.20	0.97116161	0.961366313	0.013852642
15	4.58	4.96	0.923320775	4.87	5.20	0.936555543	0.929938159	0.009358394
20	4.47	4.96	0.901124158	4.81	5.20	0.925020187	0.913072172	0.016897044
25	4.41	4.96	0.889016912	4.68	5.20	0.900026916	0.894521914	0.007785249
30	4.18	4.96	0.842605802	4.64	5.20	0.892336679	0.86747124	0.03516504
35	4.05	4.96	0.816373436	4.49	5.20	0.863498289	0.839935862	0.033322303
40	3.92	4.96	0.79014107	4.38	5.20	0.842350137	0.816245603	0.036917385
45	3.83	4.96	0.771980201	4.28	5.20	0.823124543	0.797552372	0.036164512
50	3.65	4.96	0.735658463	4.17	5.20	0.801976391	0.768817427	0.046893857
55	3.54	4.96	0.713461845	4.08	5.20	0.784673357	0.749067601	0.050354143
60	3.38	4.96	0.681175856	3.95	5.20	0.759680086	0.720427971	0.055510874
65	3.33	4.96	0.671086484	3.69	5.20	0.709693544	0.690390014	0.027299314
70	3.22	4.96	0.648889866	3.57	5.20	0.686622832	0.667756349	0.026681236
75	3.09	4.96	0.6226575	3.52	5.20	0.677010036	0.649833768	0.038433047
80	2.86	4.96	0.576246391	3.39	5.20	0.652016765	0.614131578	0.053577745
85	2.76	4.96	0.556067647	3.32	5.20	0.63855885	0.597313248	0.058330089
90	2.86	4.96	0.576246391	2.97	5.20	0.571269274	0.573757832	0.003519353
95	2.58	4.96	0.519745909	2.91	5.20	0.559733918	0.539739914	0.028275792
100	2.51	4.96	0.505620789	2.84	5.20	0.546276003	0.525948396	0.028747577
105	2.43	4.96	0.489477794	2.67	5.20	0.513592494	0.501535144	0.017051668
110	2.40	4.96	0.483424171	2.57	5.20	0.494366901	0.488895536	0.007737679
115	2.31	4.96	0.465263302	2.54	5.20	0.488599223	0.476931263	0.016500988
120	2.20	4.96	0.443066685	2.40	5.20	0.461683393	0.452375039	0.013164001
125	2.13	4.96	0.428941564	2.35	5.20	0.452070596	0.44050608	0.016354695
130	2.06	4.96	0.414816444	2.18	5.20	0.419387088	0.417101766	0.003231933
135	1.95	4.96	0.392619826	2.29	5.20	0.440535241	0.416577533	0.033881314
140	1.93	4.96	0.388584078	2.18	5.20	0.419387088	0.403985583	0.021781017
145	1.92	4.96	0.386566203	2.16	5.20	0.415541969	0.401054086	0.020488961
150	1.82	4.96	0.36638746	2.08	5.20	0.400161495	0.383274478	0.023881849
155	1.82	4.96	0.36638746	2.03	5.20	0.390548698	0.378468079	0.017084575
160	1.82	4.96	0.36638746	2.03	5.20	0.390548698	0.378468079	0.017084575
165	1.82	4.96	0.36638746	2.01	5.20	0.38670358	0.37654552	0.014365666
170	1.81	4.96	0.364369586	2.01	5.20	0.38670358	0.375536583	0.015792519
175	1.81	4.96	0.364369586	2.00	5.20	0.38478102	0.374575303	0.014433064
180	1.80	4.96	0.362351711	2.00	5.20	0.38478102	0.373566366	0.015859917

Table D. 7 Efficiency removal of PCO of effect catalyst (TiO_2) dosage (5.0 % wt.TiO_2/vol.sol.) in a small modeling room

Time (min)	Test 1st	C_{CO} Test 1st	$C_{CO}/C_{CO,0}$	Test 2nd	C_{CO} Test 2nd	$C_{CO}/C_{CO,0}$	Average $C_{CO}/C_{CO,0}$	error
0	5.01	5.01	1	4.92	4.92	1	1	0
5	4.95	5.01	0.988027298	4.85	4.92	0.985786311	0.986906805	0.001584617
10	4.85	5.01	0.968072794	4.71	4.92	0.957358934	0.962715864	0.007575843
15	4.65	5.01	0.928163787	4.45	4.92	0.904565234	0.91636451	0.016686697
20	4.55	5.01	0.908209283	4.33	4.92	0.88019891	0.894204097	0.019806324
25	4.45	5.01	0.888254779	4.20	4.92	0.85380206	0.87102842	0.024361751
30	4.22	5.01	0.842359421	4.06	4.92	0.825374683	0.833867052	0.012010023
35	3.96	5.01	0.790477711	3.96	4.92	0.805069414	0.797773562	0.010317892
40	3.86	5.01	0.770523207	3.85	4.92	0.782733617	0.776628412	0.008634064
45	3.77	5.01	0.752564154	3.76	4.92	0.764458875	0.758511514	0.008410838
50	3.70	5.01	0.738596001	3.67	4.92	0.746184132	0.742390067	0.005365619
55	3.61	5.01	0.720636948	3.57	4.92	0.725878863	0.723257905	0.003706594
60	3.36	5.01	0.670750688	3.40	4.92	0.691359905	0.681055297	0.014572917
65	3.24	5.01	0.646805284	3.30	4.92	0.671054635	0.65892996	0.017146881
70	3.13	5.01	0.62485533	3.23	4.92	0.656840947	0.640848138	0.022617247
75	3.03	5.01	0.604900826	3.05	4.92	0.620291462	0.612596144	0.010882823
80	2.82	5.01	0.562996368	2.89	4.92	0.587803031	0.5753997	0.017540959
85	2.74	5.01	0.547032765	2.77	4.92	0.563436707	0.555234736	0.011599339
90	2.58	5.01	0.515105559	2.60	4.92	0.528917749	0.522011654	0.009766693
95	2.49	5.01	0.497146506	2.56	4.92	0.520795642	0.508971074	0.016722464
100	2.44	5.01	0.487169254	2.39	4.92	0.486276684	0.486722969	0.000631143
105	2.26	5.01	0.451251147	2.32	4.92	0.472062995	0.461657071	0.014716199
110	2.18	5.01	0.435287544	2.21	4.92	0.449727199	0.442507372	0.010210377
115	2.12	5.01	0.423314842	2.16	4.92	0.439574564	0.431444703	0.01149736
120	2.07	5.01	0.41333759	1.99	4.92	0.405055606	0.409196598	0.005856247
125	1.94	5.01	0.387396735	1.96	4.92	0.398964025	0.39318038	0.008179309
130	1.87	5.01	0.373428583	1.81	4.92	0.368506121	0.370967352	0.003480706
135	1.84	5.01	0.367442232	1.77	4.92	0.360384013	0.363913122	0.004990914
140	1.82	5.01	0.363451331	1.69	4.92	0.344139798	0.353795564	0.013655316
145	1.77	5.01	0.353474079	1.65	4.92	0.33601769	0.344745885	0.012343531
150	1.69	5.01	0.337510476	1.60	4.92	0.325865055	0.331687766	0.008234556
155	1.58	5.01	0.315560522	1.59	4.92	0.323834528	0.319697525	0.005850606
160	1.56	5.01	0.311569621	1.55	4.92	0.315712421	0.313641021	0.002929401
165	1.54	5.01	0.307578721	1.53	4.92	0.311651367	0.309615044	0.002879796
170	1.54	5.01	0.307578721	1.53	4.92	0.311651367	0.309615044	0.002879796
175	1.54	5.01	0.307578721	1.53	4.92	0.311651367	0.309615044	0.002879796
180	1.53	5.01	0.30558327	1.53	4.92	0.311651367	0.308617318	0.004290792

Table D. 8 Efficiency removal of PCO of effect catalyst (TiO2) dosage (7.5 %

wt.TiO$_2$/vol.sol.) in a small modeling room

Time (min)	Test 1st	C_{CO} Test 1st	$C_{CO}/C_{CO,0}$	Test 2nd	C_{CO} Test 2nd	$C_{CO}/C_{CO,0}$	Average $C_{CO}/C_{CO,0}$	error
0	4.67	4.67	1	5.27	5.27	1	1	0
5	4.56	4.67	0.976452607	5.2	5.27	0.986717268	0.981584937	0.007258211
10	4.49	4.67	0.961467902	5	5.27	0.948766603	0.955117253	0.008981174
15	4.41	4.67	0.944342525	4.85	5.27	0.920303605	0.932323065	0.016998083
20	4.32	4.67	0.925076476	4.79	5.27	0.908918406	0.916997441	0.01142548
25	4.25	4.67	0.910091771	4.64	5.27	0.880455408	0.895273589	0.020956073
30	4.22	4.67	0.903669754	4.57	5.27	0.867172676	0.885421215	0.025807332
35	4.10	4.67	0.877981689	4.34	5.27	0.823529412	0.85075555	0.038503574
40	3.95	4.67	0.845871607	4.28	5.27	0.812144213	0.82900791	0.023848869
45	3.85	4.67	0.824464885	4.23	5.27	0.802656546	0.813560716	0.015420824
50	3.77	4.67	0.807339508	4.17	5.27	0.791271347	0.799305428	0.011361906
55	3.72	4.67	0.796636148	4.1	5.27	0.777988615	0.787312381	0.013185797
60	3.60	4.67	0.770948082	4.05	5.27	0.768500949	0.769724516	0.001730385
65	3.53	4.67	0.755963377	4.02	5.27	0.762808349	0.759385863	0.004840126
70	3.49	4.67	0.747400689	3.88	5.27	0.736242884	0.741821787	0.007889759
75	3.44	4.67	0.736697328	3.82	5.27	0.724857685	0.730777507	0.008371892
80	3.40	4.67	0.72813464	3.74	5.27	0.709677419	0.71890603	0.013051226
85	3.29	4.67	0.704587246	3.72	5.27	0.705882353	0.7052348	0.000915779
90	3.22	4.67	0.689602541	3.63	5.27	0.688804554	0.689203548	0.000564262
95	3.04	4.67	0.651070443	3.56	5.27	0.675521822	0.663296132	0.017289736
100	2.99	4.67	0.640367082	3.53	5.27	0.669829222	0.655098152	0.020832879
105	2.96	4.67	0.633945066	3.45	5.27	0.654648956	0.644297011	0.014639861
110	2.94	4.67	0.629663722	3.33	5.27	0.631878558	0.63077114	0.001566126
115	2.90	4.67	0.621101033	3.24	5.27	0.614800759	0.617950896	0.004454967
120	2.73	4.67	0.584709607	3.19	5.27	0.605313093	0.59501135	0.014568865
125	2.68	4.67	0.574006246	3.16	5.27	0.599620493	0.58681337	0.018112008
130	2.55	4.67	0.546177509	3.14	5.27	0.595825427	0.571001468	0.03510638
135	2.53	4.67	0.541896165	3.1	5.27	0.588235294	0.565065729	0.032766713
140	2.52	4.67	0.539755492	3.05	5.27	0.578747628	0.55925156	0.027571604
145	2.51	4.67	0.53761482	3.01	5.27	0.571157495	0.554386158	0.023718253
150	2.48	4.67	0.531192804	3.01	5.27	0.571157495	0.55117515	0.028259304
155	2.48	4.67	0.531192804	2.98	5.27	0.565464896	0.54832885	0.024234028
160	2.48	4.67	0.531192804	2.97	5.27	0.563567362	0.547380083	0.02289227
165	2.48	4.67	0.531192804	2.96	5.27	0.561669829	0.546431317	0.021550511
170	2.48	4.67	0.531192804	2.96	5.27	0.561669829	0.546431317	0.021550511
175	2.48	4.67	0.531192804	2.96	5.27	0.561669829	0.546431317	0.021550511
180	2.48	4.67	0.531192804	2.96	5.27	0.561669829	0.546431317	0.021550511

Table D. 9 Efficiency removal of PCO of effect air flow rate (3 L/min.) in a small modeling room

Time (min)	Test 1st	C_{CO} Test 1st	$C_{CO}/C_{CO,0}$	Test 2nd	C_{CO} Test 2nd	$C_{CO}/C_{CO,0}$	Average $C_{CO}/C_{CO,0}$	error
0	4.87	4.87	1	5.08	5.08	1	1	0
5	4.82	4.87	0.989730107	4.94	5.08	0.972450164	0.981090136	0.012218765
10	4.67	4.87	0.958920429	4.87	5.08	0.958675246	0.958797838	0.00017337
15	4.61	4.87	0.946596558	4.81	5.08	0.946868174	0.946732366	0.000192062
20	4.47	4.87	0.917840858	4.66	5.08	0.917350493	0.917595675	0.00034674
25	4.43	4.87	0.909624944	4.61	5.08	0.907511266	0.908568105	0.001494596
30	4.28	4.87	0.878815265	4.46	5.08	0.877993585	0.878404425	0.000581016
35	4.25	4.87	0.872653329	4.38	5.08	0.862250822	0.867452076	0.007355684
40	4.21	4.87	0.864437415	4.25	5.08	0.836668831	0.850553123	0.019635354
45	4.16	4.87	0.854167522	4.17	5.08	0.820926068	0.837546795	0.023505258
50	4.11	4.87	0.84389763	4.14	5.08	0.815022532	0.829460081	0.020417778
55	4.04	4.87	0.82951978	4.04	5.08	0.795344078	0.812431929	0.024165871
60	3.97	4.87	0.81514193	4.01	5.08	0.789440542	0.802291236	0.018173626
65	3.93	4.87	0.806926016	3.90	5.08	0.767794242	0.787360129	0.027670342
70	3.90	4.87	0.80076408	3.83	5.08	0.754019324	0.777391702	0.033053534
75	3.86	4.87	0.792548166	3.81	5.08	0.750083633	0.7713159	0.030026959
80	3.84	4.87	0.788440209	3.74	5.08	0.736308716	0.762374462	0.036862532
85	3.82	4.87	0.784332252	3.72	5.08	0.732373025	0.758352638	0.036740722
90	3.79	4.87	0.778170316	3.71	5.08	0.730405179	0.754287748	0.033775052
95	3.77	4.87	0.774062359	3.65	5.08	0.718598107	0.746330233	0.039219149
100	3.75	4.87	0.769954402	3.60	5.08	0.70875888	0.739356641	0.043271768
105	3.67	4.87	0.753522573	3.60	5.08	0.70875888	0.731140727	0.031652711
110	3.66	4.87	0.751468595	3.57	5.08	0.702855344	0.727161969	0.034374759
115	3.63	4.87	0.745306659	3.54	5.08	0.696951807	0.721129233	0.034192043
120	3.58	4.87	0.735036766	3.52	5.08	0.693016117	0.714026441	0.029713086
125	3.53	4.87	0.724766873	3.48	5.08	0.685144735	0.704955804	0.028017083
130	3.47	4.87	0.712443002	3.46	5.08	0.681209044	0.696826023	0.022085743
135	3.42	4.87	0.702173109	3.44	5.08	0.677273353	0.689723231	0.017606786
140	3.42	4.87	0.702173109	3.40	5.08	0.669401972	0.685787541	0.023172694
145	3.40	4.87	0.698065152	3.37	5.08	0.663498436	0.680781794	0.02444236
150	3.40	4.87	0.698065152	3.37	5.08	0.663498436	0.680781794	0.02444236
155	3.39	4.87	0.696011174	3.35	5.08	0.659562745	0.677786959	0.025772931
160	3.39	4.87	0.696011174	3.33	5.08	0.655627054	0.675819114	0.028555885
165	3.39	4.87	0.696011174	3.31	5.08	0.651691363	0.673851268	0.031338839
170	3.39	4.87	0.696011174	3.28	5.08	0.645787827	0.6708995	0.035513269
175	3.38	4.87	0.693957195	3.26	5.08	0.641852136	0.667904666	0.036843841
180	3.38	4.87	0.693957195	3.26	5.08	0.641852136	0.667904666	0.036843841

Table D. 10 Efficiency removal of PCO of effect air flow rate (4 L/min.) in a small modeling room

Time (min)	Test 1st	C_{CO} Test 1st	$C_{CO}/C_{CO,0}$	Test 2nd	C_{CO} Test 2nd	$C_{CO}/C_{CO,0}$	Average $C_{CO}/C_{CO,0}$	error
0	4.93	4.93	1	5.18	5.18	1	1	1.57009E-16
5	4.85	4.93	0.983772819	5.02	5.18	0.96912389	0.976448355	0.010358357
10	4.78	4.93	0.969574037	4.89	5.18	0.944037051	0.956805544	0.018057375
15	4.72	4.93	0.957403651	4.78	5.18	0.922809726	0.940106689	0.024461599
20	4.44	4.93	0.900608519	4.73	5.18	0.913160942	0.90688473	0.008875903
25	4.34	4.93	0.880324544	4.65	5.18	0.897722887	0.889023715	0.012302487
30	4.27	4.93	0.866125761	4.48	5.18	0.86491702	0.865521391	0.000854708
35	4.11	4.93	0.8336714	4.40	5.18	0.849478966	0.841575183	0.011177637
40	4.03	4.93	0.817444219	4.30	5.18	0.830181397	0.823812808	0.009006545
45	3.97	4.93	0.805273834	4.07	5.18	0.78579699	0.795535412	0.013772209
50	3.8	4.93	0.770791075	4.02	5.18	0.776148205	0.77346964	0.003788063
55	3.73	4.93	0.756592292	3.94	5.18	0.760710151	0.758651221	0.002911766
60	3.59	4.93	0.728194726	3.80	5.18	0.733693555	0.73094414	0.003888259
65	3.5	4.93	0.709939148	3.68	5.18	0.710536472	0.71023781	0.000422372
70	3.4	4.93	0.689655172	3.65	5.18	0.704747202	0.697201187	0.010671676
75	3.31	4.93	0.671399594	3.50	5.18	0.675800849	0.673600222	0.003112157
80	3.17	4.93	0.643002028	3.39	5.18	0.654573524	0.648787776	0.008182283
85	3.09	4.93	0.626774848	3.27	5.18	0.631416442	0.629095645	0.003282102
90	3.03	4.93	0.614604462	3.24	5.18	0.625627171	0.620115817	0.007794232
95	2.97	4.93	0.602434077	3.07	5.18	0.592821305	0.597627691	0.006797257
100	2.94	4.93	0.596348884	3.01	5.18	0.581242763	0.588795824	0.010681641
105	2.87	4.93	0.582150101	2.90	5.18	0.560015438	0.57108277	0.015651571
110	2.78	4.93	0.563894523	2.82	5.18	0.544577383	0.554235953	0.013659281
115	2.74	4.93	0.555780933	2.78	5.18	0.536858356	0.546319644	0.013380283
120	2.68	4.93	0.543610548	2.77	5.18	0.534928599	0.539269573	0.006139065
125	2.73	4.93	0.553752535	2.75	5.18	0.531069085	0.54241081	0.016039621
130	2.63	4.93	0.53346856	2.70	5.18	0.521420301	0.52744443	0.008519405
135	2.58	4.93	0.523326572	2.66	5.18	0.513701274	0.518513923	0.006806114
140	2.57	4.93	0.521298174	2.61	5.18	0.504052489	0.512675332	0.012194541
145	2.55	4.93	0.517241379	2.60	5.18	0.502122733	0.509682056	0.010690498
150	2.51	4.93	0.509127789	2.60	5.18	0.502122733	0.505625261	0.004953323
155	2.5	4.93	0.507099391	2.60	5.18	0.502122733	0.504611062	0.003519029
160	2.49	4.93	0.505070994	2.60	5.18	0.502122733	0.503596863	0.002084736
165	2.48	4.93	0.503042596	2.58	5.18	0.498263219	0.500652908	0.00337953
170	2.48	4.93	0.503042596	2.58	5.18	0.498263219	0.500652908	0.00337953
175	2.48	4.93	0.503042596	2.58	5.18	0.498263219	0.500652908	0.00337953
180	2.48	4.93	0.503042596	2.58	5.18	0.498263219	0.500652908	0.00337953

Table D. 11 Efficiency removal of PCO of effect air flow rate (5 L/min.) in a small modeling room

Time (min)	Test 1st	C_{CO} Test 1st	$C_{CO}/C_{CO,0}$	Test 2nd	C_{CO} Test 2nd	$C_{CO}/C_{CO,0}$	Average $C_{CO}/C_{CO,0}$	error
0	5.01	5.01	1	4.92	4.92	1	1	0
5	4.95	5.01	0.988027298	4.85	4.92	0.985786311	0.986906805	0.001584617
10	4.85	5.01	0.968072794	4.71	4.92	0.957358934	0.962715864	0.007575843
15	4.65	5.01	0.928163787	4.45	4.92	0.904565234	0.91636451	0.016686697
20	4.55	5.01	0.908209283	4.33	4.92	0.88019891	0.894204097	0.019806324
25	4.45	5.01	0.888254779	4.20	4.92	0.85380206	0.87102842	0.024361751
30	4.22	5.01	0.842359421	4.06	4.92	0.825374683	0.833867052	0.012010023
35	3.96	5.01	0.790477711	3.96	4.92	0.805069414	0.797773562	0.010317892
40	3.86	5.01	0.770523207	3.85	4.92	0.782733617	0.776628412	0.008634064
45	3.77	5.01	0.752564154	3.76	4.92	0.764458875	0.758511514	0.008410838
50	3.70	5.01	0.738596001	3.67	4.92	0.746184132	0.742390067	0.005365619
55	3.61	5.01	0.720636948	3.57	4.92	0.725878863	0.723257905	0.003706594
60	3.36	5.01	0.670750688	3.40	4.92	0.691359905	0.681055297	0.014572917
65	3.24	5.01	0.646805284	3.30	4.92	0.671054635	0.65892996	0.017146881
70	3.13	5.01	0.62485533	3.23	4.92	0.656840947	0.640848138	0.022617247
75	3.03	5.01	0.604900826	3.05	4.92	0.620291462	0.612596144	0.010882823
80	2.82	5.01	0.562996368	2.89	4.92	0.587803031	0.5753997	0.017540959
85	2.74	5.01	0.547032765	2.77	4.92	0.563436707	0.555234736	0.011599339
90	2.58	5.01	0.515105559	2.60	4.92	0.528917749	0.522011654	0.009766693
95	2.49	5.01	0.497146506	2.56	4.92	0.520795642	0.508971074	0.016722464
100	2.44	5.01	0.487169254	2.39	4.92	0.486276684	0.486722969	0.000631143
105	2.26	5.01	0.451251147	2.32	4.92	0.472062995	0.461657071	0.014716199
110	2.18	5.01	0.435287544	2.21	4.92	0.449727199	0.442507372	0.010210377
115	2.12	5.01	0.423314842	2.16	4.92	0.439574564	0.431444703	0.01149736
120	2.07	5.01	0.41333759	1.99	4.92	0.405055606	0.409196598	0.005856247
125	1.94	5.01	0.387396735	1.96	4.92	0.398964025	0.39318038	0.008179309
130	1.87	5.01	0.373428583	1.81	4.92	0.368506121	0.370967352	0.003480706
135	1.84	5.01	0.367442232	1.77	4.92	0.360384013	0.363913122	0.004990914
140	1.82	5.01	0.363451331	1.69	4.92	0.344139798	0.353795564	0.013655316
145	1.77	5.01	0.353474079	1.65	4.92	0.33601769	0.344745885	0.012343531
150	1.69	5.01	0.337510476	1.60	4.92	0.325865055	0.331687766	0.008234556
155	1.58	5.01	0.315560522	1.59	4.92	0.323834528	0.319697525	0.005850606
160	1.56	5.01	0.311569621	1.55	4.92	0.315712421	0.313641021	0.002929401
165	1.54	5.01	0.307578721	1.53	4.92	0.311651367	0.309615044	0.002879796
170	1.54	5.01	0.307578721	1.53	4.92	0.311651367	0.309615044	0.002879796
175	1.54	5.01	0.307578721	1.53	4.92	0.311651367	0.309615044	0.002879796
180	1.53	5.01	0.30558327	1.53	4.92	0.311651367	0.308617318	0.004290792

Table D. 12 Efficiency HCHO removal by using pure SF filter in small modeling room (adsorption)

Time (min)	Test 1st	C_{CO} Test 1st	$C_{CO}/C_{CO,0}$	Test 2nd	C_{CO} Test 2nd	$C_{CO}/C_{CO,0}$	Average $C_{CO}/C_{CO,0}$	error
0	4.86	4.86	1	4.96	4.96	1	1	2.22045E-16
5	4.75	4.86	0.977366255	4.80	4.96	0.967725668	0.972545962	0.006816924
10	4.66	4.86	0.958847737	4.56	4.96	0.91931417	0.939080954	0.027954453
15	4.56	4.86	0.938271605	4.43	4.96	0.893091276	0.91568144	0.031947317
20	4.46	4.86	0.917695473	4.25	4.96	0.856782653	0.887239063	0.043071869
25	4.4	4.86	0.905349794	4.14	4.96	0.834594049	0.869971922	0.050031867
30	4.35	4.86	0.895061728	4.02	4.96	0.810388301	0.852725014	0.059873155
35	4.29	4.86	0.882716049	4.01	4.96	0.808371155	0.845543602	0.052569779
40	4.26	4.86	0.87654321	3.83	4.96	0.772062532	0.824302871	0.073878996
45	4.22	4.86	0.868312757	3.78	4.96	0.761976803	0.81514478	0.075190874
50	4.17	4.86	0.858024691	3.72	4.96	0.749873928	0.80394931	0.076474138
55	4.13	4.86	0.849794239	3.68	4.96	0.741805345	0.795799792	0.076359679
60	4.08	4.86	0.839506173	3.62	4.96	0.729702471	0.784604322	0.077642942
65	3.95	4.86	0.812757202	3.56	4.96	0.717599597	0.765178399	0.067286588
70	3.93	4.86	0.808641975	3.53	4.96	0.711548159	0.760095067	0.068655696
75	3.8	4.86	0.781893004	3.44	4.96	0.693393848	0.737643426	0.062578354
80	3.67	4.86	0.755144033	3.40	4.96	0.685325265	0.720234649	0.049369324
85	3.65	4.86	0.751028807	3.29	4.96	0.663136662	0.707082734	0.062149132
90	3.45	4.86	0.709876543	3.10	4.96	0.624810893	0.667343718	0.060150498
95	3.41	4.86	0.701646091	3.04	4.96	0.612708018	0.657177054	0.062888714
100	3.48	4.86	0.716049383	3.01	4.96	0.606656581	0.661352982	0.077352392
105	3.45	4.86	0.709876543	2.98	4.96	0.600605144	0.655240843	0.077266548
110	3.44	4.86	0.70781893	2.96	4.96	0.596570852	0.652194891	0.07866427
115	3.42	4.86	0.703703704	2.95	4.96	0.594553707	0.649128705	0.077180703
120	3.26	4.86	0.670781893	2.93	4.96	0.590519415	0.630650654	0.056754142
125	3.15	4.86	0.648148148	2.92	4.96	0.588502269	0.618325209	0.042176005
130	3.09	4.86	0.635802469	2.92	4.96	0.588502269	0.612152369	0.033446292
135	2.99	4.86	0.615226337	2.90	4.96	0.584467978	0.599847158	0.021749445
140	2.94	4.86	0.604938272	2.89	4.96	0.582450832	0.593694552	0.015901021
145	2.92	4.86	0.600823045	2.89	4.96	0.582450832	0.591636939	0.012991117
150	2.89	4.86	0.594650206	2.87	4.96	0.578416541	0.586533373	0.011478935
155	2.89	4.86	0.594650206	2.89	4.96	0.582450832	0.588550519	0.00862626
160	2.88	4.86	0.592592593	2.85	4.96	0.574382249	0.583487421	0.012876657
165	2.88	4.86	0.592592593	2.87	4.96	0.578416541	0.585504567	0.010023982
170	2.88	4.86	0.592592593	2.85	4.96	0.574382249	0.583487421	0.012876657
175	2.88	4.86	0.592592593	2.85	4.96	0.574382249	0.583487421	0.012876657
180	2.88	4.86	0.592592593	2.84	4.96	0.572365103	0.582478848	0.014302995

Table D. 13 Efficiency HCHO removal by using pure SF filter in small modeling room (photolysis)

Time (min)	Test 1st	C_{CO} Test 1st	$C_{CO}/C_{CO,0}$	Test 2nd	C_{CO} Test 2nd	$C_{CO}/C_{CO,0}$	Average $C_{CO}/C_{CO,0}$	error
0	5.31	5.31	1	5.13	5.13	1	1	0
5	4.99	5.31	0.939679548	4.84	5.13	0.943469786	0.941574667	0.002680103
10	4.84	5.31	0.911404336	4.69	5.13	0.914230019	0.912817178	0.00199806
15	4.81	5.31	0.905749293	4.6	5.13	0.89668616	0.901217726	0.006408603
20	4.69	5.31	0.883129123	4.46	5.13	0.869395712	0.876262417	0.009710989
25	4.58	5.31	0.862393968	4.32	5.13	0.842105263	0.852249616	0.014346281
30	4.49	5.31	0.845428841	4.28	5.13	0.834307992	0.839868416	0.007863627
35	4.43	5.31	0.834118756	4.2	5.13	0.81871345	0.826416103	0.010893196
40	4.38	5.31	0.824693685	4.15	5.13	0.808966862	0.816830273	0.011120544
45	4.34	5.31	0.817153629	4.01	5.13	0.781676413	0.799415021	0.02508618
0	4.31	5.31	0.811498586	3.9	5.13	0.760233918	0.785866252	0.036249594
55	4.24	5.31	0.798303487	3.88	5.13	0.756335283	0.777319385	0.029676002
60	4.22	5.31	0.794533459	3.8	5.13	0.740740741	0.7676371	0.038037196
65	4.09	5.31	0.770028275	3.69	5.13	0.719298246	0.74466326	0.035871548
70	3.96	5.31	0.745523091	3.64	5.13	0.709551657	0.727537374	0.025435645
75	3.91	5.31	0.736098021	3.4	5.13	0.662768031	0.699433026	0.051852133
80	3.78	5.31	0.711592837	3.34	5.13	0.651072125	0.681332481	0.042794606
85	3.60	5.31	0.677662582	3.29	5.13	0.641325536	0.659494059	0.025694172
90	3.39	5.31	0.638077286	3.22	5.13	0.627680312	0.632878799	0.007351771
95	3.37	5.31	0.634307257	3.17	5.13	0.617933723	0.62612049	0.011577837
100	3.36	5.31	0.632422243	3.12	5.13	0.608187135	0.620304689	0.01713681
105	3.33	5.31	0.626767201	3.06	5.13	0.596491228	0.611629214	0.021408346
110	3.31	5.31	0.622997172	3.02	5.13	0.588693957	0.605845565	0.024256036
115	3.24	5.31	0.609802074	2.99	5.13	0.582846004	0.596324039	0.01906082
120	3.19	5.31	0.600377003	2.93	5.13	0.571150097	0.58576355	0.020666543
125	3.11	5.31	0.58529689	2.88	5.13	0.561403509	0.573350199	0.016895172
130	3.04	5.31	0.572101791	2.85	5.13	0.555555556	0.563828673	0.011699955
135	3.02	5.31	0.568331762	2.84	5.13	0.553606238	0.560969	0.010412518
140	2.93	5.31	0.551366635	2.8	5.13	0.545808967	0.548587801	0.003929865
145	2.92	5.31	0.549481621	2.79	5.13	0.543859649	0.546670635	0.003975335
150	2.87	5.31	0.54005655	2.78	5.13	0.541910331	0.540983441	0.001310821
155	2.83	5.31	0.532516494	2.78	5.13	0.541910331	0.537213413	0.006642446
160	2.82	5.31	0.53063148	2.77	5.13	0.539961014	0.535296247	0.006596977
165	2.76	5.31	0.519321395	2.77	5.13	0.539961014	0.529641204	0.014594414
170	2.75	5.31	0.517436381	2.77	5.13	0.539961014	0.528698697	0.015927321
175	2.75	5.31	0.517436381	2.77	5.13	0.539961014	0.528698697	0.015927321
180	2.75	5.31	0.517436381	2.77	5.13	0.539961014	0.528698697	0.015927321

Table D. 14 Efficiency HCHO removal by using commercial filters (Polyester class Eu 2) in small modeling room (adsorption)

Time (min)	Test 1st	C_{CO} Test 1st	$C_{CO}/C_{CO,0}$	Test 2nd	C_{CO} Test 2nd	$C_{CO}/C_{CO,0}$	Average $C_{CO}/C_{CO,0}$	error
0	5.21	5.21	1	4.75	4.75	1	1	0
5	5.03	5.21	0.965444423	4.63	4.75	0.974758098	0.970101261	0.006585763
10	4.87	5.21	0.934728355	4.52	4.75	0.951619689	0.943174022	0.011943977
15	4.52	5.21	0.867536955	4.48	4.75	0.943205721	0.905371338	0.053505898
20	4.39	5.21	0.84258015	4.16	4.75	0.875893984	0.859237067	0.023556438
25	4.34	5.21	0.832981378	4.11	4.75	0.865376525	0.849178952	0.022906828
30	4.31	5.21	0.827222116	4.07	4.75	0.856962558	0.842092337	0.021029668
35	4.28	5.21	0.821462853	4.00	4.75	0.842238115	0.831850484	0.014690329
40	4.27	5.21	0.819543098	3.91	4.75	0.823306689	0.821424894	0.00266126
45	4.25	5.21	0.81570359	3.88	4.75	0.816996214	0.816349902	0.000914023
50	4.23	5.21	0.811864081	3.82	4.75	0.804375263	0.808119672	0.005295394
55	4.21	5.21	0.808024573	3.74	4.75	0.787547329	0.797785951	0.014479598
60	4.19	5.21	0.804185064	3.71	4.75	0.781236853	0.792710959	0.016226836
65	4.14	5.21	0.794586293	3.69	4.75	0.77702987	0.785808081	0.012414266
70	4.12	5.21	0.790746784	3.64	4.75	0.766512411	0.778629598	0.01713629
75	4.09	5.21	0.784987522	3.61	4.75	0.760201935	0.772594728	0.017526056
80	4.06	5.21	0.779228259	3.58	4.75	0.75389146	0.766559859	0.017915822
85	4.04	5.21	0.77538875	3.54	4.75	0.745477493	0.760433121	0.021150453
90	4.01	5.21	0.769629487	3.52	4.75	0.741270509	0.755449998	0.020052826
95	3.92	5.21	0.752351699	3.50	4.75	0.737063525	0.744707612	0.010810371
100	3.85	5.21	0.738913419	3.43	4.75	0.722339083	0.730626251	0.011719826
105	3.83	5.21	0.735073911	3.38	4.75	0.711821624	0.723447767	0.01644185
110	3.82	5.21	0.733154156	3.32	4.75	0.699200673	0.716177415	0.024008738
115	3.80	5.21	0.729314648	3.28	4.75	0.690786706	0.710050677	0.027243369
120	3.78	5.21	0.725475139	3.16	4.75	0.665544804	0.695509972	0.042377146
125	3.73	5.21	0.715876368	3.13	4.75	0.659234329	0.687555348	0.04005197
130	3.65	5.21	0.700518334	3.11	4.75	0.655027345	0.67777284	0.032166986
135	3.51	5.21	0.673641774	3.08	4.75	0.64871687	0.661179322	0.017624569
140	3.49	5.21	0.669802265	3.08	4.75	0.64871687	0.659259568	0.014909626
145	3.48	5.21	0.667882511	3.06	4.75	0.644509886	0.656196199	0.016526941
150	3.47	5.21	0.665962757	3.05	4.75	0.642406395	0.654184576	0.016656863
155	3.44	5.21	0.660203494	3.01	4.75	0.633992427	0.647097961	0.018534023
160	3.43	5.21	0.65828374	2.99	4.75	0.629785444	0.644034592	0.020151338
165	3.42	5.21	0.656363985	2.99	4.75	0.629785444	0.643074715	0.018793867
170	3.42	5.21	0.656363985	2.99	4.75	0.629785444	0.643074715	0.018793867
175	3.42	5.21	0.656363985	2.99	4.75	0.629785444	0.643074715	0.018793867
180	3.42	5.21	0.656363985	2.99	4.75	0.629785444	0.643074715	0.018793867

Table D. 15 Efficiency HCHO removal by using commercial filters (Polyester class Eu 2) in small modeling room (photolysis)

Time (min)	Test 1st	C_{CO} Test 1st	$C_{CO}/C_{CO,0}$	Test 2nd	C_{CO} Test 2nd	$C_{CO}/C_{CO,0}$	Average $C_{CO}/C_{CO,0}$	error
0	5.11	5.11	1	4.69	4.69	1	1	0
5	4.93	5.11	0.964774951	4.59	4.69	0.978663025	0.971718988	0.009820351
10	4.77	5.11	0.933463796	4.46	4.69	0.950924958	0.942194377	0.012346906
15	4.73	5.11	0.925636008	4.29	4.69	0.914652101	0.920144054	0.007766795
20	4.66	5.11	0.911937378	4.19	4.69	0.893315126	0.902626252	0.013167921
25	4.46	5.11	0.872798434	4.14	4.69	0.882646638	0.877722536	0.006963732
30	4.31	5.11	0.843444227	4.04	4.69	0.861309664	0.852376945	0.012632771
35	4.18	5.11	0.818003914	3.76	4.69	0.801566134	0.809785024	0.011623266
40	4.11	5.11	0.804305284	3.66	4.69	0.780229159	0.792267221	0.017024391
45	4.02	5.11	0.786692759	3.57	4.69	0.761025882	0.773859321	0.018149223
0	3.94	5.11	0.771037182	3.48	4.69	0.741822604	0.756429893	0.020657826
55	3.88	5.11	0.759295499	3.47	4.69	0.739688907	0.749492203	0.013863954
60	3.82	5.11	0.747553816	3.44	4.69	0.733287814	0.740420815	0.010087586
65	3.77	5.11	0.73776908	3.42	4.69	0.729020419	0.73339475	0.006186237
70	3.71	5.11	0.726027397	3.40	4.69	0.724753025	0.725390211	0.000901118
75	3.65	5.11	0.714285714	3.37	4.69	0.718351932	0.716318823	0.00287525
80	3.60	5.11	0.704500978	3.36	4.69	0.716218235	0.710359607	0.008285351
85	3.57	5.11	0.698630137	3.35	4.69	0.714084537	0.706357337	0.010927911
90	3.51	5.11	0.686888454	3.31	4.69	0.705549747	0.696219101	0.013195527
95	3.47	5.11	0.679060665	3.26	4.69	0.69488126	0.686970963	0.01118685
100	3.42	5.11	0.66927593	3.19	4.69	0.679945377	0.674610653	0.007544439
105	3.37	5.11	0.659491194	3.12	4.69	0.665009495	0.662250344	0.003902028
110	3.33	5.11	0.651663405	3.08	4.69	0.656474705	0.654069055	0.003402103
115	3.28	5.11	0.641878669	3.04	4.69	0.647939915	0.644909292	0.004285948
120	3.25	5.11	0.636007828	3.00	4.69	0.639405125	0.637706476	0.002402252
125	3.20	5.11	0.626223092	2.93	4.69	0.624469243	0.625346167	0.001240159
130	3.16	5.11	0.618395303	2.88	4.69	0.613800755	0.616098029	0.003248836
135	3.13	5.11	0.612524462	2.80	4.69	0.596731175	0.604627819	0.01116754
140	3.08	5.11	0.602739726	2.74	4.69	0.583928991	0.593334358	0.013301199
145	3.02	5.11	0.590998043	2.72	4.69	0.579661596	0.585329819	0.008016079
150	2.98	5.11	0.583170254	2.69	4.69	0.573260503	0.578215379	0.007007252
155	2.96	5.11	0.57925636	2.68	4.69	0.571126806	0.575191583	0.005748463
160	2.89	5.11	0.56555773	2.67	4.69	0.568993108	0.567275419	0.002429179
165	2.88	5.11	0.563600783	2.67	4.69	0.568993108	0.566296945	0.00381295
170	2.87	5.11	0.561643836	2.67	4.69	0.568993108	0.565318472	0.00519672
175	2.85	5.11	0.557729941	2.67	4.69	0.568993108	0.563361525	0.007964262
180	2.85	5.11	0.557729941	2.67	4.69	0.568993108	0.563361525	0.007964262

APPENDIX E

Efficiency of the removal of HCHO in large modeling room

Table E. 1 Efficiency removal of photocatalytic oxidation (PCO) of initial HCHO concentration about 5.00 ± 0.50 ppm in large modeling room

Time (hr)	Test 1st	C_{CO} Test 1st	$C_{CO}/C_{CO,0}$	Test 2nd	C_{CO} Test 2nd	$C_{CO}/C_{CO,0}$	Average $C_{CO}/C_{CO,0}$	error
0	5.74	5.74	1	5.46	5.46	1	1	0
1	4.94	5.74	0.860627178	4.35	5.46	0.796703297	0.828665238	0.04520101
2	3.77	5.74	0.656794425	3.7	5.46	0.677655678	0.667225052	0.014751133
3	3.05	5.74	0.531358885	3.24	5.46	0.593406593	0.562382739	0.043874355
4	2.96	5.74	0.515679443	3.05	5.46	0.558608059	0.537143751	0.030355115
5	2.97	5.74	0.517421603	2.76	5.46	0.505494505	0.511458054	0.008433732
6	2.84	5.74	0.494773519	2.64	5.46	0.483516484	0.489145002	0.007959926
7	2.7	5.74	0.470383275	2.4	5.46	0.43956044	0.454971858	0.021795036
8	2.64	5.74	0.459930314	2.41	5.46	0.441391941	0.450661128	0.013108609

Table E. 2 Efficiency removal of photocatalytic oxidation (PCO) of initial HCHO concentration about 7.50 ± 0.50 ppm. in large modeling room

Time (hr)	Test 1st	C_{CO} Test 1st	$C_{CO}/C_{CO,0}$	Test 2nd	C_{CO} Test 2nd	$C_{CO}/C_{CO,0}$	Average $C_{CO}/C_{CO,0}$	error
0	7.53	7.53	1	7.19	7.19	1	1	0
1	4.83	7.53	0.641434263	5.19	7.19	0.721835883	0.681635073	0.056852531
2	4.95	7.53	0.657370518	4.1	7.19	0.570236439	0.613803479	0.061613098
3	4.76	7.53	0.632138114	4	7.19	0.556328234	0.594233174	0.05360568
4	4.55	7.53	0.604249668	3.89	7.19	0.541029207	0.572639438	0.044703617
5	4.64	7.53	0.616201859	3.84	7.19	0.534075104	0.575138482	0.058072385
6	4.14	7.53	0.549800797	3.73	7.19	0.518776078	0.534288438	0.021937789
7	4.22	7.53	0.560424967	3.64	7.19	0.506258693	0.53334183	0.03830134
8	4.1	7.53	0.544488712	3.56	7.19	0.495132128	0.51981042	0.034900375

Table E. 3 Efficiency removal of photocatalytic oxidation (PCO) of initial HCHO concentration about 10.00 ± 0.50 ppm in large modeling room

Time (hr)	Test 1st	C_{CO} Test 1st	$C_{CO}/C_{CO,0}$	Test 2nd	C_{CO} Test 2nd	$C_{CO}/C_{CO,0}$	Average $C_{CO}/C_{CO,0}$	error
0	9.95	9.95	1	11.35	11.35	1	1	0
1	7.94	9.95	0.79798995	9.73	11.35	0.857268722	0.827629336	0.041916422
2	7.17	9.95	0.720603015	8.61	11.35	0.758590308	0.739596662	0.026861072
3	6.44	9.95	0.647236181	8.4	11.35	0.740088106	0.693662144	0.065656226
4	6.06	9.95	0.609045226	7.84	11.35	0.690748899	0.649897063	0.057773221
5	5.39	9.95	0.541708543	7.36	11.35	0.64845815	0.595083347	0.075483371
6	4.93	9.95	0.495477387	6.79	11.35	0.598237885	0.546857636	0.072662645
7	4.79	9.95	0.481407035	6.4	11.35	0.563876652	0.522641844	0.058314825
8	4.5	9.95	0.452261307	6.05	11.35	0.533039648	0.492650478	0.057118913

จุฬาลงกรณ์มหาวิทยาลัย
CHULALONGKORN UNIVERSITY

VITA

Name: Miss. Janjira Triped

Date of Birth: January 5, 1985

Nationality: Thai

Education:

2007-2008 Master's Degree in Environmental Management (International Program), Chulalongkorn University, Bangkok, Thailand

2003-2007 Bachelor Degree of Science in Biotechnology, Faculty of Technology, Khon Kean University, Khon Kean, Thailand

Publication and Presentation:

2014, Janjira Triped, Wipada Sanongraj, and Wipawee Khamwichit. Photocatalytic Oxidation of Gaseous Formaldehyde Using the TiO_2 Coated SF Filter. International Journal of Chemical, Molecular, Nuclear, Materials and Metallurgical Engineering. 8(5), (2014) 439-442.

2014, Janjira Triped, Wipada Sanongraj, and Wipawee Khamwichit. Formaldehyde Exposure of Medical Students during Gross Anatomy Laboratory. The 2nd International Global Health Forum(IGHF). "Situation and Challenge in Global Health" October2 - 3, 2014 at Thailand. Organized by Chulalongkorn University, Bangkok, Thailand